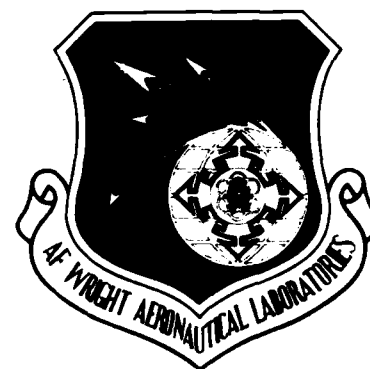


12



## THROTTLE DEPENDENT FORCES - A PRIMER

Douglas L. Bowers  
Airframe Propulsion Integration Group  
Aeromechanics Division

November 1985



Final Report for Period August 1982 - November 1984

Approved for Public Release; Distribution Unlimited

DTIC FILE COPY

FLIGHT DYNAMICS LABORATORY  
AIR FORCE WRIGHT AERONAUTICAL LABORATORIES  
AIR FORCE SYSTEMS COMMAND  
WRIGHT-PATTERSON AIR FORCE BASE, OHIO 45433-6553

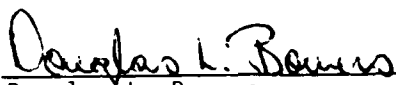
86 1 6 - 073

AD-A162 939

## NOTICE

When Government drawings, specifications, or other data are used for any purpose other than in connection with a definitely related Government procurement operation, the United States Government thereby incurs no responsibility nor any obligation whatsoever; and the fact that the government may have formulated, furnished, or in any way supplied the said drawings, specifications, or other data, is not to be regarded by implication or otherwise as in any manner licensing the holder or any other person or corporation, or conveying any rights or permission to manufacture, use, or sell any patented invention that may in any way be related thereto.

This technical report has been reviewed and is approved for publication.

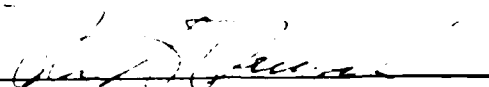


Douglas L. Bowers  
Project Engineer



TOMMY J. KENT, MAJ, USAF  
Chief, Aerodynamics and  
Airframe Branch  
Aeromechanics Division

FOR THE COMMANDER:



DONALD A. DREESBACH  
Colonel, USAF  
Chief, Aeromechanics Division  
Flight Dynamics Laboratory

"If your address has changed, if you wish to be removed from our mailing list, or if the addressee is no longer employed by your organization please notify AEWAL/FIMM, W-P AFB, OH 45433 to help maintain a current mailing list".

Copies of this report should not be returned unless return is required by security considerations, contractual obligations, or notice on a specific document.

UNCLASSIFIED

SECURITY CLASSIFICATION OF THIS PAGE

## REPORT DOCUMENTATION PAGE

1a. REPORT SECURITY CLASSIFICATION UNCLASSIFIED			1b. RESTRICTIVE MARKINGS <b>A162 939</b>			
2a. SECURITY CLASSIFICATION AUTHORITY			3. DISTRIBUTION/AVAILABILITY OF REPORT Approved for Public Release; Distribution Unlimited			
2b. DECLASSIFICATION/DOWNGRADING SCHEDULE						
4. PERFORMING ORGANIZATION REPORT NUMBER(S) AFWAL-TR-85-3055			5. MONITORING ORGANIZATION REPORT NUMBER(S)			
6a. NAME OF PERFORMING ORGANIZATION AFWAL/FIMM		6b. OFFICE SYMBOL (If applicable)		7a. NAME OF MONITORING ORGANIZATION		
6c. ADDRESS (City, State and ZIP Code) AFWAL/FIMM Wright-Patterson AFB, OH 45433-6553			7b. ADDRESS (City, State and ZIP Code)			
8a. NAME OF FUNDING/SPONSORING ORGANIZATION		8b. OFFICE SYMBOL (If applicable)		9. PROCUREMENT INSTRUMENT IDENTIFICATION NUMBER		
8c. ADDRESS (City, State and ZIP Code)			10. SOURCE OF FUNDING NOS.			
			PROGRAM ELEMENT NO.	PROJECT NO.	TASK NO.	WORK UNIT NO.
11. TITLE (Include Security Classification) THROTTLE DEPENDENT FORCES - A PRIMER			62201F	7500	70	32
12. PERSONAL AUTHOR(S) Bowers, Douglas L.						
13a. TYPE OF REPORT Final		13b. TIME COVERED FROM 82 Aug TO 84 Nov		14. DATE OF REPORT (Yr., Mo., Day) November 1985		15. PAGE COUNT 117
16. SUPPLEMENTARY NOTATION						
17. COSATI CODES			18. SUBJECT TERMS (Continue on reverse if necessary and identify by block number)			
FIELD	GROUP	SUB. GR.	Aircraft, Exhaust Nozzles, Inlets, Airbreathing Propulsion Subsonic, Transonic, Supersonic.			
01	01	00				
21	01	00				
19. ABSTRACT (Continue on reverse if necessary and identify by block number)						
<p>This report is intended to provide an introduction to the broad area of throttle dependent forces for airbreathing aircraft, primarily subsonic to supersonic capable. Basic concepts and examples are presented for subsonic, supersonic and transonic inlet and nozzle applications. Experimental and analytical determination of throttle-dependent forces is discussed, including approaches and potential problems. A final reference section of basic definitions is included for completeness.</p>						
20. DISTRIBUTION/AVAILABILITY OF ABSTRACT UNCLASSIFIED/UNLIMITED <input checked="" type="checkbox"/> SAME AS RPT. <input type="checkbox"/> DTIC USERS <input type="checkbox"/>				21. ABSTRACT SECURITY CLASSIFICATION Unclassified		
22a. NAME OF RESPONSIBLE INDIVIDUAL Douglas L. Bowers				22b. TELEPHONE NUMBER (Include Area Code) 513-255-6207		22c. OFFICE SYMBOL AFWAL/FIMM

## FOREWORD

This summary of throttle dependent forces was generated as a chapter in an AIAA Progress In Aeronautics Series book, "Turbine-Engine Airframe Integration: Prediction and Verification of Thrust and Drag." It has been updated to reflect the constructive comments of a peer review group. This document could be used well as an introductory reference text for new propulsion integration engineers or as a reference for non-propulsion engineers.

The author acknowledges the contribution to this work by Gordon Tamplin, specifically the Basic Definitions Section, and by members of the Airframe Propulsion Integration Group, specifically Donald Stava, Dennis Sedlock and Lewis Surber.

The author would be pleased to review constructive comments for future revisions.

Accession For	
NTIS CRA&I	<input checked="" type="checkbox"/>
DTIC TAB	<input type="checkbox"/>
Unannounced	<input type="checkbox"/>
Justification	
By	
Distribution /	
Availability Codes	
Dist	Avail and/or Special
A-1	



## TABLE OF CONTENTS

SECTION	PAGE
I INTRODUCTION	1
II BASIC CONCEPTS AND EXAMPLES	4
1. Supersonic/Transonic Aircraft Inlets	4
2. Supersonic/Transonic Aircraft Nozzles	6
3. Other Tactical Aircraft Throttle Dependent Forces	11
4. Examples - Supersonic/Transonic Aircraft Throttle Dependent Forces	14
5. Subsonic Aircraft Inlets/Nozzles	21
6. Examples - Subsonic Aircraft Throttle Dependent Forces	24
III DETERMINATION OF THROTTLE DEPENDENT FORCES	31
1. Experimental Techniques	31
2. Difficulties in Experimental Testing	37
3. Qualitative Techniques to Assess Throttle-Dependent Forces	51
4. Analytical Techniques	51
5. Inlet Analytical Techniques	52
6. Afterbody/Nozzle Analytical Techniques	55
7. Transport Nacelle Analytical Techniques	60
IV WIND TUNNEL/ANALYSIS DETERMINATION OF THROTTLE-DEPENDENT FORCES IN FLIGHT	68
1. Sources of Error-Wind Tunnel/Analysis to Flight	68
2. Wind Tunnel/Analysis to Flight Correlation - Examples	70
V FINAL REMARKS	94
REFERENCES	95
BASIC DEFINITIONS	98

## LIST OF ILLUSTRATIONS

FIGURE		PAGE
1	Typical Installed Propulsion System Performance (Reference 2)	2
2	Required Variation of Nozzle Geometry (Reference 3)	2
3	Typical Subsonic Spillage Drag Curves (Reference 4)	3
4	Inlet/Engine Flow Matching for a Supersonic Cruise Sizing Point (Reference 5)	5
5	Inlet Spillage Flow Schematic (Reference 6)	5
6	Spillage Drag (Reference 4)	7
7	Tradeoff of Spillage and Bypass Drag (Reference 6)	7
8	Nozzle Internal Performance Map (Reference 5)	9
9	Variable Geometry Nozzle	9
10	Aft End Drag Map (Reference 5)	10
11	Jet Interference (Reference 3)	10
12	Effect of Base Size on Boattail-, Base-, and Total Pressure Drag (Reference 3)	12
13	Inlet/Nozzle Throttle Dependent Forces (Reference 7)	12
14	Jet Efflux on Tail Normal Force (Reference 3)	13
15	Chordwise Pressure Distributions - Thrust Vectoring; 45° Primary Nozzle (Reference 8)	13
16	F-15 Three-view Drawing (Reference 9)	15
17	Inlet Longitudinal Control Effectiveness (Reference 10)	15
18	General Terms for Pressure-Integrated Inlet Drags and Inlet Capture Ratios (Reference 9)	16
19	Typical Pressure Integrated Inlet Drag Components from F-15 Flight Data (Reference 11)	17
20	Comparison of Inlet and Aircraft Drag Data, $M_0 = 0.9$ $\alpha = 0^\circ$ (Reference 12)	17
21	Nozzle Surface Pressure Instrumentation and Boattail Drag Coefficient versus Mach Number (Reference 11)	18

## LIST OF ILLUSTRATIONS (Cont'd)

FIGURE		PAGE
22	XB-70 Inlet Bypass and Boundary Layer Bleed Exits (Reference 13)	19
23	Variation in Measured Inlet Bypass and Bleed Drag with Mach Number for Typical In Flight Condition for the XB-70 Airplane (Reference 13)	19
24	Effect of Bypass Operation on Aircraft Stability (Reference 6)	20
25	Changes in Drag with Engine Power Lever Angle (Reference 13)	20
26	Major Elements of Wing/Pylon/Nacelle Flow Field (Reference 14)	22
27	Boeing Advanced Medium STOL Transport (Reference 15)	22
28	Definition of Inlet Capture Area, $A_i$ , and Characterization of Flow Incidence Approaching Inlet via Mass Flows Ratio $A_o/A_i$ (Reference 5)	23
29	A300R Nacelle (Reference 16)	25
30	Pressure Distribution on Wing, Pylon, Core Engine, and Fan Cowl (Reference 16)	26
31	$\Delta C_{D_{pjet}}$ versus $\alpha$ for Wing, Pylon, Fan and Core Engine Cowl (Reference 16)	27
32	OSRA Design and Configuration Data (Reference 17)	27
33	Upper Surface Blowing Aerodynamics (Reference 17)	28
34	AGM-109 Three View Drawing (Reference 18)	29
35	Subcritical Inlet Spillage Drag Variation with Inlet Mass Flow Ratio (Reference 18)	29
36	Noattail-base Drag Variation with Nozzle Pressure Ratio (Reference 18)	30
37	Projection of Full Scale Aircraft Performance (Reference 7)	32
38	Inlet Model Balance Arrangement (Reference 9)	34
39	Jet Effects Model Support Systems (Reference 7)	35
40	Transport Testing Techniques (Reference 19)	36
41	Current Engine Simulation Techniques for Wind Tunnel Testing (Reference 21)	38
42	Types of Nacelle Simulators (Reference 23)	40
43	Principles of Jet Engine Simulation in Wind Tunnels (Reference 24)	41

## LIST OF ILLUSTRATIONS (Cont'd)

FIGURE		PAGE
44	Concept of Annular-jet Plume Simulation with Sting Support of a Jet Effects Model (Reference 22)	42
45	Inlet Fairing Effects on Afterbody Drag (Reference 7)	44
46	Examples of Wind Tunnel Model Mounting Techniques (Reference 5)	45
47	Jet Effects Model Support Options (Reference 1)	45
48	Typical Afterbody Test Rig with Subdivided Boattail (Reference 23)	46
49	Force Balance Nacelle Configuration (Reference 25)	48
50	Nacelle Axial-Force Components (Reference 25)	49
51	Effect of Nozzle Position on Pressure Distribution (Reference 27)	50
52	Inlet Drag Correlations (Reference 29)	53
53	Theoretical Peak Velocities on Lips of a 2-Dimensional Staggered Intake (Reference 31)	54
54	Predicted Twin-Jet Nozzle Pressure Distributions (Reference 29)	54
55	Inlet Flow Field Correlation for Side-Mounted Inlet: $M = 2.5$ , $\alpha = 15^\circ$ (Reference 32)	56
56	Static Pressures on Inlet Ramp and Cowl (Reference 30)	56
57	Schematic of Nozzle Afterbody Flow (Reference 33)	57
58	IMS Data Correlation (Reference 7)	59
59	Analytical Prediction of Nacelle Boattail Pressures (Reference 5)	59
60	Comparison of Predictions of Patched Method with Experiment (Reference 33)	59
61	Navier-Stokes Solution by Swanson for Circular Arc Boattail Nozzles with Solid Plume Simulators (Reference 33)	61
62	Comparison of Calculated and Measured Internal Surface Pressure Distributions (Reference 5)	61
63	Transonic Cowl Pressure Comparison of Analysis and Test (Reference 5)	62
64	Comparison of Analytical vs. Measured Pressures for Installed Powered Nacelle (Reference 5)	62



## LIST OF ILLUSTRATIONS (Cont'd)

FIGURE		PAGE
65	Wing Pressures at Engine Position (Reference 40)	64
66	Pressure Distribution at an Axisymmetric Inlet NACA 1-85-100 (Reference 37)	64
67	Comparison of Surface Pressure Coefficient $M_\infty = 0.79$ , $MFR = 0.69$ , $\alpha = 3.06$ (Reference 38)	65
68	Calculated Mach Contours for Inlet at Angle of Attack (Reference 38)	65
69	Navier-Stokes Solution of Peery and Forester (Reference 41)	66
70	X-15 Fuselage Base Pressure Coefficients (Reference 43)	69
71	Comparison of Flight-Measured XB-70 Average Base Pressure Coefficient with Predicted Values (Reference 43)	69
72	Sources of Error in Throttle Dependent Drag Predictions (Reference 46)	71
73	B-1 Nacelle Instrumented Regions (Reference 47)	73
74	Inlet Surface Pressure Instrumentation Common to the Wind Tunnel Models and Aircraft (Reference 47)	73
75	Aircraft and Model Inlet Cowl Pressures (Reference 47)	74
76	Drag Coefficient Variation with Mass Flow Ratio (Reference 47)	75
77	Aft Nacelle Isometric Showing Measurement Locations (Reference 48)	76
78	Aft Nacelle Drag - Model and Aircraft (Reference 47)	77
79	MFR Effect on Aft Nacelle/Nozzle Drag (Reference 48)	78
80	Model Installations (Reference 48)	78
81	Sting Effects (Nozzle/Afterbody Tests) (Reference 48)	80
82	F-15 Inlet Pressure Orifices (Reference 49)	81
83	Comparison of Flight and Wind Tunnel Pressure Coefficients for Upper Cowl Surface (Reference 9)	82
84	Effect of Capture Area Ratio on Wing Fairing Pressure Coefficients (Reference 49)	83

## LIST OF ILLUSTRATIONS (Concluded)

FIGURE		PAGE
85	Comparison of Wind Tunnel and Flight Pressure-Integrated Drag (Reference 9)	84
86	F-15 Nozzle Pressure Orifices (Reference 50)	85
87	Upper Fuselage Pressure Coefficient (Reference 49)	86
88	Pressure Orifice Locations-Left Engine Nacelle and Nozzle (Reference 51)	88
89	Support System Interference Models and YF-17 Aircraft (Reference 51)	88
90	Surface Pressure Distributions-Cruise Nozzle Configuration (Reference 51)	89
91	Surface Pressure Distribution Reheat Nozzle Configuration (Reference 51)	90
92	Tornado Prototype Afterbody (Reference 52)	91
93	Tornado Afterbody Model (Reference 52)	91
94	Boattail Surface Static Pressure Distributions (Reference 52)	92
95	Comparison of In-Flight and Wind Tunnel Base Pressures (Reference 52)	93

## LIST OF SYMBOLS

$A_c, A_i$	inlet capture area
$A_e$	nozzle exit area
$A_{max}, A_{10}$	afterbody maximum cross-sectional area
$A_o/A_i, A_o/A_c$	inlet capture area ratio
$A_t$	nozzle throat area
$A_{th}$	inlet throat thickness-subsonic cowl
$A_8$	nozzle throat area
$A_9$	nozzle exit area
$C_D$	drag coefficient
$C_{DIP}, C_D, p$	pressure integrated drag
$C_{D_{SPILL}}$	spillage drag
$C_L$	lift coefficient
$\bar{C}$	centerline
$C_{m_{\delta I}}$	pitching moment rate of change with inlet ramp deflection
$C_N$	normal force coefficient
$C_p$	pressure coefficient
$C_T$	thrust coefficient
$d_B$	nozzle base diameter
$D_e, D_{eq}$	diameter of circle of equivalent cross-sectional area
ECS	environmental control system
IMS	integral mean slope
MFR, $m/m_o$	inlet mass flow ratio
$M_o, M_\infty$	Mach number
NPR	nozzle pressure ratio, $P_{T_j}/P_\infty$

## LIST OF SYMBOLS (Concluded)

$NS$	nacelle station
$P_0, P_\infty$	freestream static pressure
$P_{Tj}$	nozzle total pressure
$P_\omega$	windward inlet surface pressure
OSRA	Quiet Short Haul Research Aircraft
$S$	stagnation point
$S_F$	fuselage cross-sectional area
SFC	specific fuel consumption
STOL	short takeoff and landing
$V_0$	freestream velocity
$\beta$	sideslip/yaw angle
$\eta$	span location referenced to wing halfspan
$\rho$	inlet cowl rotation angle

## SECTION I

## INTRODUCTION

Aircraft propulsion systems are sized to satisfy critical mission points, such as subsonic cruise or high altitude takeoff for transports and maximum acceleration or high altitude dash for tactical aircraft. This sizing determines the flow areas required and the extent of variable geometry to be incorporated in the inlet and nozzle. Any time the aircraft flies at other than these design points, the propulsion system is operating in an off-design condition with resultant performance penalties. Throttle dependent forces are a result of changes in engine power setting and the subsequent inlet and nozzle geometry and flow variations. The issue of throttle dependent forces becomes more critical as aircraft are required to operate over wider Mach number ranges, as is the case for tactical aircraft, or to finer performance tolerances, as is the case for transports.

For tactical aircraft, Reference 1 points out that increasing the maximum design Mach number leads to larger inlet capture areas and therefore greater off-design losses when operating at subsonic cruise Mach numbers. In addition, the required nozzle area is increased, producing large drag penalties as a result of high nozzle boattail angles at reduced Mach numbers. Two examples of inlet/nozzle area variability for a Mach 2.5 tactical aircraft are shown in Figures 1 and 2. For this aircraft's mission, the engine airflow requirement can range from 60 to 100 percent of that air which can be brought into the propulsion system. When operating at capture area ratios that are substantially less than 1.0, the penalty from spilled excess air can be substantial. The nozzle area variation, as a function of Mach number and engine flow, is shown in Figure 2. For efficient internal performance across the aircraft mission profile, the nozzle exit to throat area ratio must vary from 1.0 to 2.6. The associated external geometry variations can result in drag penalties during subsonic cruise. The combined impact (inlet and nozzle flow and geometry) of these penalties on specific fuel consumption (pounds of fuel per pound of thrust per hour...obviously the smaller the better) for a Mach 2.5 aircraft at Mach 0.9 cruise can be large.

Although not required to operate over the wide Mach number range required for tactical aircraft, the subsonic transport is driven by a requirement for finely

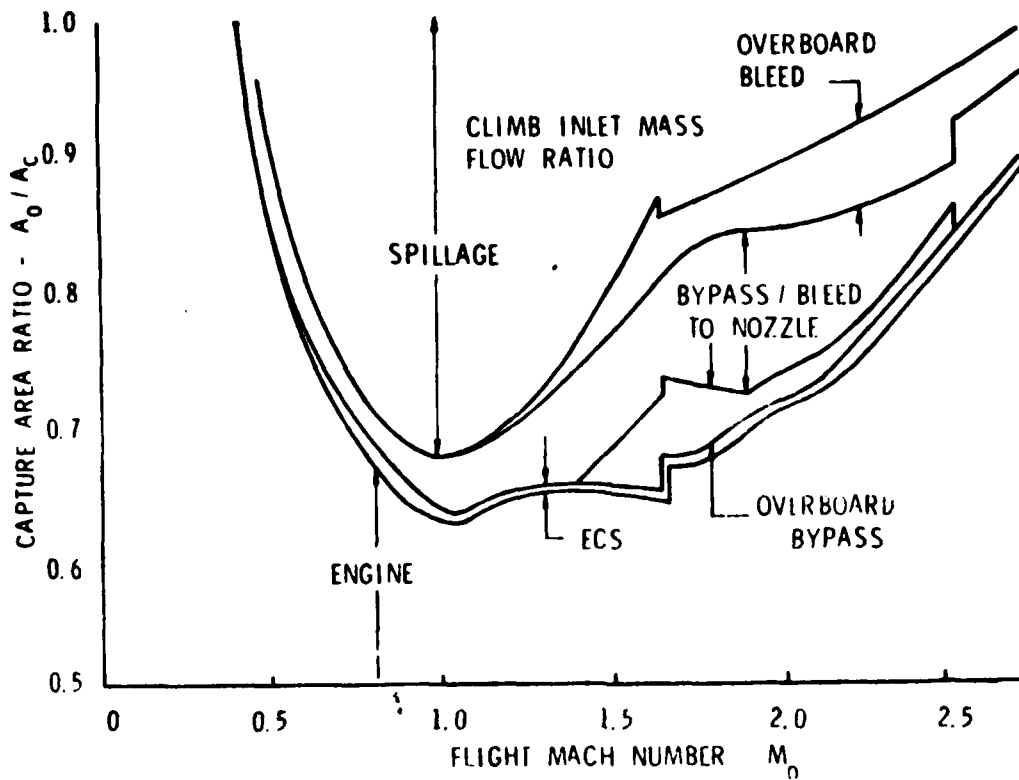


Figure 1. Typical Installed Propulsion System Performance (Reference 2)

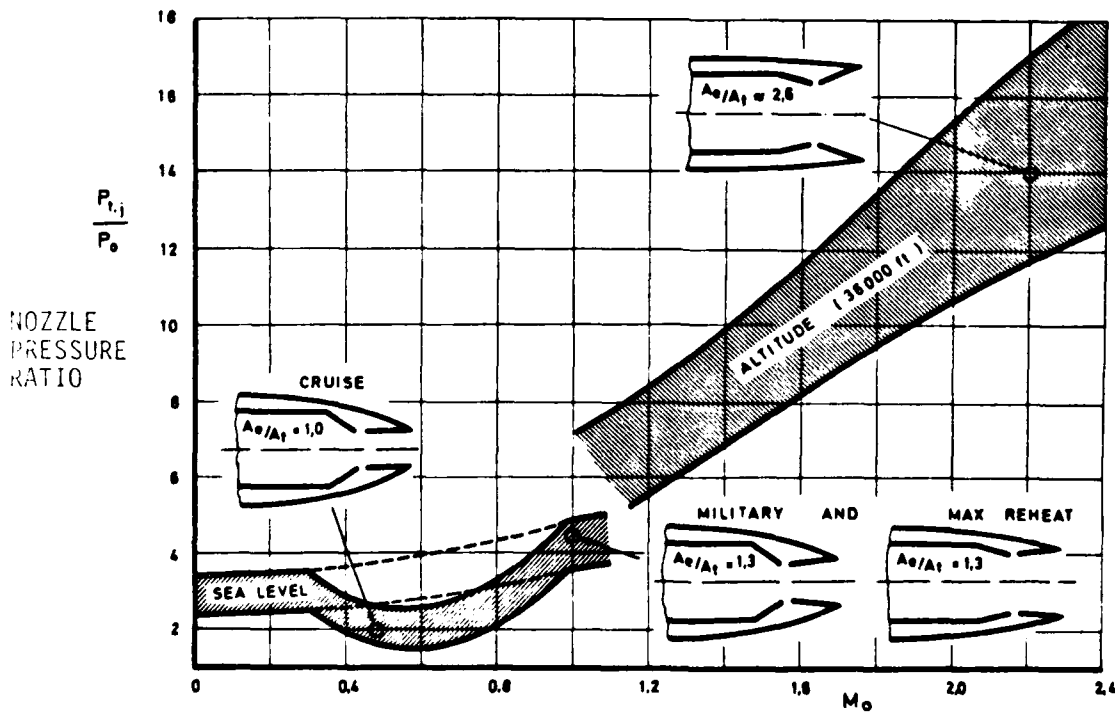


Figure 2. Required Variation of Nozzle Geometry (Reference 3)

tuned performance. The subsonic inlet is sized for cruise altitude and Mach number and generally carries no variable geometry other than blow-in doors for additional inlet area at takeoff. For this class of installation, correct determination of throttle dependent forces is necessary to guarantee the minimum required installed engine performance crucial to the air transport industry. The relative values of spillage drag for a supersonic inlet versus a subsonic inlet are shown in Figure 3.

The importance attributed to throttle dependent forces, for both tactical and subsonic transport aircraft, is demonstrated by the many past and ongoing efforts to determine their consequence across the flight regime. To aid in the understanding of this critical area, this report will provide basic definitions, examples at various flight points, and an examination of techniques for determining these forces.

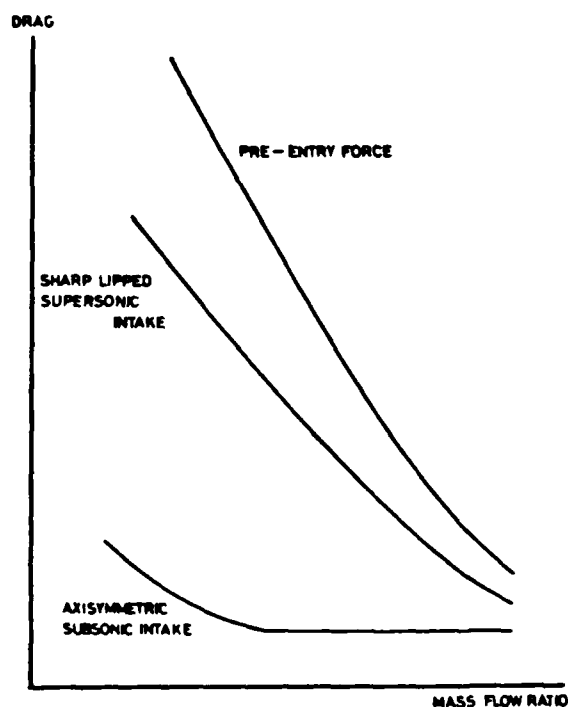


Figure 3. Typical Subsonic Spillage Drag Curves (Reference 4)

## SECTION II

## BASIC CONCEPTS AND EXAMPLES

Throttle dependent forces include all internal and external forces acting on the aircraft that are produced when the engine power setting is changed. These forces are not only the forces on the engine streamtube but also the external forces on the aircraft related to the inlet and nozzle flow fields. A complete set of basic definitions relevant to throttle dependent forces are included at the end of this report. This section will present concepts and examples relating to primary inlet and nozzle throttle dependent forces.

## 1. SUPERSONIC/TRANSONIC AIRCRAFT INLETS

An aircraft inlet captures freestream air and reduces its velocity so the engine can process it in a stable and efficient manner. In order to minimize compressor work, inlet diffusion should be accomplished with a minimum of total pressure loss. The inlet should also deliver the working fluid with minimum distortion, all over a wide range of Mach number, angle-of-attack, angle-of-sideslip, and engine demand. The supersonic inlet for a tactical aircraft must also be sized to provide a maximum demand airflow which usually occurs at maneuver or acceleration conditions. When the aircraft is at a subsonic cruise condition, however, the engine needs to process only a limited mass flow associated with 40-60 percent maximum dry thrust. The inlet, however, is still capable of processing larger mass flow closer to maximum demand. Figure 4 illustrates the excess airflow the inlet provides at flight conditions below the Mach 3.0 design condition. The forces resulting from handling this excess air are referred to as spillage drag and bypass drag. The general flow conditions for a supersonic inlet are shown in Figure 5.

Spillage drag is the result of the inlet operating on freestream air beyond that demanded by the engine and consists of additive drag and lip suction components. Additive drag (also referred to as pre-entry drag) is a calculated force used in thrust-drag bookkeeping procedures and is the loss in momentum from the freestream to the inlet entrance of the flow influenced by the inlet capture area,  $A_c$ . For a Mach 3.0 cruise aircraft, the additive drag can be as much as 20 percent of the total drag at subsonic cruise point (Reference 6). Lip suction, sometimes



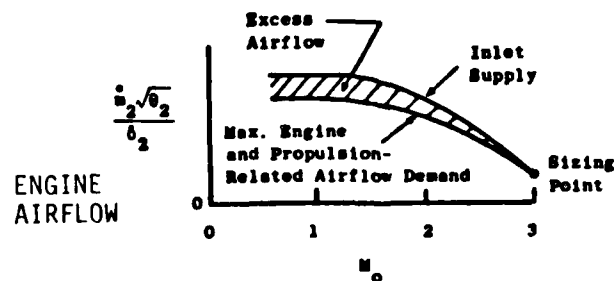


Figure 4. Inlet/Engine Flow Matching for a Supersonic Cruise Sizing Point (Reference 5)

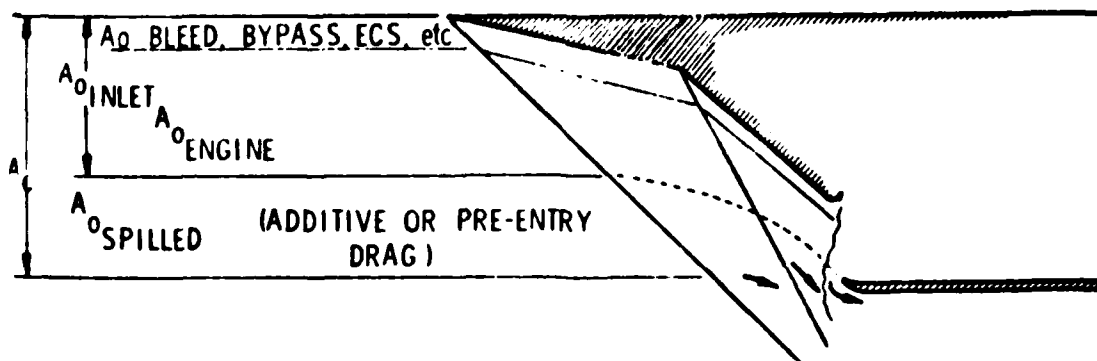


Figure 5. Inlet Spillage Flow Schematic (Reference 6)

referred to as cowl drag or cowl suction, is the result of the spilled inlet airflow moving along the external inlet cowl surface. This term may be a positive or negative (usually) axial force depending on the flow characteristics and surface contours. Spillage drag is the sum of additive drag and lip suction and is a function of inlet mass flow (or throttle setting). Generally, the spillage drag decreases as engine demand mass flow increases (Figure 6).

A portion of the air taken into the inlet may not be used to produce engine thrust. This excess airflow, or bypass air, is brought on board the aircraft, worked by the inlet compression system and then dumped overboard upstream of the engine face through doors or slots or routed to the nozzle. This results in a force due to the loss in momentum in the flight direction between freestream and the door or slot exit conditions and the change in local forces on external surfaces influenced by the bypassed air. As will be seen in the examples, this bypass flow can affect not only lift and drag, but also aircraft stability and control. The bypass drag and spillage drag are related and can be traded off against each other. Both are a function of inlet mass flow (Figure 7) and are counted as a part of the inlet drag. Advanced technology engines such as the variable cycle engine or high airflow engine may reduce spillage and bypass drag by keeping engine airflow demand high over all operating conditions. Engine weight, size, and complexity, however, must be traded against reduced inlet throttle dependent forces.

The control of the shock wave position and prevention of shock induced flow separation in the inlet can be accomplished by bleeding boundary air from the inlet ramps, cowls, or sidewalls and dumping that flow overboard. This produces forces similar to the bypass flow which must be considered in supersonic inlet throttle dependent forces.

## 2. SUPERSONIC/TRANSONIC AIRCRAFT NOZZLES

Traditionally, the nozzle has functioned as an engine control valve and as a device to accelerate the engine flow, converting the thermal energy of the engine flow to jet kinetic energy. For these processes to be efficient, geometry should be variable. The forces related to throttle position changes are gross thrust (internal) and external nozzle boattail and base drag. Another related throttle dependent force is jet interference, the aerodynamic interaction of the exhaust

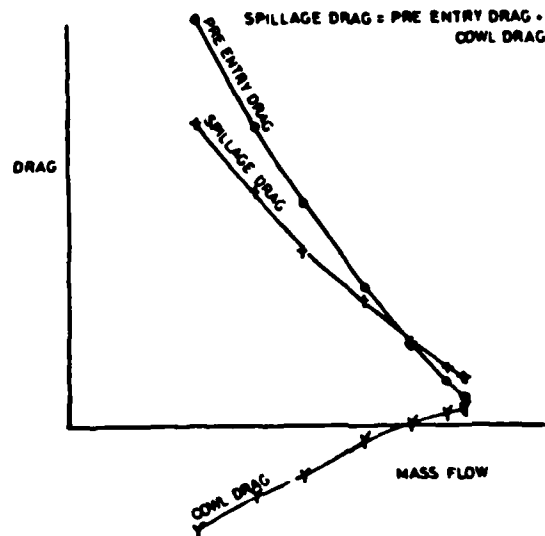


Figure 6. Spillage Drag (Reference 4)

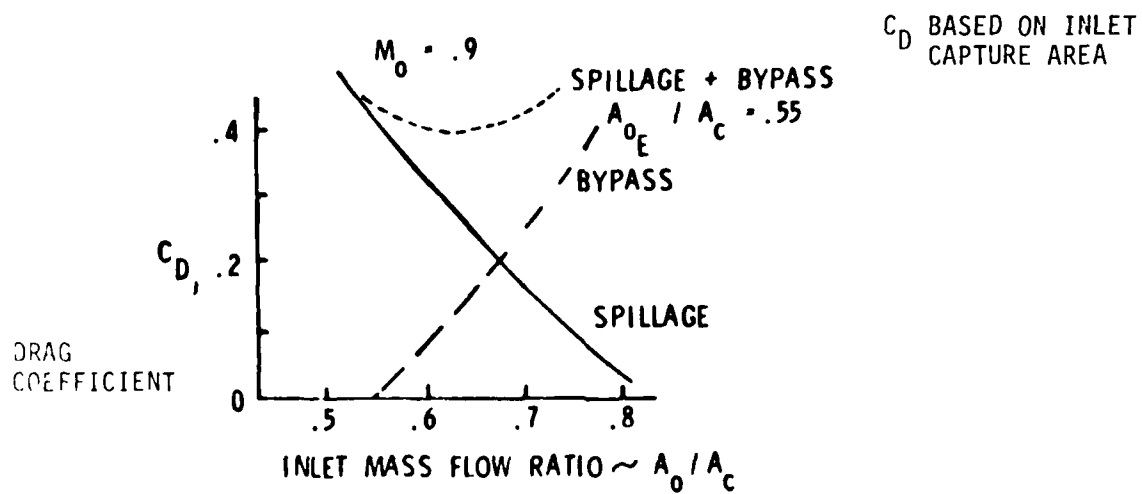


Figure 7. Tradenoff of Spillage and Bypass Drag (Reference 6)

plume with nearby aircraft surfaces. Nozzle pressure ratio is a parameter which relates freestream Mach number and engine airflow at the nozzle throat (especially at afterburning power and above) and is dependent on engine airflow in much the same way as mass flow ratio relates inlet performance to engine airflow. It is defined as the ratio of the total pressure at the nozzle throat to the freestream static pressure.

Typical nozzle internal performance, as a function of nozzle pressure ratio and nozzle area ratio, is shown in Figure 8. No one area ratio provides optimum thrust across the nozzle pressure ratio range. This leads to variable area nozzles and the geometry changes which create external throttle dependent forces. Representative variable geometry nozzle changes are shown in Figure 9. Note the area ratio ( $A_9/A_8$ ) and boattail angle changes at the three power settings. Typical external drag coefficients as a function of nozzle exit area are shown in Figure 10. With the maximum external cross sectional area ( $A_{10}$ ) fixed, the changing exit area ( $A_9$ ) results in external geometry changes and drag variations across the Mach number spectrum. Also as nozzle airflow and exit pressure vary, the plume shape and its influence changes the afterbody drag. Figure 11 illustrates the influence of the plume at subsonic and supersonic freestream conditions. In subsonic flow, the plume turns and entrains the external flow, producing a strong upstream influence. In supersonic freestream flow, the typical plume becomes "solid" and produces a shock system which can impact adjacent aircraft surfaces. In addition, even in supersonic flow, the jet exhaust can influence the external nozzle forces for a short distance upstream through the subsonic boundary layer. Boattail drag results from external air flowing over the afterbody and producing a nonpotential flow pressure distribution. This flow is affected by boundary layer displacement on the boattail surface which can be large due to an adverse pressure gradient at the nozzle/plume junction. In the extreme case, a large boattail angle or a strong shock at the nozzle plume junction can result in flow separation and increased drag.

The base drag of the nozzle is dependent on the nozzle pressure ratio. For small base areas, increasing nozzle pressure ratio pressurizes the base area and decreases drag. Larger base areas may result in increased drag, due to steeper turning angles at the boattail plume junction. A typical functional relationship

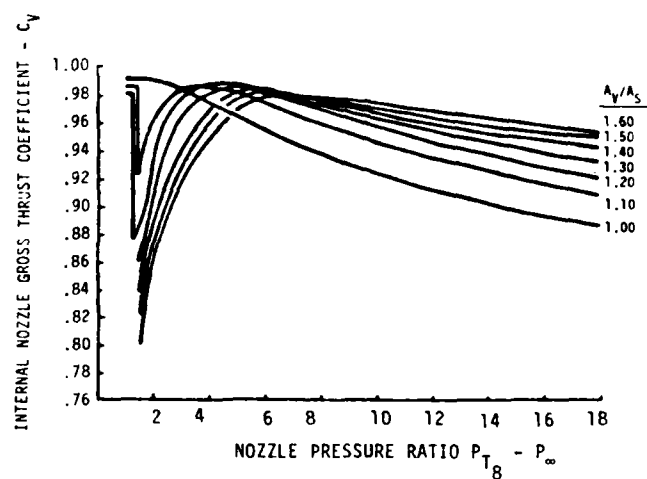


Figure 8. Nozzle Internal Performance Map (Reference 5)

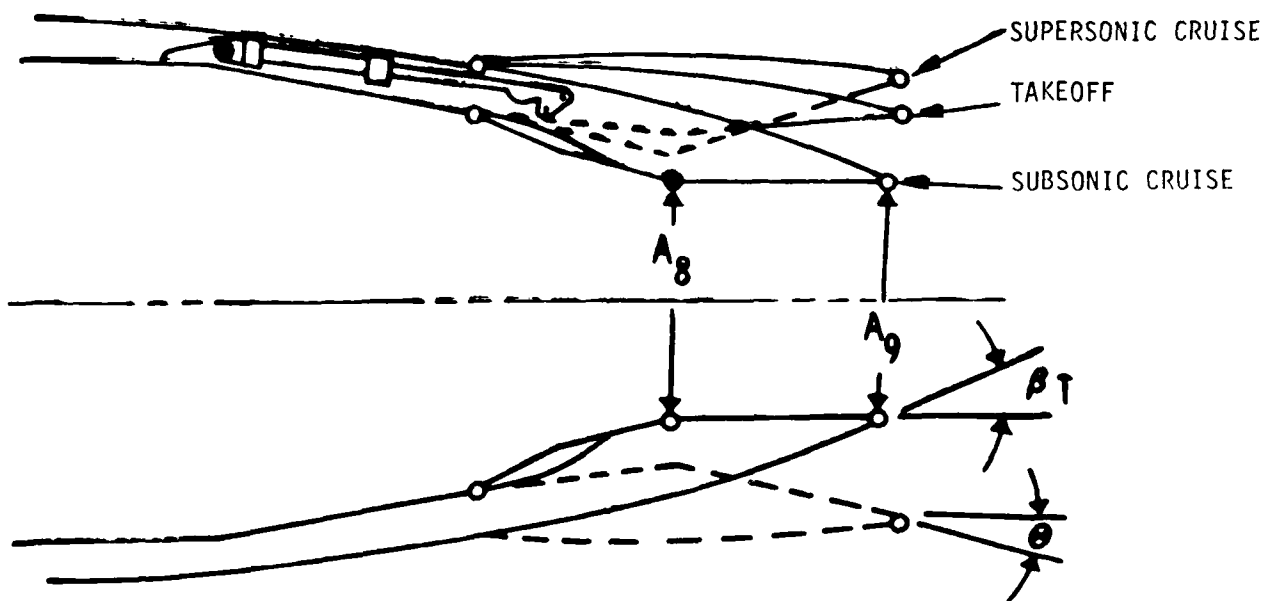


Figure 9. Variable Geometry Nozzle

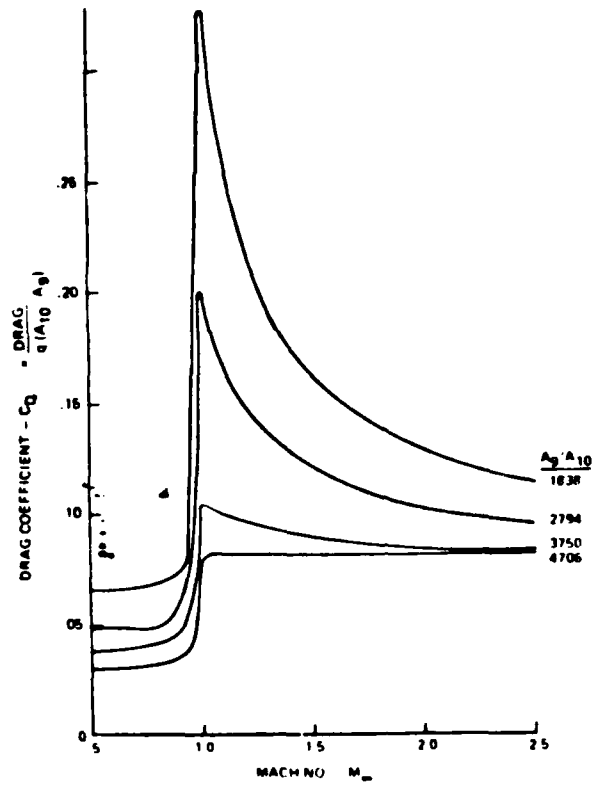


Figure 10. Aft End Drag Map (Reference 5)

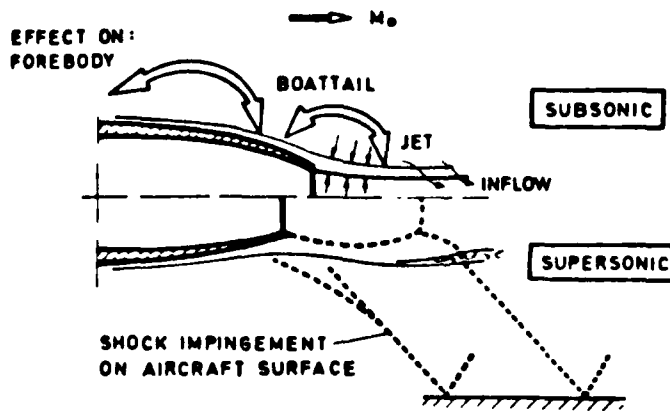


Figure 11. Jet Interference (Reference 3)

between base area and base, boattail, and total afterbody drag is shown in Figure 12. It should be noted that most modern aircraft have extremely small base areas.

A summary of the primary throttle dependent forces for supersonic/transonic aircraft is presented in Figure 13. Inlet capture area and nozzle exit areas become larger as the maximum Mach number, which usually sizes the propulsion system, is increased. Thus inlet spillage drag and afterbody drag become strong factors during off design operation, especially during the subsonic cruise mission leg.

### 3. OTHER TACTICAL AIRCRAFT THROTTLE DEPENDENT FORCES

Other related throttle dependent considerations are inlet total pressure distortion and pressure recovery, tail interference and jet-induced effects.

One measure of the quality of the flow that the inlet provides to the engine face is the total pressure distortion. This phenomenon is always present in some degree but is not a factor unless the engine surges and there is a loss of thrust. Inlet pressure recovery, the measure of total pressure loss of the inlet streamtube from freestream to the engine face, is not a direct throttle dependent force, but is directly related to changing engine mass flow or inlet geometry.

Any aircraft surface near the jet plume can be influenced by throttle position. An example of the change in normal force on a horizontal tail, as a function of angle-of-attack and jet on/off, is presented in Figure 14. The high tail shows no jet influence, while the low tail is strongly influenced by the presence of the jet.

Further indirect throttle dependent forces can result from lift and moments generated on inlet and nozzle surfaces and from induced lift and moments on adjacent aircraft lifting surfaces. If trim changes are required to balance these forces, a throttle dependent trim drag will occur. A graphical presentation of the change in pressure distribution on a wing with close coupled jet plume is shown in Figure 15. This change in pressure distribution produces an increment of total aircraft lift, drag, and pitching moment which is dependent on engine throttle setting. This influence is well documented and advanced aircraft are currently being configured to take advantage of this effect.

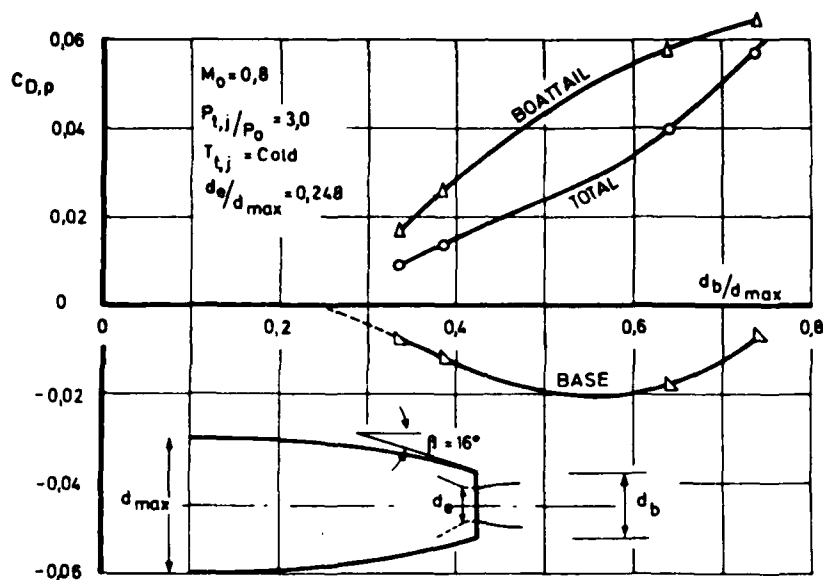


Figure 12. Effect of Base Size on Boattail-, Base-, and Total Pressure Drag (Reference 3)

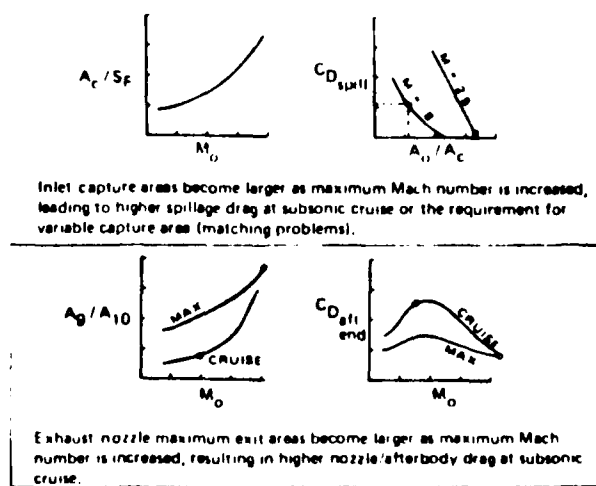


Figure 13. Inlet/Nozzle Throttle Dependent Forces (Reference 7)



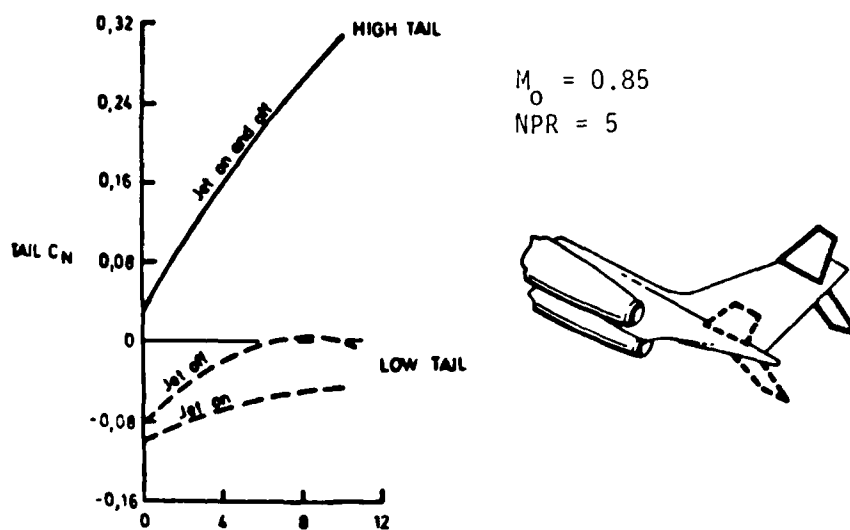


Figure 14. Jet Efflux on Tail Normal Force (Reference 3)

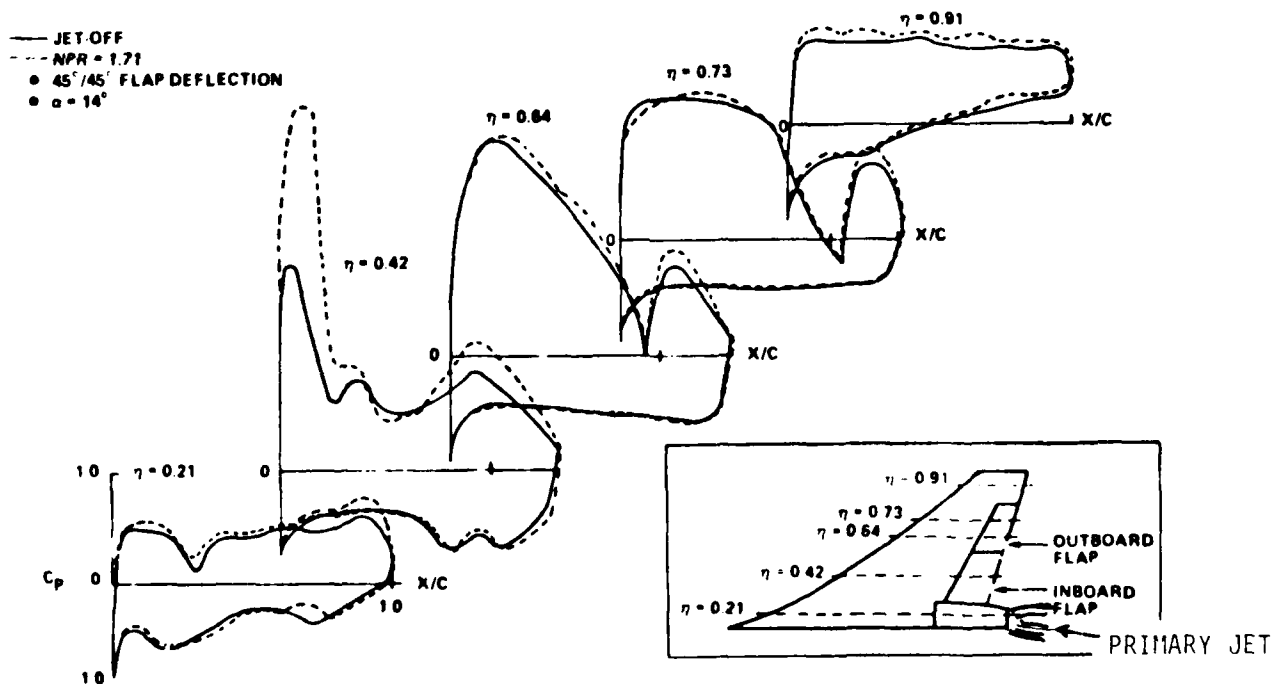


Figure 15. Chordwise Pressure Distributions - Thrust Vectoring; 45° Primary Nozzle (Reference 8)

#### 4. EXAMPLES - SUPERSONIC/TRANSONIC AIRCRAFT THROTTLE DEPENDENT FORCES

##### F-15

The F-15 aircraft, shown in Figure 16, has variable inlets and exhaust nozzles and offers good examples of throttle dependent forces. The inlet (Figure 17) has a variable second and third ramp and variable capture area achieved by rotating the inlet about a transverse hinge point at the lower cowl lip. This rotating inlet, which is well forward of the center-of-gravity, has a significant effect on aircraft longitudinal stability and control across the subsonic/transonic Mach number spectrum of the F-15. Other components of throttle dependent forces, spillage drag and bleed/bypass drag are illustrated in Figure 18. The resulting forces and their contribution to the total inlet drag as a function of inlet capture ratio is presented in Figure 19. Note, as discussed earlier, the cowl drag partially offsets the additive drag. A wind tunnel model with independent inlet and airframe force balances provided an indication of the effect of varying inlet mass flow on separate inlet and aircraft forces. When comparing these forces (Figure 20) a favorable interaction is evident above an inlet capture area ratio of 0.5 as the inlet drag is increasing as the aircraft drag is decreasing. This interaction was identified by surface pressures to be at least partially the result of flow over the boundary layer diverter and gun fairing surfaces. The F-15 nozzle, required to pass engine airflows for flight up to 2.5 Mach number and efficiently produce thrust, can have boattail angles ranging from 8 to 18 degrees. The resulting nozzle drag variation (Figure 21) across the flight regime can be from 2 to 44 drag counts as boattail angle increases.

##### XB-70

For large supersonic/transonic aircraft with high airflow propulsion systems, the throttle dependent forces are reflected in total drag and aircraft stability and control. The XB-70, with 6 engines, dumped bleed and bypass flow at various locations around the aircraft (Figure 22). As a result, the percent of total airplane drag attributed to these flows is as much as 10 percent in supersonic flight (Figure 23). The bypass operation also affected aircraft stability and control illustrated in Figure 24. It is seen that rolling moment and pitching moment were strong functions of bypass door opening. The overall aircraft drag change with power lever angle at two Mach numbers is shown in Figure 25. While this

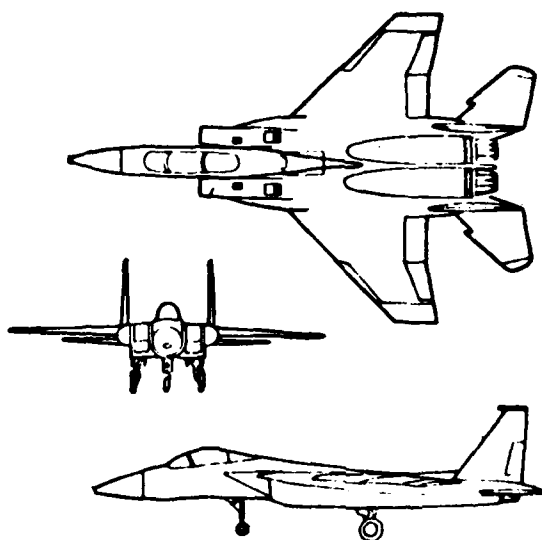


Figure 16. F-15 Three-view Drawing (Reference 9)

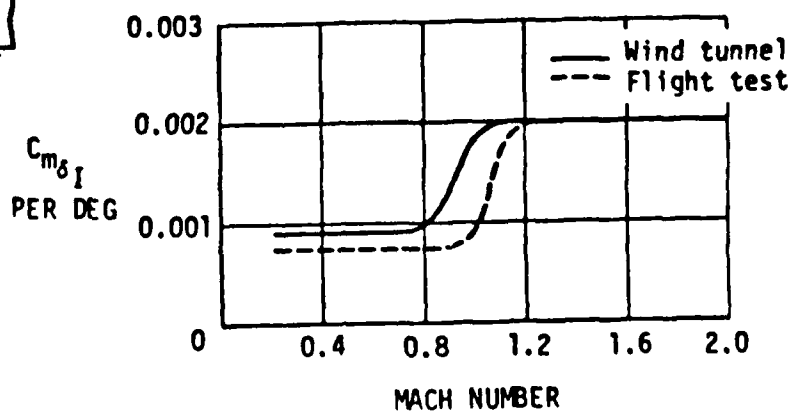
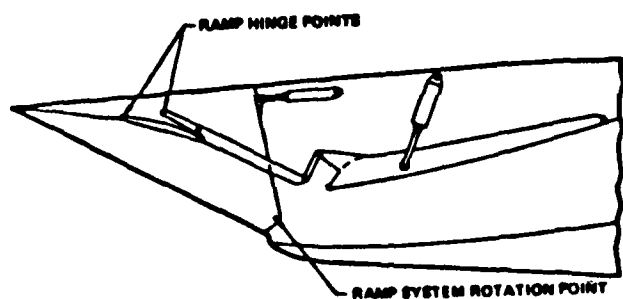
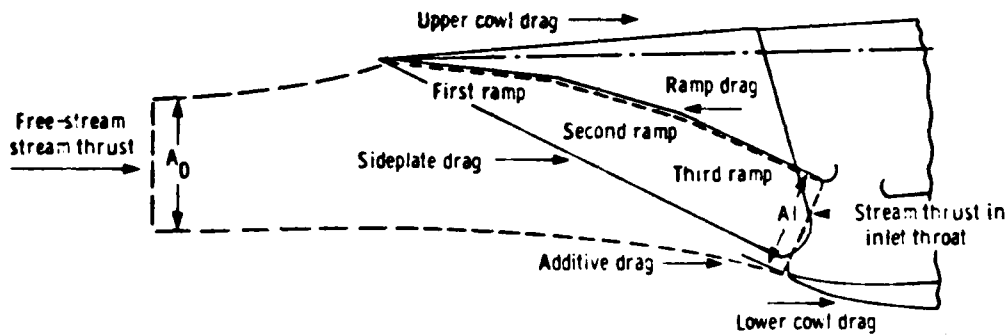


Figure 17. Inlet Longitudinal Control Effectiveness (Reference 10)

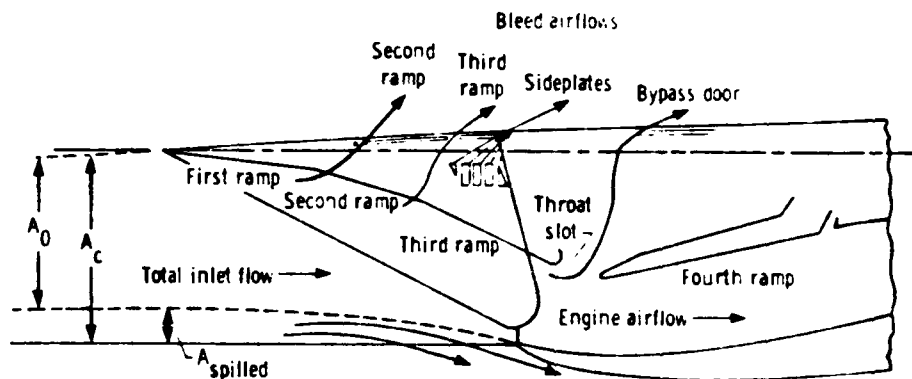


$$\text{Inlet drag} = \text{Additive drag} + \text{Upper cowl drag} + \text{Lower cowl drag} + \text{Sideplate drag}$$

where

$$\text{Additive drag} = \text{Drag on three ramps} + \text{Stream thrust in inlet throat} - \text{Free-stream stream thrust}$$

(a) Relationships used in the calculation of pressure integrated inlet drag



$$A_0 = \sum (\text{Bleed airflows}) + \text{Engine airflow}$$

(b) Diagram showing sum of inlet captured stream tube area ( $A_0$ ) and geometric capture area ( $A_c$ ).

Figure 18. General Terms for Pressure-Integrated Inlet Drags and Inlet Capture Ratios (Reference 9)

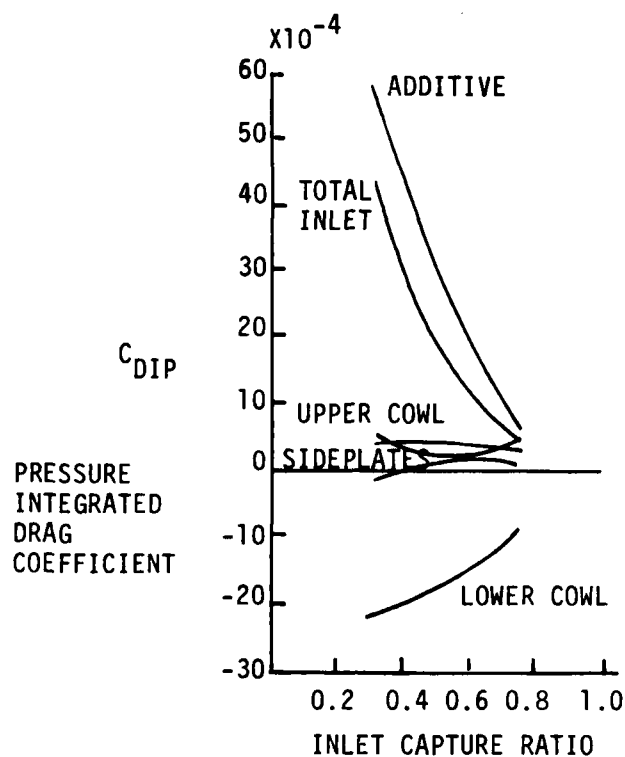


Figure 19. Typical Pressure Integrated Inlet Drag Components from F-15 Flight Data (Reference 11)

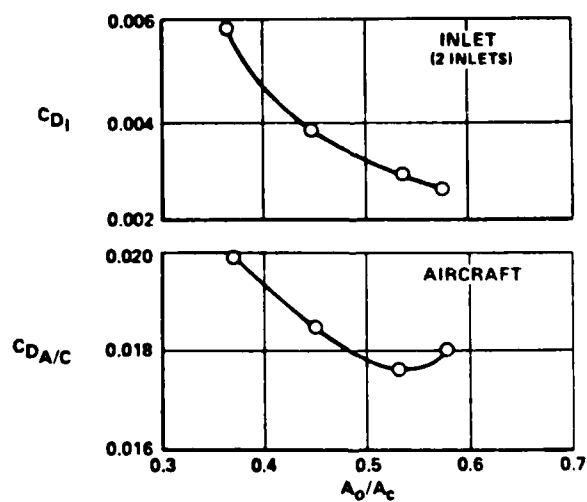


Figure 20. Comparison of Inlet and Aircraft Drag Data,  $M_0 = 0.9$   $\alpha = 0^\circ$  (Reference 12)

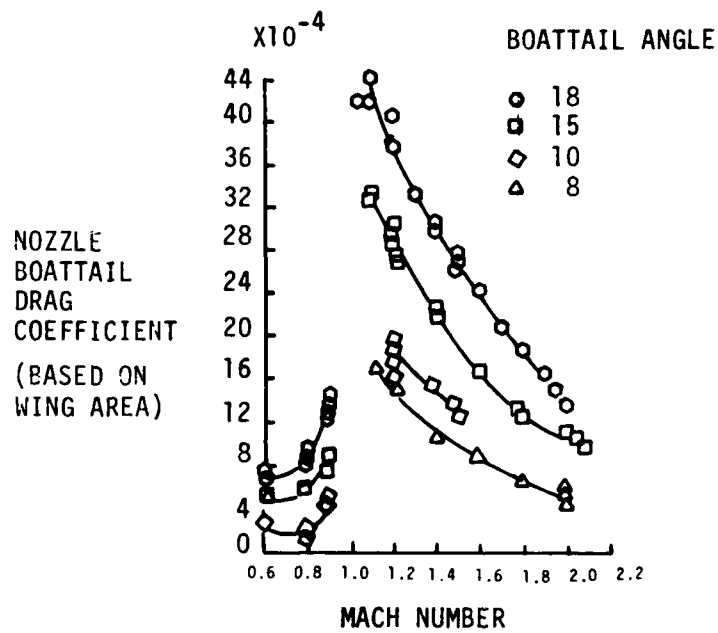


Figure 21. Nozzle Surface Pressure Instrumentation and Boattail Drag Coefficient versus Mach Number (Reference 11)

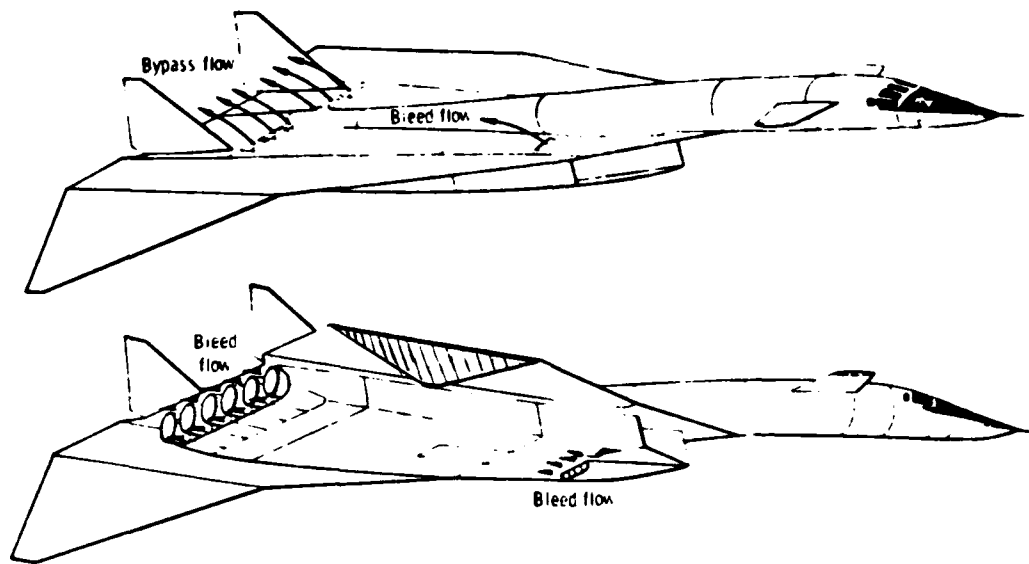


Figure 22. XB-70 Inlet Bypass and Boundary Layer Bleed Exits (Reference 13)

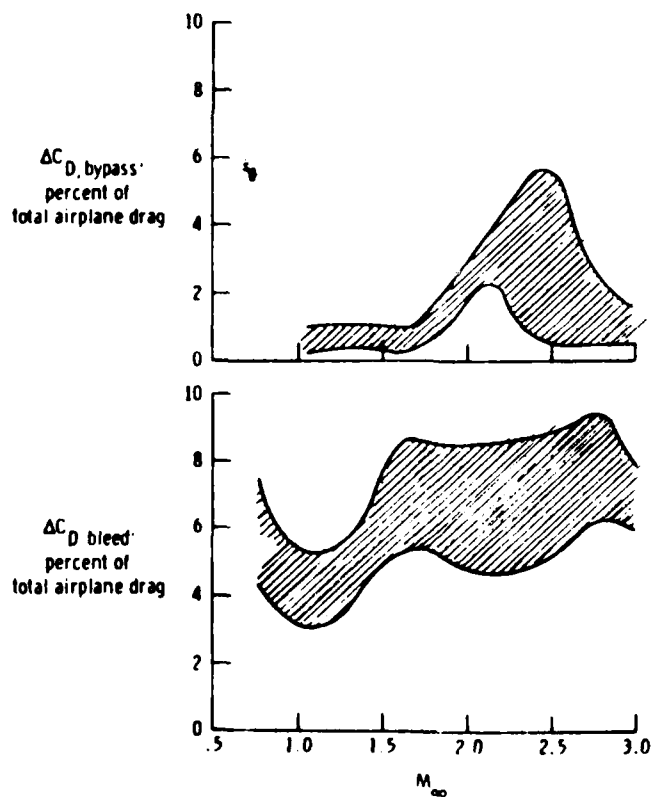


Figure 23. Variation in Measured Inlet Bypass and Bleed Drag with Mach Number for Typical 1g Flight Condition for the XB-70 Airplane (Reference 13)

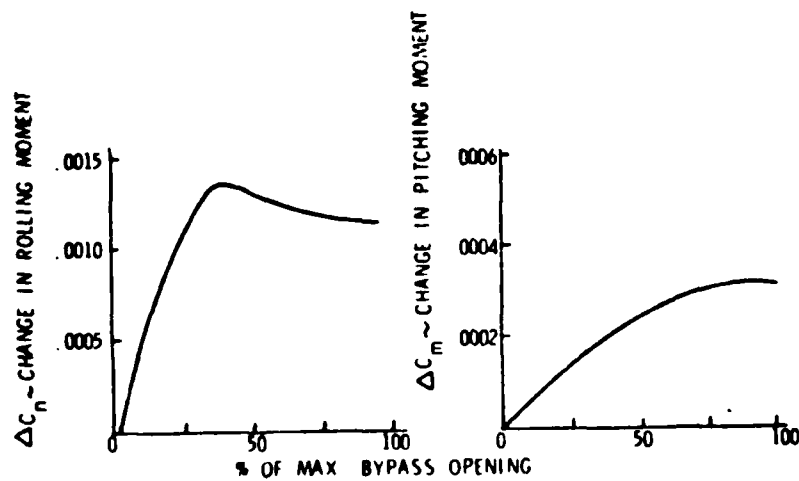


Figure 24. Effect of Bypass Operation on Aircraft Stability (Reference 6)

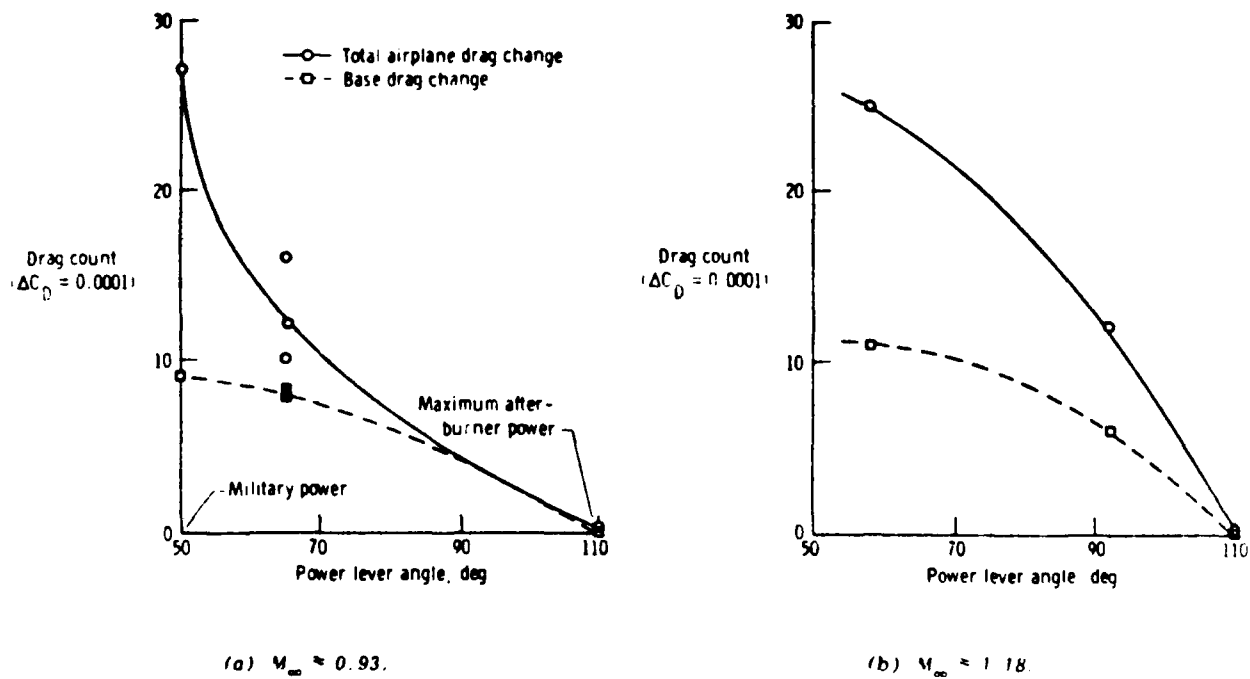


Figure 25. Changes in Drag with Engine Power Lever Angle (Reference 13)



six engine installation is not typical, note that nearly one-third of the change is base drag.

#### 5. SUBSONIC AIRCRAFT INLETS/NOZZLES

The propulsion system for subsonic aircraft, while not required to respond to the large engine mass flow changes of supersonic aircraft, is required to produce high levels of performance in sometimes very complicated aircraft integrations. The engine is usually podded under a wing or on the fuselage to take advantage of high energy freestream flow and is usually designed to satisfy the maximum airflow requirement with the smallest possible inlet capture area. Further, driven by weight considerations, the subsonic inlet design will not likely have bleed/bypass provisions and the problems of off-design operation increase. The inlet may incorporate blow-in-doors to handle the extra airflow required for takeoff (compared with cruise airflow) to avoid an oversized inlet for cruise. A typical wing pylon/nacelle installation (Figure 26) shows the potential for throttle dependent forces around the inlet, the afterbody/nozzle, the pylon and the wing. For an aircraft with short takeoff and landing (STOL) requirements, configurations such as the Boeing YC-14 (Figure 27) with upper surface blowing have been proposed. The high degree of potential engine/aircraft interaction is obvious. Any engine airflow changes will affect not only the inlet flow field and the airframe in the proximity of the inlet but also the flow on the wing upper surface, changing the lift, drag, and pitching moment characteristics of the aircraft.

The subsonic inlet generally has rounded cowl lips and is sized for a capture ratio ( $A_o/A_i$ ) near unity at cruise. Figure 28 presents the subsonic inlet flow character for a range of mass flows and illustrates the changing stagnation point,  $S$ , which directly relates to both components of spillage drag, i.e. additive drag and cowl lip suction. With a velocity ratio greater than 1, the flow stagnates outside the cowl and part of the captured flow rapidly accelerates around the cowl. This can produce flow separation on inside cowl surfaces, resulting in reduced engine face total pressure recovery and reduced thrust. This problem is especially critical for STOL aircraft, which have climb-out angles typically around 40-50 degrees and flow stagnation on part of the nacelle on the outside cowl surfaces.

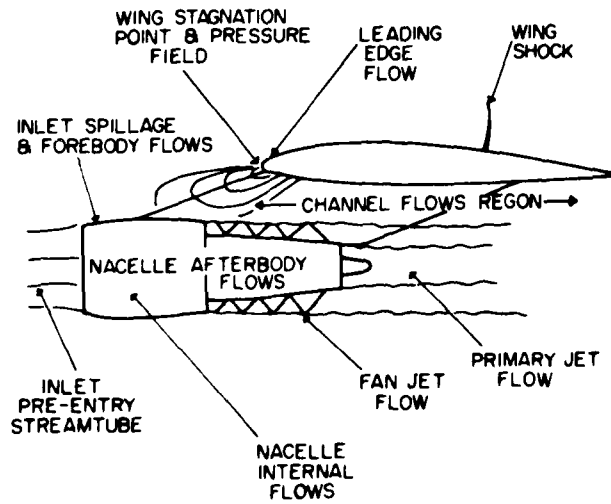


Figure 26. Major Elements of Wing/Pylon/Nacelle Flow Field (Reference 14)



Figure 27. Boeing Advanced Medium STOL Transport (Reference 15)

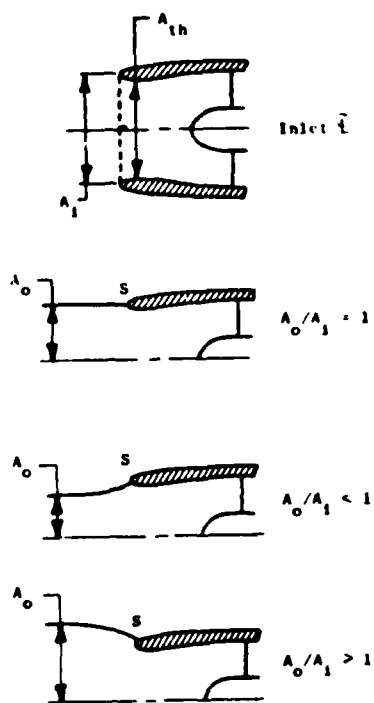


Figure 28. Definition of Inlet Capture Area,  $A_i$ , and Characterization of Flow Incidence Approaching Inlet via Mass Flows Ratio  $A_o/A_i$  (Reference 5)

Changes in inlet and nozzle flow can affect the engine cowl, pylon and wing surface pressures. Reference 16 attributes up to 2.5 percent of the total aircraft drag to this interaction, a significant factor for transports where a few drag counts are critical to the success of a commercial operator. For an aircraft with upper surface blowing, the jet obviously changes the wing forces and both conventional and advanced installations will experience throttle dependent lift, drag, and pitching moment changes.

## 6. EXAMPLES-SUBSONIC AIRCRAFT THROTTLE DEPENDENT FORCES

### Airbus A300B

The Airbus A300B nacelle (Figure 29) is a good example of a transport propulsion installation with throttle dependent forces. The changes in pressure distribution on the wing lower surface, pylon, core engine cowl, and fan cowl as the jet is changed from flow-through (natural flow) to an exhaust flow simulation are presented in Figure 30. The largest change in pressure distribution is on the core engine cowl, with smaller changes on the pylon, fan cowl and wing. These pressure distribution changes with different jet conditions result in the pressure drag coefficient increments shown in Figure 31. Note the core engine cowl drag is somewhat offset by the other contributors.

### OSRA

The NASA Quiet Short-Haul Research Aircraft (OSRA) is an example of propulsive lift transport with strong throttle dependent effects. The aircraft (Figure 32) has a 4 engine nacelle-over-wing propulsion installation similar to other upper surface blowing configurations. The engine exhaust flows over the upper wing and flaps so changes in throttle setting affect aircraft lift, drag and pitching moment. Total aircraft lift coefficient at takeoff, Figure 33, shows the lift dependence on engine rpm. Total lift coefficient at 100 percent thrust (curve A) is appreciably greater than the total lift coefficient at 60 percent thrust (curve B). When the total lift generated with the direct thrust component is removed from both curves A and B, Curve C results. This lift curve is approximately 17 percent higher across the angle-of-attack range than the basic wing lift curve, curve D. Clearly, the throttle dependent interaction of the propulsive flow and the airframe is a large contributor to the mission performance of this aircraft.

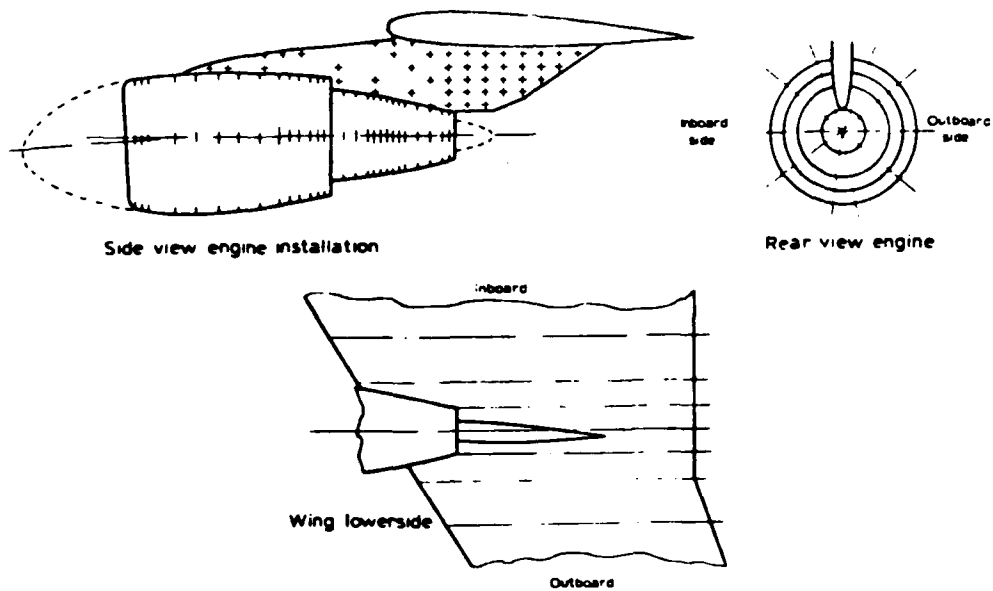


Figure 29. A300B Nacelle (Reference 16)

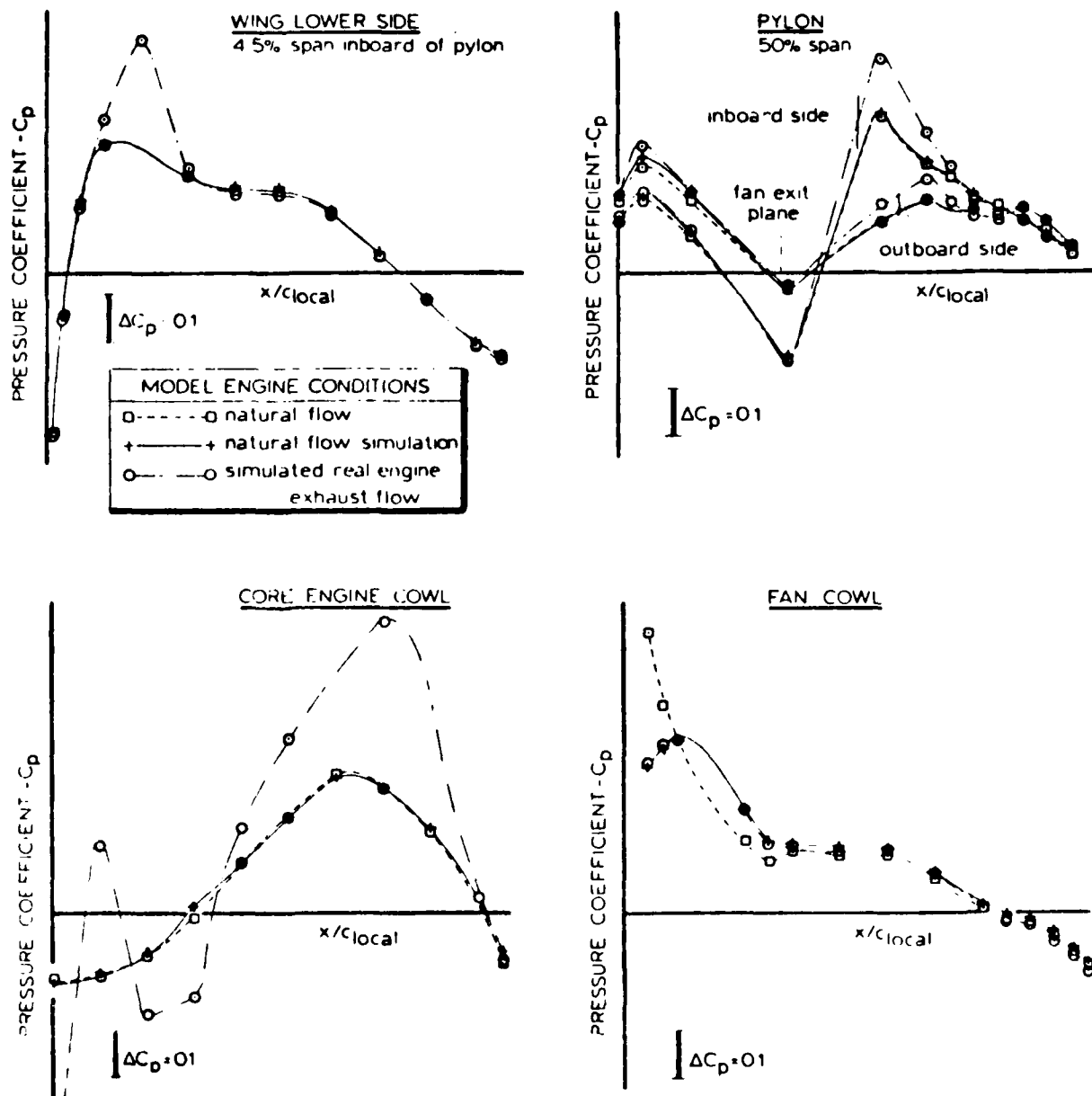


Figure 30. Pressure Distribution on Wing, Pylon, Core Engine, and Fan Cowl (Reference 16)

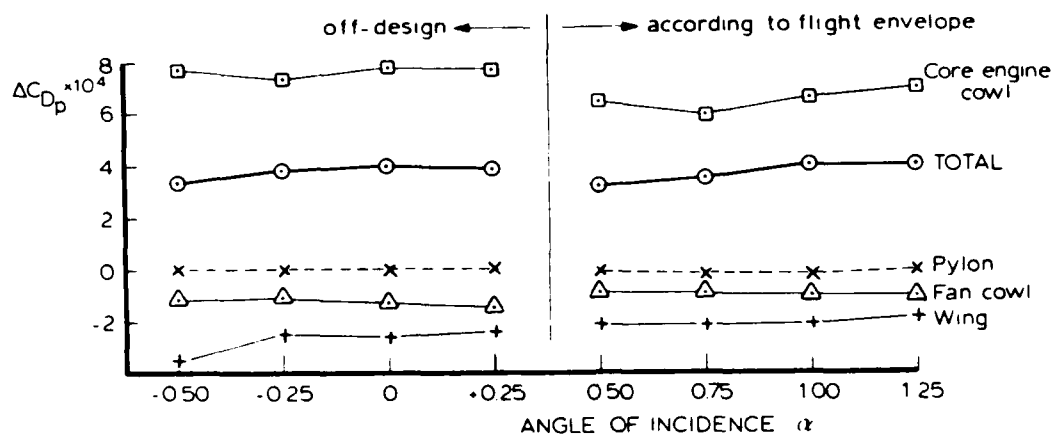


Figure 31.  $\Delta C_{Dp}$  versus  $\alpha$  for Wing, Pylon, Fan and Core Engine Cowl (Reference 16)

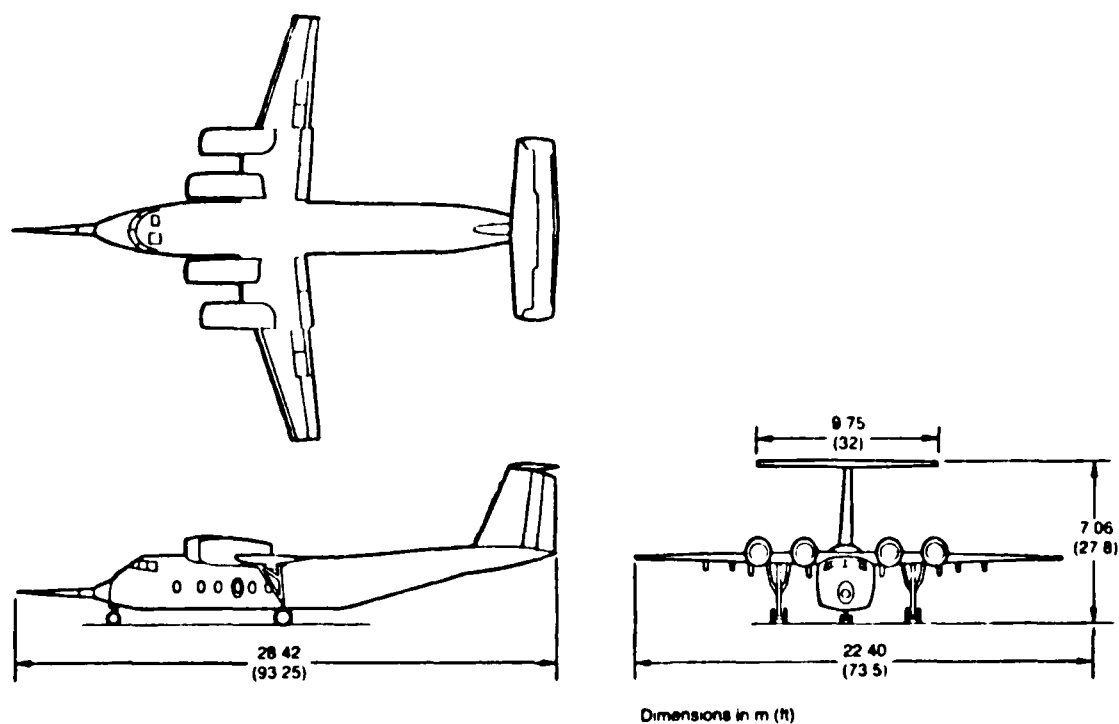


Figure 32. QSRA Design and Configuration Data (Reference 17)

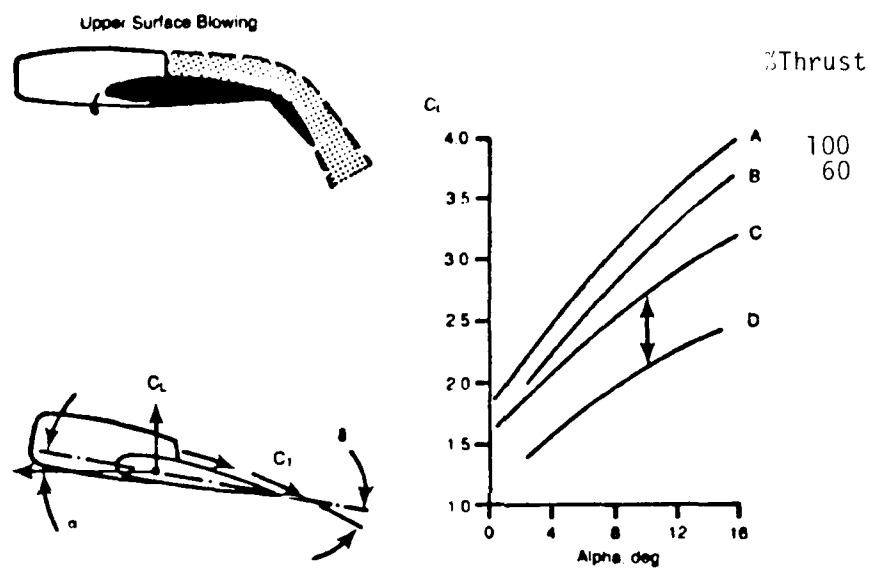


Figure 33. Upper Surface Blowing Aerodynamics (Reference 17)



## AGM-109

The throttle dependent forces for cruise missiles follow the trends exhibited in larger aircraft. For the AGM-109 cruise missile (Figure 34) spillage drag increases with decreasing engine mass flow demand (Figure 35) and the boattail/base drag first decreases and then increases with increasing nozzle pressure ratio (Figure 36).

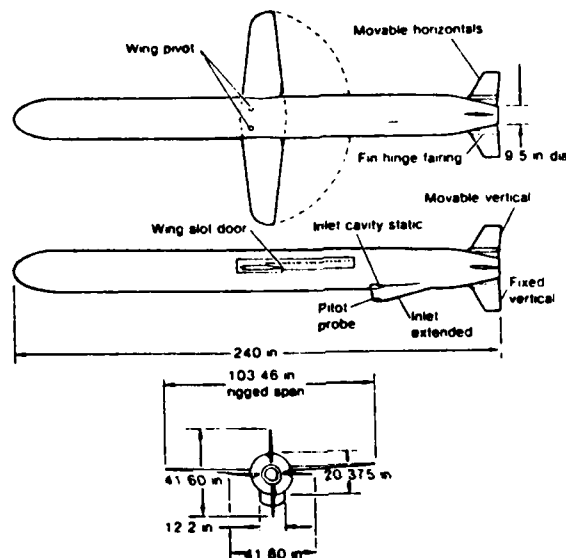


Figure 34. AGM-109 Three View Drawing (Reference 18)

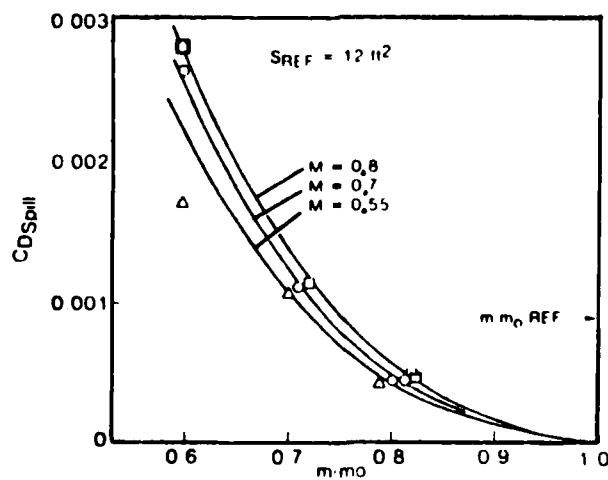


Figure 35. Subcritical Inlet Spillage Drag Variation with Inlet Mass Flow Ratio (Reference 18)

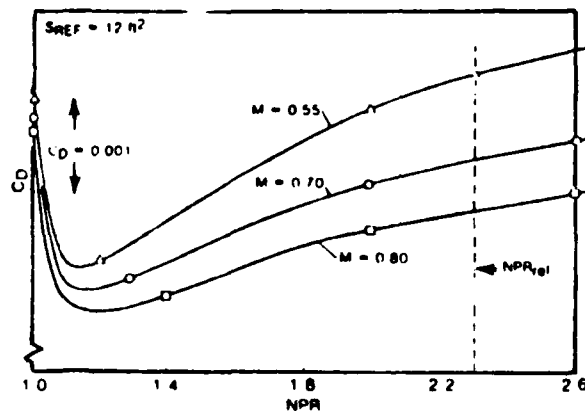


Figure 36. Boattail-base Drag Variation with Nozzle Pressure Ratio (Reference 18)

## SECTION III

## DETERMINATION OF THROTTLE DEPENDENT FORCES

Since the measurement of throttle dependent forces in flight is generally not possible, experimental results from wind tunnels and analytical techniques are used. This section will present tools and techniques for the experimental and analytical estimation of these forces.

## 1. EXPERIMENTAL TECHNIQUES

The experimental approach for determining throttle dependent forces is based on the thrust/drag accounting system typically established for aircraft systems. This system orderly assembles force increments from various wind tunnel models to correct a reference configuration to a full scale aircraft. Three different models are typically used: an aerodynamic force and moment model, an inlet model, and a nozzle (jet effects) model (Figure 37). The aerodynamic force and moment model is the aerodynamic reference configuration which usually has a simple inlet and nozzle geometry representation. This model is typically 4-7% scale for fighter aircraft, usually sting supported, fully metric, and uses a flow-through duct propulsion system simulation.

The inlet spillage model, or inlet drag model, usually simulates only a partial aircraft. The fuselage forebody and inlet are modeled, though the fuselage is often only represented to approximately 3 inlet heights downstream (Reference 4). At least partial span wings should be present to the extent needed to account for all areas affected by the inlet flow field. This model is larger than the aerodynamic force and moment model (10-15 percent scale); is equipped with suction at low speed or relies on ram air for inlet flow; is instrumented with pressures at the engine face (rake) and on cowl surfaces; accurately represents the inlet geometry; incorporates simulation of bleed, bypass and auxiliary doors if necessary; and measures the total inlet forces with a force balance.

The accuracy of the mass flow through the inlet is especially important with typical accuracies of mass flow quoted to  $\pm 0.5$  percent (Reference 16). The spillage drag, as well as bleed and bypass forces, can be determined from pressures or

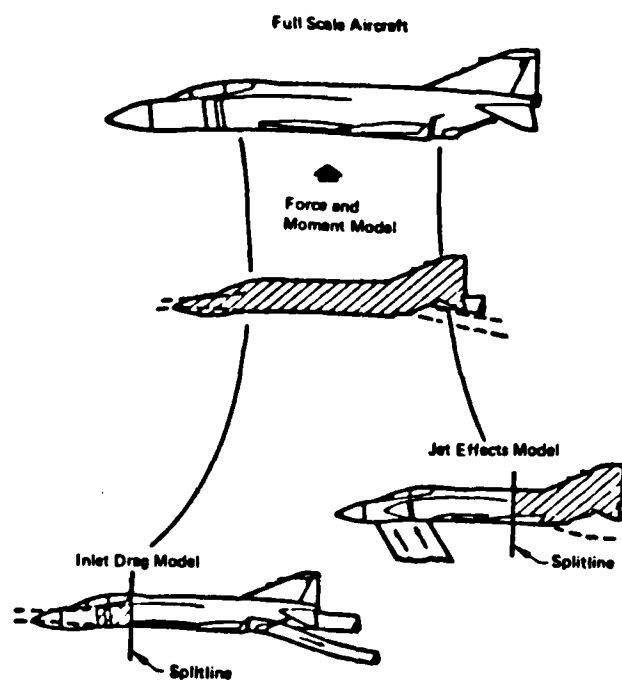


Figure 37. Projection of Full Scale Aircraft Performance (Reference 7)

force balances. Representative inlet spillage models are shown in Figure 38. The F-15 model in this example is supported by two flow-through sting tubes and is instrumented with two force balances and multiple surface pressures.

The jet effects model is used to determine throttle dependent forces due to the exhaust plume and to the variable geometry. The model generally duplicates aircraft lines although usually only the afterbody is metric, i.e. on the force balance. High pressure cold air over a range of nozzle pressure ratios is generally used to represent the nozzle flow. The model may be supported in a number of ways (Figure 39) though the wingtip support is often preferred. Experimental parameters include nozzle pressure ratio, nozzle boattail angle, nozzle internal area ratio, angle-of-attack and Mach number. Instrumentation for this model generally consists of force balances which measure afterbody drag or thrust-minus-drag and surface pressures which may be integrated to determine the nozzle forces.

While experimental determination of throttle dependent forces for subsonic transports uses an approach similar to that used for tactical aircraft, the requirement to guarantee aircraft performance to the commercial operator prior to the aircraft sale puts increased emphasis on accuracy. Propulsion forces which depend on nacelle shape, pylon placement and complex jet exhaust interactions require careful calibration of massflow and controlled testing. On a short nacelle, the simultaneous simulation of the inlet and nozzle flow often requires the use of propulsion simulators, which add to cost and model complexity. Typical model testing techniques for transport aircraft are shown in Figure 40.

The selection of model hardware to determine throttle dependent forces is driven by factors present in all wind tunnel tests. The resources available limit the overall achievable test objectives which in turn define the model complexity and therefore the test approach. Issues include: model size versus accuracy; use of force balances versus pressure area integration; extent of aircraft and propulsion stream simulation; Reynolds number simulation; available hardware, facility, and cost. Each test presents individual problems in sizing, model internal space, data reduction and corrections, and other items which impact the desired and achievable accuracy (Reference 20). All test variables involved must be closely examined and compared, so that the most effective compromises can be made between what is desired and what is feasible.

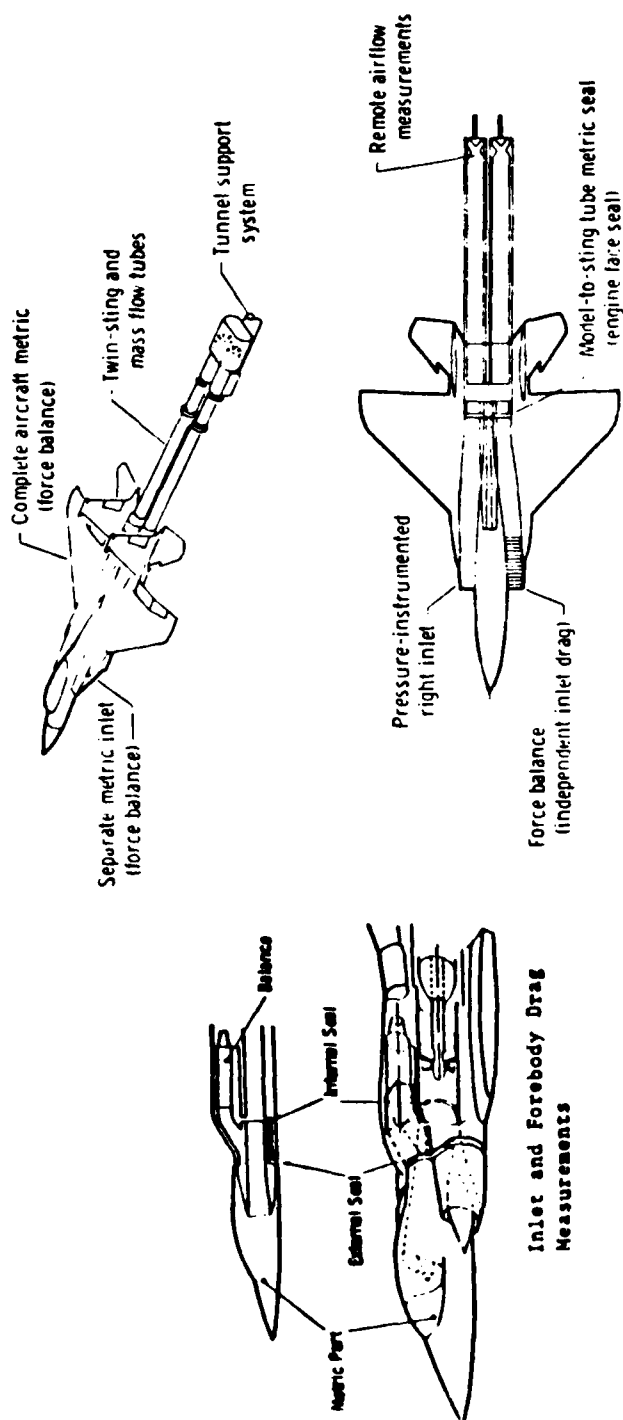


Figure 38. Inlet Model Balance Arrangement (Reference 9)

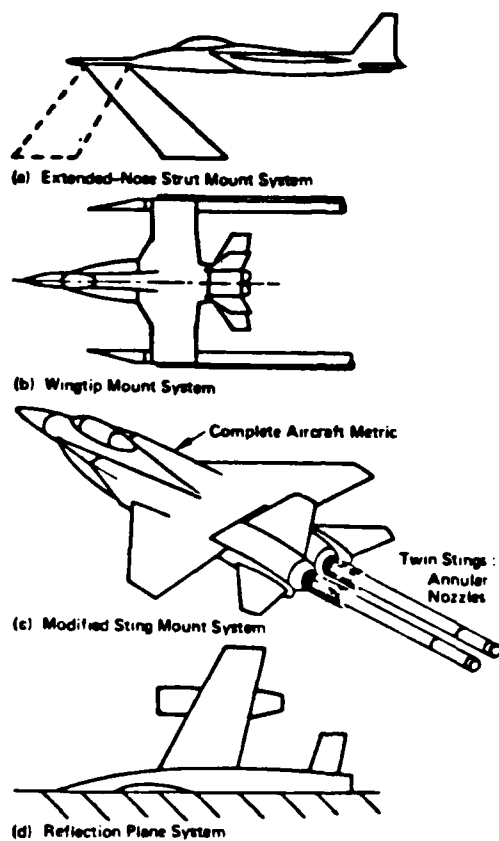
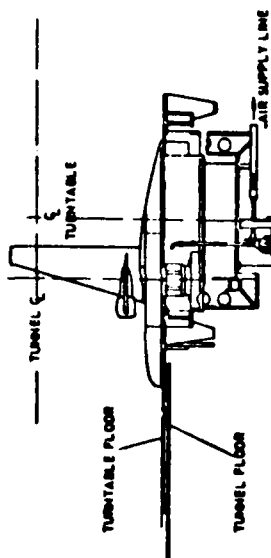
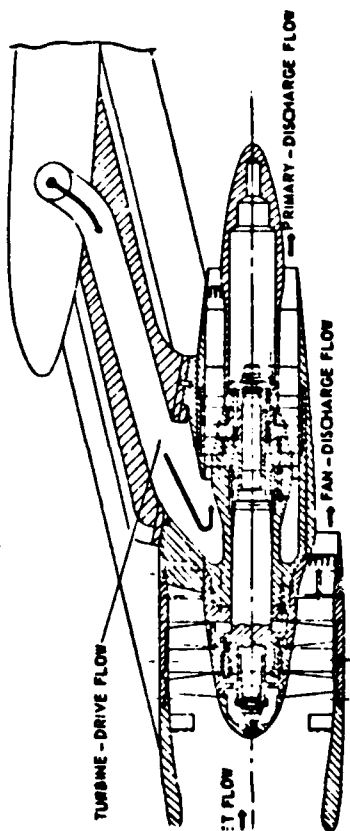


Figure 39. Jet Effects Model Support Systems (Reference 7)



ii-span model tunnel installation with powered nacelle.

-sectional view of a miniature turbo-driven fan simulator.

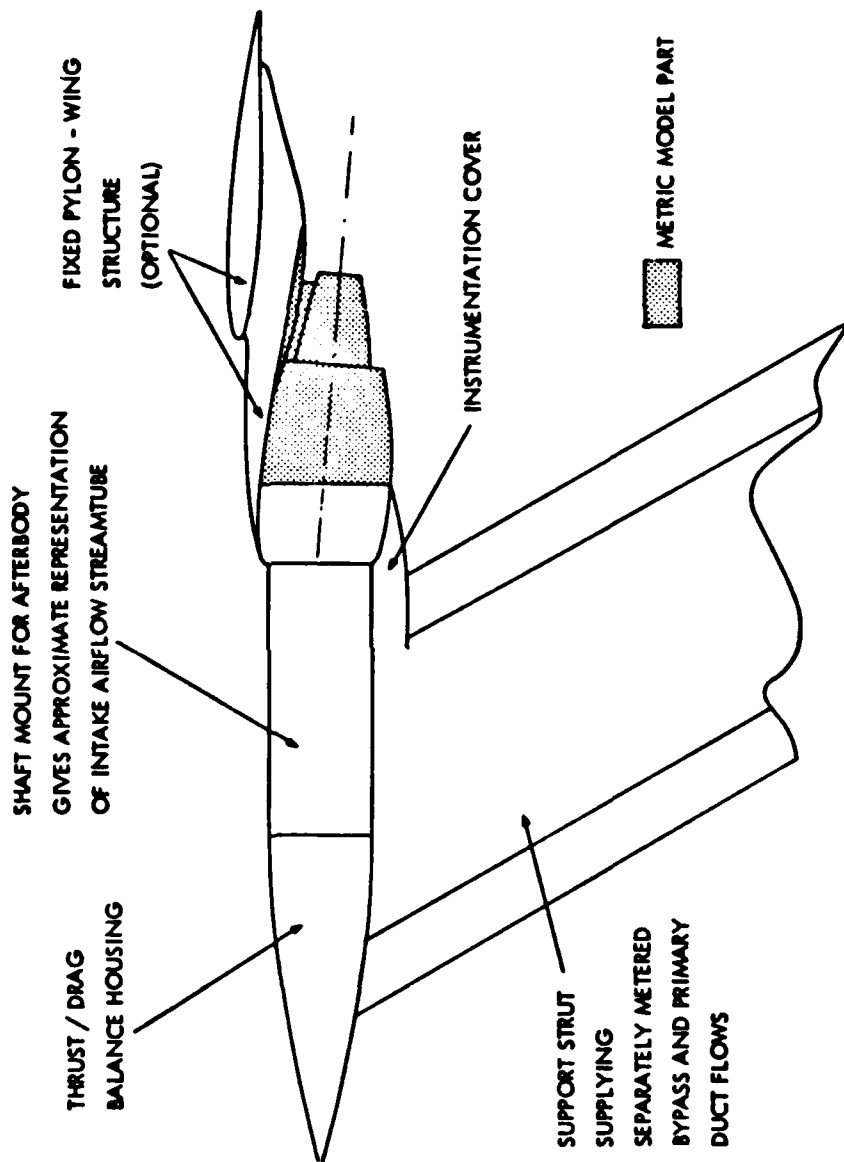


Figure 40. Transport Testing Techniques (Reference 19)



## 2. DIFFICULTIES IN EXPERIMENTAL TESTING

Reference 1 identifies several difficulties in wind tunnel determination of inlet and nozzle throttle dependent forces, including errors in parameter matching, inadequate flow field simulation, model support influence, and tunnel effects such as blockage and buoyancy. Other wind tunnel considerations are the method of propulsion flow simulation, model support testing options, measurement and determination of forces, and determination of accuracy and repeatability.

The simulation of the propulsion stream has been and is currently the subject of a great deal of research and debate. Current techniques used in wind tunnel testing are presented in Figure 41. For the inlet spillage model, the inlet flow must be correctly simulated to give proper levels of spillage drag, cowl drag and inlet flow/aircraft interactions. The location of the stagnation point on a transport nacelle, for example, should match between wind tunnel and flight to provide comparable inlet flow. This flow can be simulated by active suction for low speed conditions or rely on ram air and a variable position mass flow plug for higher Mach numbers. For aircraft that have independent inlet and nozzle flow fields, these techniques are adequate. When changes in the inlet mass flow and/or geometry do not affect the aircraft afterbody flow, or if changes in the exhaust nozzle geometry or exhaust flow do not appear to affect the flow around the inlet, the inlet and nozzle flowfields are determined to be independent. If the flowfields do interact, as in a transport nacelle, the propulsion system is called "short coupled" or "closely coupled". There is no convention for determining if an aircraft propulsion system is close coupled or independent. Depending on the particular installation and the overall propulsion system length, interactions can range from none at all to major. This issue has been the driver behind development of turbine and ejector powered propulsion stream simulators for tactical aircraft wind tunnel models. For closely coupled inlet/nozzle flows, typically encountered in transports, these special techniques may be required. Turbine simulators are small compressors with high pressure air turbine or electric motor drive. This technique has been utilized with success on transport nacelles and is being investigated for close-coupled fighter aircraft. The turbine simulator matches most inlet and nozzle flow conditions, but can be mechanically complex and does not account for temperature. Ejector simulators use a propulsive pumping action to control the inlet/nozzle flow at point design conditions. Although primarily emphasized in the European technical community,

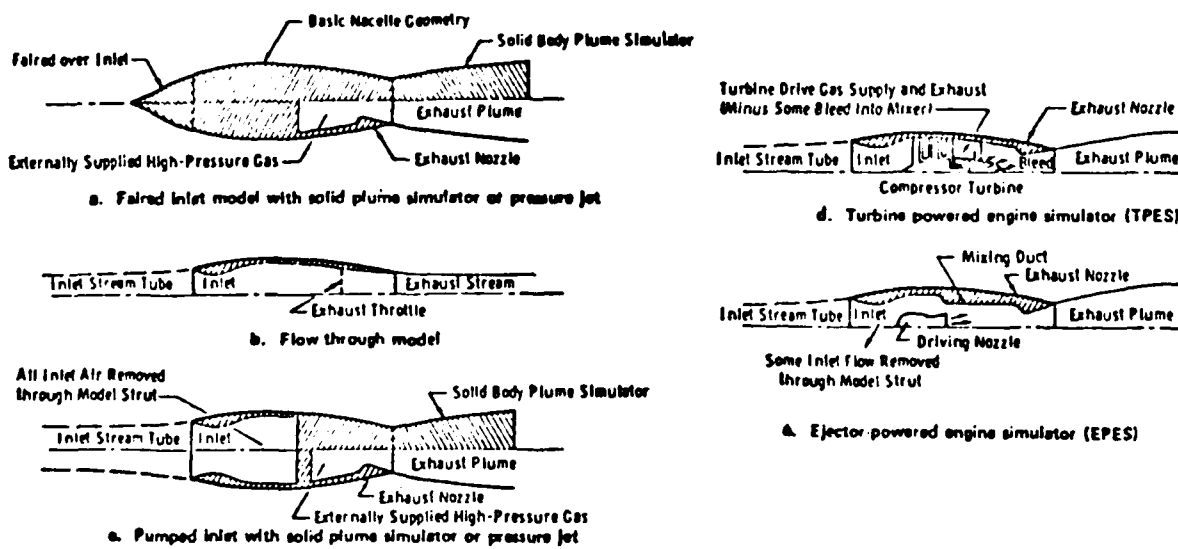


Figure 41. Current Engine Simulation Techniques for Wind Tunnel Testing (Reference 21)

these simulators have been investigated at Arnold Engineering Development Center, with best results achieved at transonic/supersonic Mach numbers. The whole array of propulsion stream simulation techniques for jet transport aircraft is shown in Figures 42 and 43. These approaches are generally applicable for fighter aircraft as well. Correct simulation of the inlet and nozzle flows must be considered when throttle dependent forces are to be determined.

Exhaust nozzle flow from a jet engine is characterized by the nozzle pressure ratio, gas temperature, gas combustion products, total pressure, total temperature distortions, swirl, and turbulence. Perhaps because it is not possible to simulate all parameters in a part scale wind tunnel model, one source (Reference 20) states: "the jet should be simulated as simply as possible." This has led to a variety of techniques for jet plume simulation, the most common being the use of high pressure cold air. Such a simulation is relatively easy to control and incorporate into a wind tunnel model. This technique, however, accounts for only the nozzle pressure ratio jet parameter. Solid plume simulators have also been used with different fairings to simulate nozzle pressure ratio changes. This technique partially accounts for the nozzle pressure ratio effect using a calculated plume shape to fabricate model plume contours but does not provide for jet entrainment/mixing effects. A hybrid jet simulation which can double as a model support system is an annular-jet. The model is supported by a sting(s) through the nozzle, and high pressure air is ducted around the sting (Figure 44). This technique offers promise but has limited angle-of-attack and jet simulation capability.

In experiments where hot and cold exhaust plumes have been utilized to determine nozzle boattail forces, the cold jet consistently had higher boattail drag values than a hot jet at similar nozzle pressure ratios. This is due to different plume shapes and entrainment characteristics, with the largest differences occurring for large boattail angles at high transonic Mach numbers. Effects of exhaust temperature has been simulated using gases having different ratios of specific heat, by burning ethylene in the nozzle plenum, or by using real engines. While these approximately simulate the real exhaust jet, it adds cost and complexity to an already difficult model. An approximate correction for temperature effects can be achieved by increasing the cold jet nozzle pressure ratio to produce a maximum plume diameter for the corresponding hot jet.

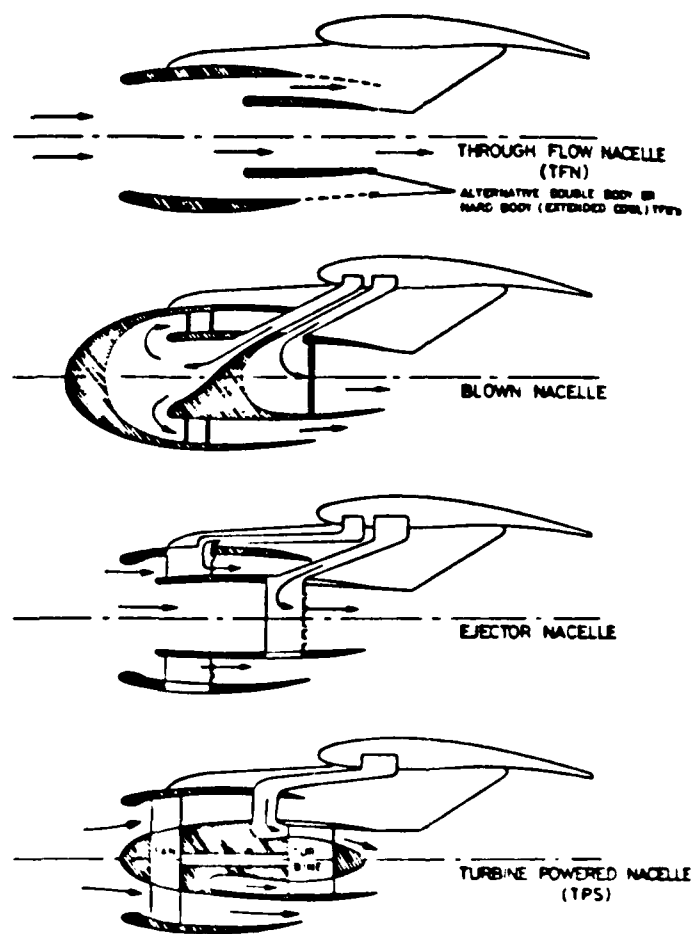


Figure 42. Types of Nacelle Simulators (Reference 23)

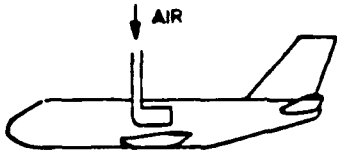
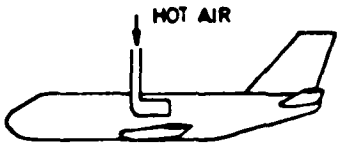
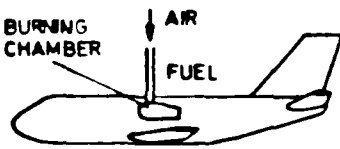
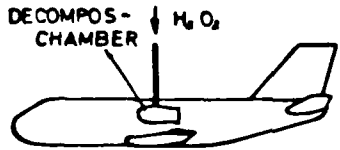
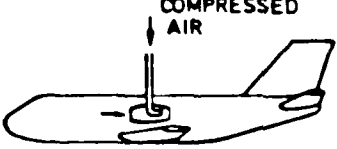
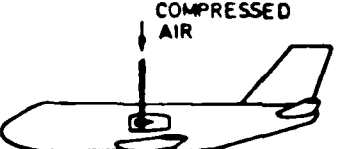
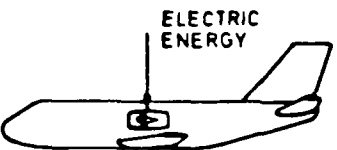
SIMULATION OF COLD JET	COMPRESSED AIR	
SIMULATION OF HOT JET	HOT COMPRESSED AIR	
	COMPRESSED AIR + BURNING	
	HYDROGEN PEROXYDE	
SIMULATION OF JET INTAKE	INJECTOR	
	TIP TURBINE DRIVEN FAN	
	ELECTRIC MOTOR DRIVEN FAN	

Figure 43. Principles of Jet Engine Simulation in Wind Tunnels (Reference 24)

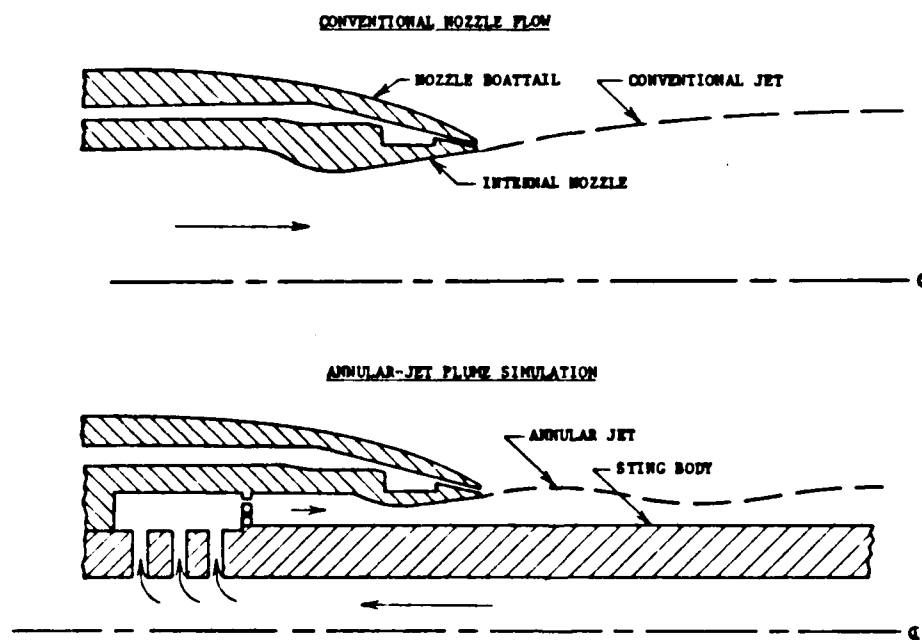


Figure 44. Concept of Annular-jet Plume Simulation with Sting Support of a Jet Effects Model (Reference 22)

The assumption that the inlet and nozzle flow fields are independent allows separate determination of inlet and nozzle throttle dependent forces. However, if the inlet is faired over, as in a jet effects model, the entire flow is spilled and can change the aerodynamic character of the afterbody/nozzle (Reference 22). Simultaneous simulation of the inlet-nozzle flow is limited by available wind tunnel testing techniques. Figure 45 demonstrates the impact of inlet fairing. The illustration compares the changes in afterbody/nozzle drag for two aircraft models. Note that probably neither the inlet fairing nor the dead end inlet is a correct simulation and that lift and pitching moment are also affected. This is a necessary compromise for most research and development efforts.

One reason it is not possible to test an accurate scale version of the complete aircraft is that wind tunnel models have support systems which interfere with the flow field and perhaps compromise the data. The quest for interference free support systems has led to a number of concepts for both transports and fighter aircraft. Figure 46 shows stings, plates, half-models, and wingtip supports, all utilized for transport configuration tests. Representative support techniques for a fighter aircraft model are presented in Figure 47. Each support system has its own set of deficiencies, and all have a strong transonic influence. According to Glidewell (Reference 22) and Kennedy (Reference 25), a strut support can be properly designed for subsonic or supersonic use; however, such a support can be a large contributor to blockage and interference transonically. The wingtip support minimizes blockage and interference but distorts aircraft wing lines on the outer wing span and limits model metric arrangements. The dual sting and annular sting support system provides minimum blockage and interference but as previously mentioned, is limited in angle-of-attack and jet simulation capability. Regardless of the support system, the support influence could be determined either by calculating local pressures near the support system, or by special support testing where an alternate support is used to hold the model and the primary support is tested on and off to measure the support interference. The choice of a model support system depends on the test objective, test facility, existing hardware, and cost. For throttle dependent force determination, the support system should be tailored for minimum interference.

The experimental techniques previously described require use of a force balance and pressure measurements. A typical jet effects model with a non-metric section and two separate metric sections is shown in Figure 48. The use of one or both

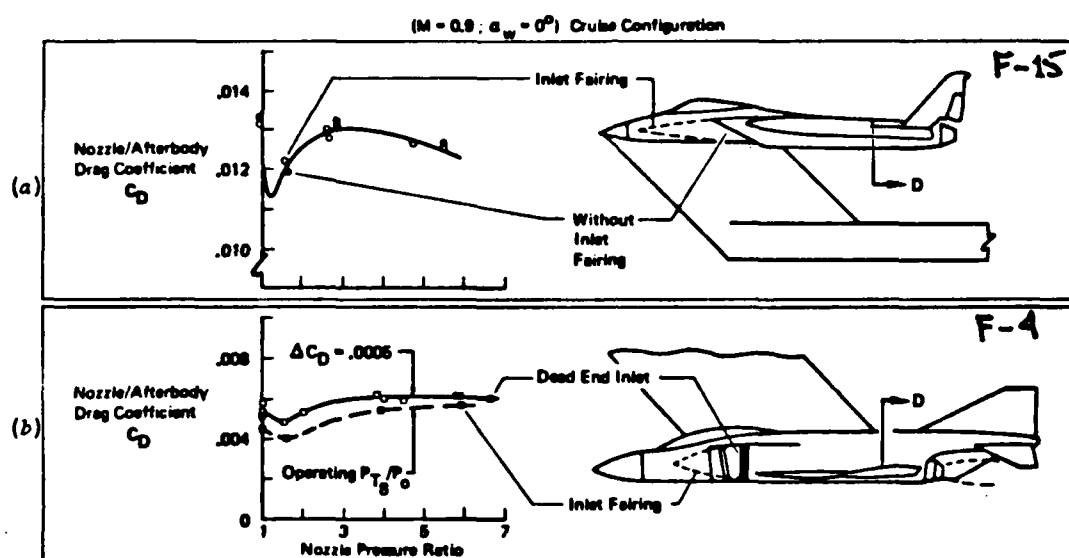


Figure 45. Inlet Fairing Effects on Afterbody Drag (Reference 7)







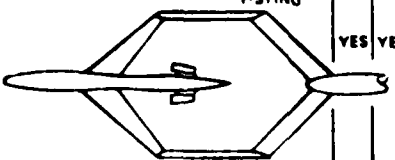
TYPE	MACH		BALANCE	
	< 1	> 1	INTERNAL	EXTERNAL
STRAIGHT STING 	YES	YES	YES	
BENT STING 	YES	NO	YES	
PLATE FAIRING FLOOR 	YES	NO	YES	YES
HALF MODEL FLOOR 	YES	YES	YES	YES
V-STING 	YES	YES	YES	

Figure 46. Examples of Wind Tunnel Model Mounting Techniques (Reference 5)

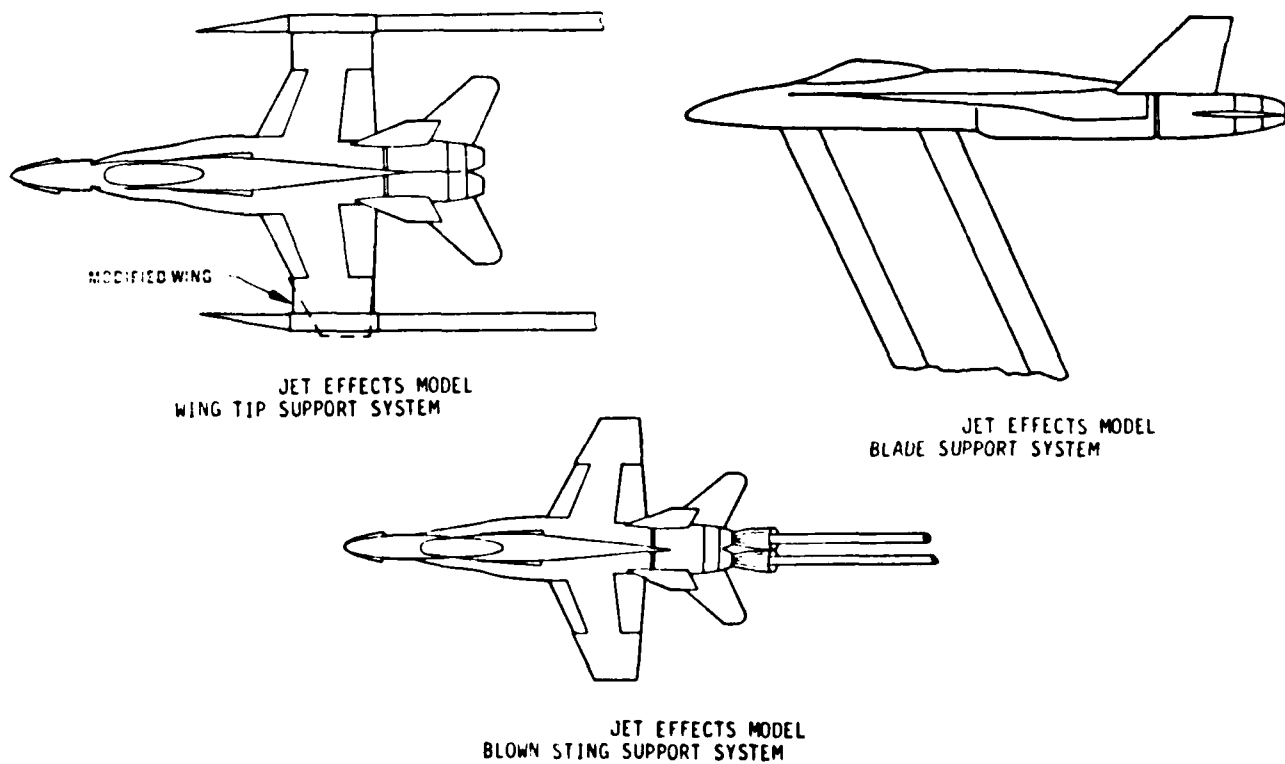


Figure 47. Jet Effects Model Support Options (Reference 1)

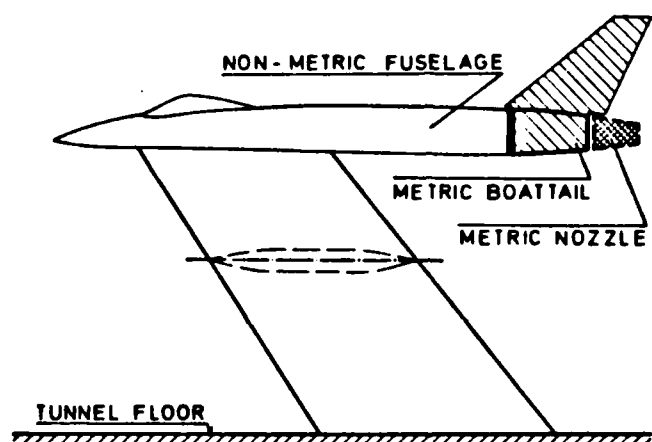


Figure 48. Typical Afterbody Test Rig with Subdivided Boattail (Reference 23)

techniques is a much discussed and controversial area. How much, if any, of the aircraft model should be metric? Can surface pressures and pressure area integration accurately determine throttle dependent forces? The presence of a metric break on a model can impact the downstream flow, creating discontinuities in surface pressure distributions. In addition, the presence of a physical gap in the model separating metric and nonmetric sections necessitates additional data corrections for metric break seal and cavity forces. Reference 25 presents data for a nacelle with a metric afterbody (Figure 49). In this test arrangement, the balance loads and the corrections (metric seal and cavity pressure) are the same magnitude at subsonic and supersonic Mach numbers, Figure 50. The issue of close coupled inlet/nozzle flows has opened the question of how much of the aircraft must be modeled and how much must be metric. Data such as Figure 51 indicates that the throttle dependent change in aircraft afterbody pressure distribution with nozzle power setting can continue upstream of the maximum cross section station usually chosen for the start of the metric section. The current "guidance" from a number of sources on metric break placement is varied:

- (1) Isolate the smallest model piece to satisfy the test objectives with greatest accuracy (Reference 7).
- (2) If disturbances from inlet/nozzle flow carry far upstream or downstream, a large part of the aircraft must not only be simulated but also must be metric.
- (3) Other sources (Reference 1, 26) recommend as much of the aircraft as possible be on a force balance with the entire aircraft metric if allowable.

Obviously the solution of the extent of the model required to be metric is not absolute. Other factors which complicate experimental determination of throttle dependent forces are accuracy and repeatability of data and wind tunnel effects. Accuracy, as defined by Reference 19, is the uncertainty of a value due to systematic or bias error. Accuracy can be improved by careful calibration and controlled test techniques; however, Jaarsma (Reference 20) notes that accuracy is difficult to assess because overall accuracy includes a combination of the effects of many instruments such as mass flow meters, pressure transducers, thermocouples, and force balances. As stated previously, each model test apparatus presents individual problems in sizing, restricted internal space, pressure corrections, metric break seal restraints, thermal expansion, clearances, and other items which make any general statement of achievable accuracy suspect (Reference 20).

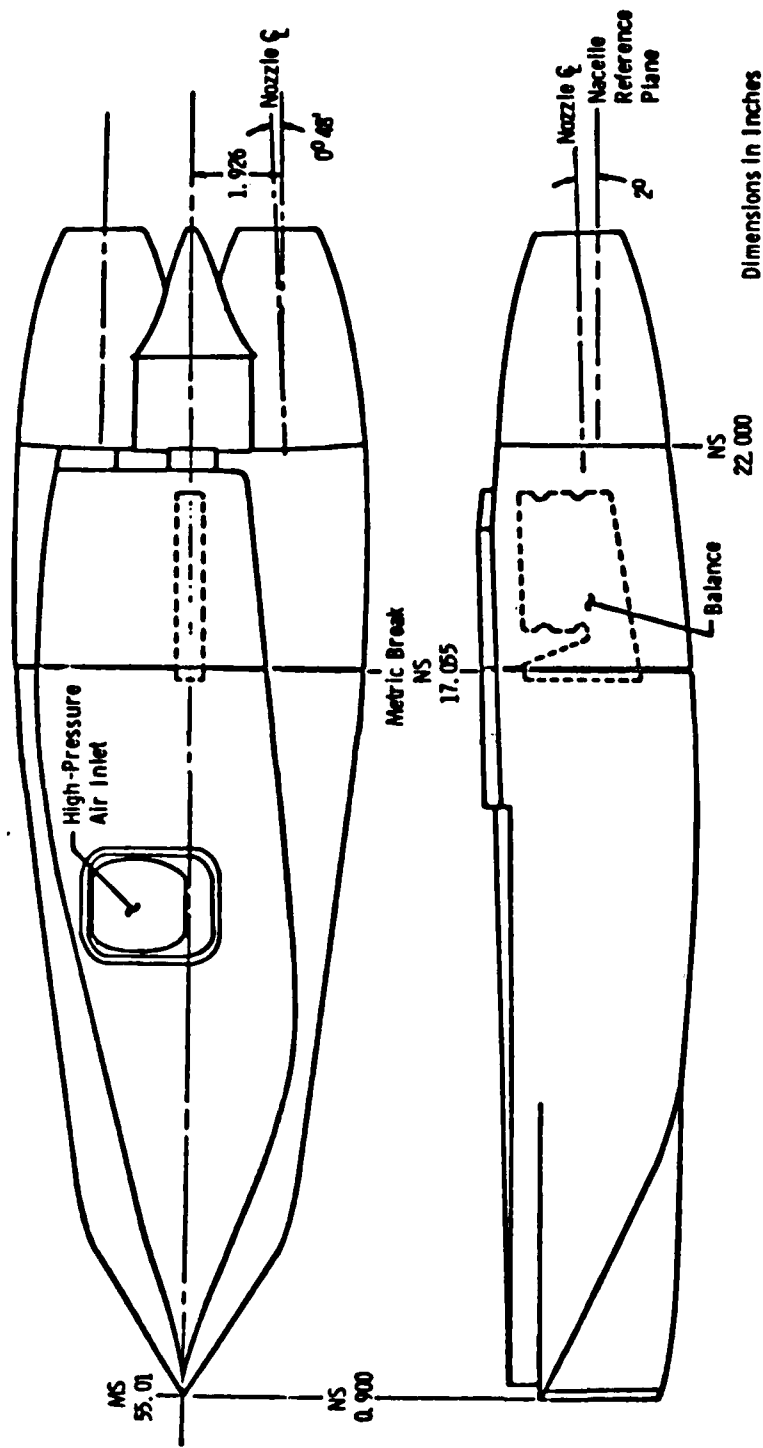


Figure 49. Force Balance Nacelle Configuration (Reference 25)

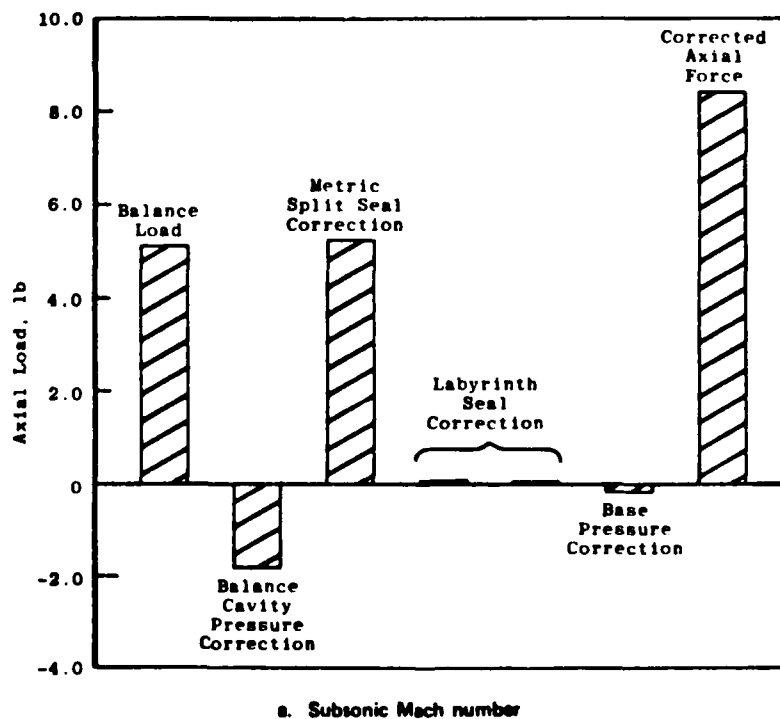
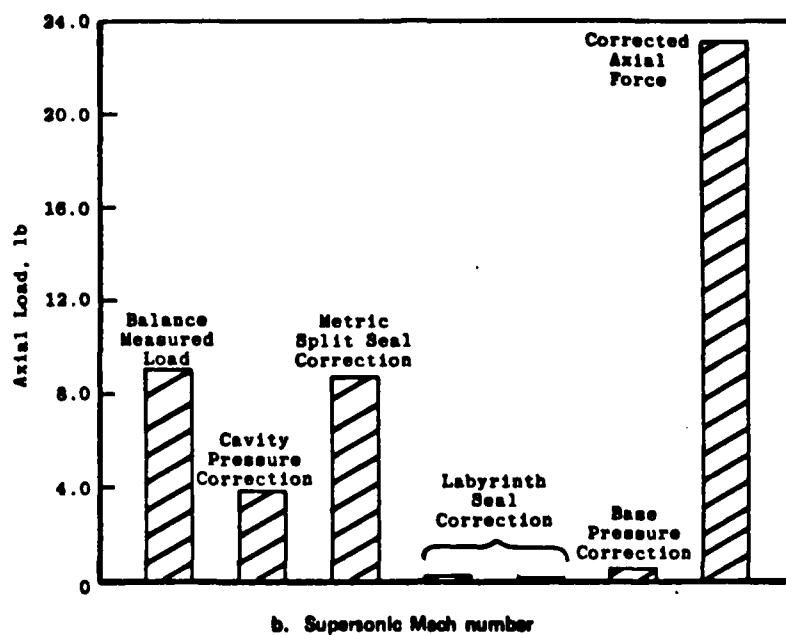


Figure 50. Nacelle Axial-Force Components (Reference 25)

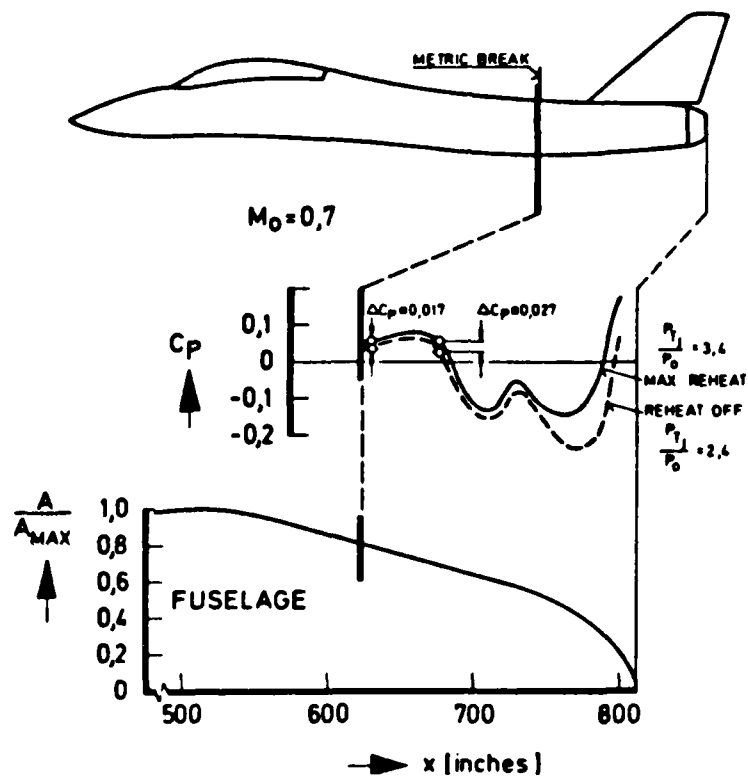


Figure 51. Effect of Nozzle Position on Pressure Distribution (Reference 27)

Repeatability is defined as the uncertainty of the measurement due to the presence of random errors. Reference 4 mentions  $\pm 1\%$  aircraft drag repeatability for a technique which measures aircraft transonic spillage drag for a supersonic aircraft. Both high repeatability and reduced bias error should be the goal when measuring throttle dependent forces.

Additional factors in experimental throttle dependent force determination are wind tunnel effects, such as buoyancy, blockage, flow quality, and Reynolds number simulation. These items will not be discussed in the report but the reader is referred to Pope (Reference 28).

### 3. QUALITATIVE TECHNIQUES TO ASSESS THROTTLE DEPENDENT FORCES

The nature and extent of the influence of the propulsion stream on the inlet/nozzle and adjacent aircraft surfaces can be determined qualitatively by various flow visualization techniques. Wind tunnel techniques include the use of tufts, dye, and oil flow, all indicating surface flow direction, the presence and location of shock waves and areas of separation, and the location of vortices. Schlieren and shadowgraph techniques can indicate in supersonic tunnel flow the presence of density gradients, i.e. primarily shock waves. A technique applicable to low speed wind tunnel work is smoke to trace streamlines influenced by the propulsion stream. Dye streams and bubbles are often used to indicate propulsion stream influence in low speed water tunnels. All of these techniques can provide the investigator further insight into the throttle dependent effects.

### 4. ANALYTICAL TECHNIQUES

In addition to experimental techniques, analytical or computational techniques can be used to predict throttle dependent forces. In general, due to the complex nature of the interaction of the propulsion stream with the external flow and adjacent surfaces, throttle dependent forces are difficult to predict. Analytical techniques vary from empirical approaches to potential flow solutions, from quasi-time dependent to time dependent, inviscid/viscous patch methods to full Navier-Stokes equations solutions. These techniques serve a useful role in evaluating and screening concepts relative to throttle dependent forces. It should be noted that these methods usually predict surface pressure distributions and throttle dependent forces are then determined from pressure area integration. Success of these

techniques varies with the level of accuracy required and level of resources available to support the prediction. The extent of the aircraft simulated also determines the success of these techniques but this simulation is limited by the computer's available storage. In this section, representative techniques will be discussed for throttle dependent forces for supersonic/transonic aircraft and for nacelle installations on transport aircraft.

## 5. INLET ANALYTICAL TECHNIQUES

Empirical procedures are correlations of experimental data which indicate trends and approximate forces for particular classes of inlet configurations. Figure 52 shows a spillage drag correlation compared with experimental data. The procedures provide adequate trends but do not reproduce the absolute values. These methods can be useful in conceptual and preliminary design procedures. The success of all empirical techniques depends on the data base and the degree of similarity of the configuration being analyzed to those in the data base. If carefully restricted and applied, these techniques can be valuable tools for determining throttle dependent forces.

Inlet surface pressures are often calculated by two-dimensional potential flow solutions over a range of angles of attack and mass flow. Boundary layer analysis is sometimes added to account for viscous effects. These techniques are moderately successful if no separation is present. Local velocity profiles on a supersonic inlet lip at subsonic conditions at different angles of attack and mass flow ratios, calculated by a two-dimensional incompressible technique are shown in Figure 53. These methods have been extended to three-dimensional potential and viscous approaches. Effects of inlet flow simulation on the engine nacelle pressure distribution, as calculated by one of these techniques, is presented in Figure 54. Note that the effect of inlet flow condition extends considerably downstream of this inlet, indicating the extent of the nacelle simulation necessary to account for the entire inlet mass flow effect.

An Euler equation solution mathematically describes the motion of an inviscid compressible fluid with variable entropy and can capture strong shocks and model jet exhausts. An inlet/forebody configuration has been analyzed with this technique to



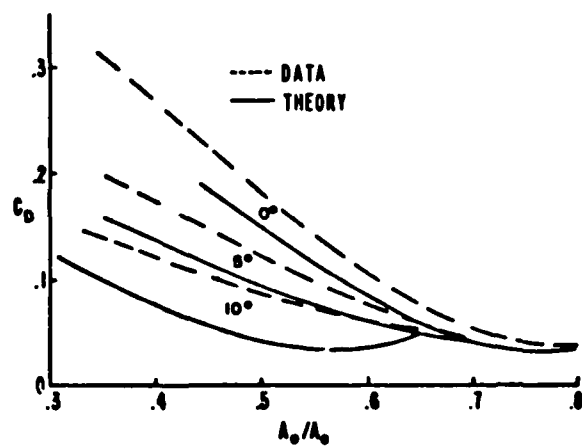


Figure 52. Inlet Drag Correlations (Reference 29)

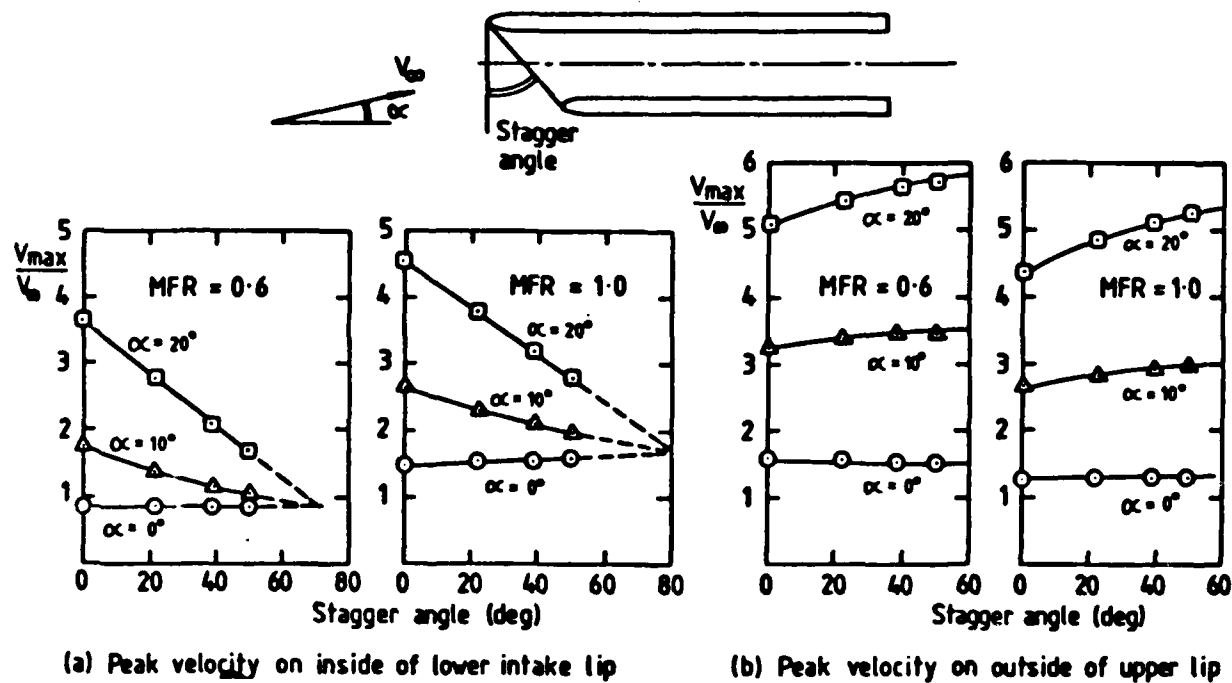


Figure 53. Theoretical Peak Velocities on Lips of a 2-Dimensional Staggered Intake (Reference 31)

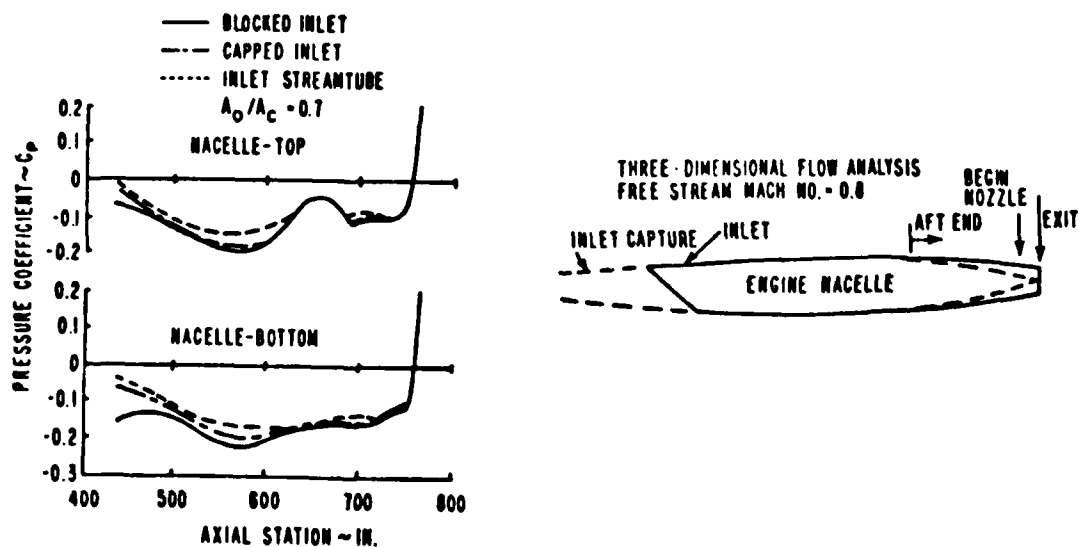


Figure 54. Predicted Twin-Jet Nozzle Pressure Distributions (Reference 29)

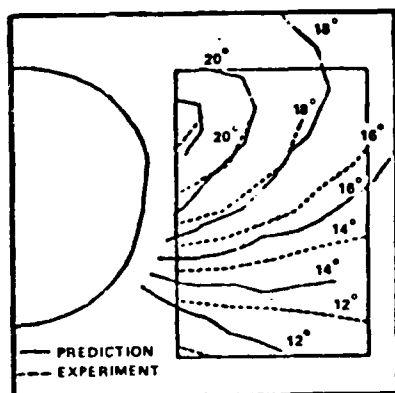
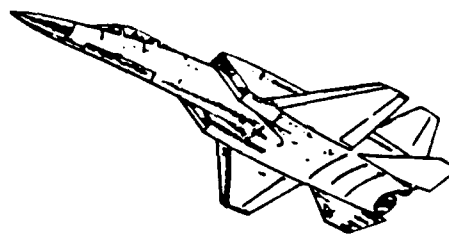
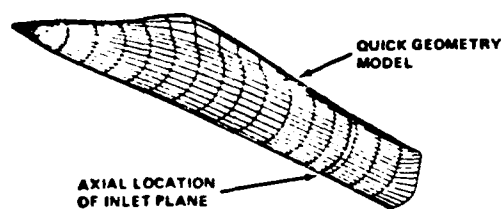
determine flow angularity near a potential inlet location (Reference 32). As shown in Figure 55, predicted flow angularities agree reasonably well with experiment.

Though not a direct example of a throttle dependent force calculation, the solution of a two-dimensional mixed compression inlet by a Navier-Stokes solution (Figure 56) indicates the potential for very detailed inlet analysis. This method (Reference 30) is described as a MacCormick explicit finite difference algorithm with modified treatment of the viscous sublayer and of the turbulent boundary layer. The method provides good agreement with experimental data, and while for the case shown, the solution ran for 1.6 hours on a CYBER 175, run times are being reduced so that practical applications can be achieved. Advanced inlet analytical techniques are being developed for three-dimensional viscous flow Navier-Stokes solutions.

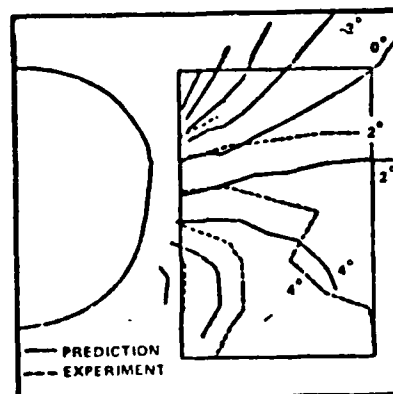
## 6. AFTERBODY/NOZZLE ANALYTICAL TECHNIQUES

References 15, 29, and 33 all point out the difficulty involved in modeling and predicting the flow over the afterbody nozzle region. Consequently, the throttle dependent forces due to changes in the nozzle boattail angle and jet plume are also difficult to predict since the afterbody/nozzle is dominated by strong viscous/inviscid interactions at subsonic and transonic speeds. As illustrated on Figure 57, this flow is characterized by pressure gradients which may cause the boundary layer to separate, a jet exhaust plume that may grow or diminish in size depending on nozzle pressure ratio (and in turn change freestream flow turning and jet entrainment), and a large viscous mixing region between the jet and external flow. If the external flow is transonic or supersonic, shock waves will also be present. Because of these strong viscous/inviscid interactions, inviscid theoretical methods have been found to be inadequate for predicting afterbody/nozzle flow. In general, nozzle surface pressures are difficult to predict, especially at transonic speeds, but trends can be predicted with more success than absolute values. As with the inlet, the full range of techniques, from empirical correlations to three-dimensional Navier-Stokes solutions, have been applied to predict afterbody nozzle forces.

Empirical force prediction techniques for exhaust nozzles are derived from parametric afterbody/nozzle data. Important geometric parameters include nozzle boattail angle, base area, initial plume angle, overall afterbody closure, nozzle

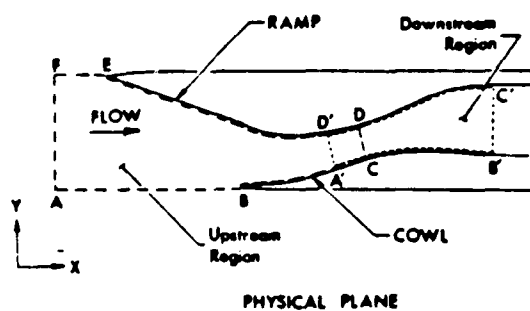


ANGLE-OF-ATTACK,  $\alpha$

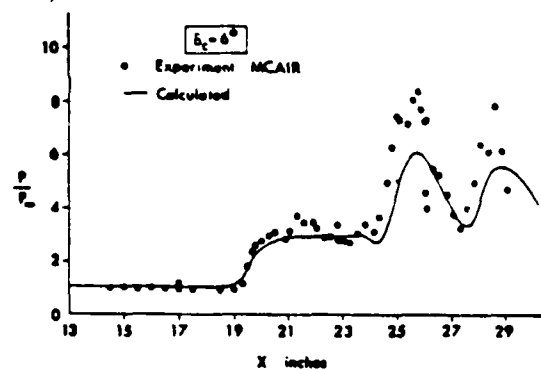


ANGLE-OF-SIDESLIP,  $\beta$

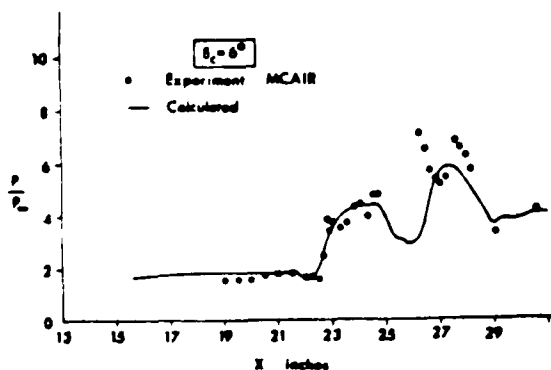
Figure 55. Inlet Flow Field Correlation for Side-Mounted Inlet:  
 $M = 2.5$ ,  $\alpha = 15^\circ$  (Reference 32)



Details of Inlet Geometry



Static Pressure on Ramp for  $\delta_c = 6^\circ$



Static Pressure on Cowl for  $\delta_c = 6^\circ$

Figure 56. Static Pressures on Inlet Ramp and Cowl (Reference 30)

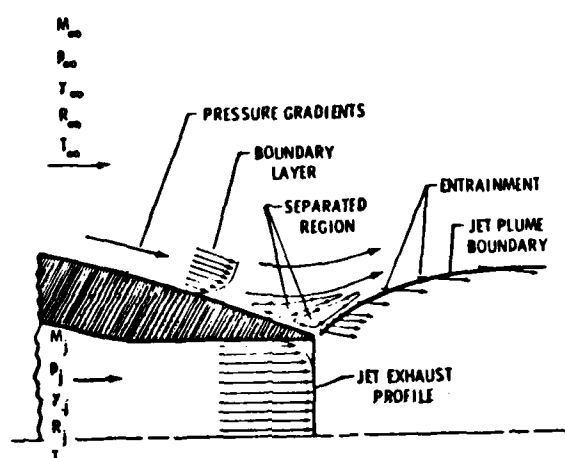


Figure 57. Schematic of Nozzle Afterbody Flow (Reference 33)

type and spacing, interfairing type, empennage location, and the proximity of lifting surfaces. In general, geometric effects and jet effects are handled separately. The geometry parameters can be characterized by the Integral Mean Slope (IMS) correlation. This parameter is an area weighted average slope of the non-dimensional cross sectional area plot and is proportional to the ideal pressure area integral of the afterbody/nozzle. The formulation and a correlation of the parameter at one Mach number are shown in Figure 58. The procedure provides a good prediction of afterbody pressure drag if the area is free of separation and is "clean", i.e., with minimum nearby empennage surfaces. This correlation is combined with a plume correlation parameter to account for the geometric as well as jet exhaust effects.

Subsonic viscous flow and patch methods which combine the inviscid regions with a boundary layer calculation and an exhaust simulation yield more rigorous subsonic/transonic solutions of the nozzle boattail flow field. These techniques include representations of the effects of skin friction, axial pressure gradients, jet entrainment, separated flow, jet mixing, and jet temperature. Two examples of these techniques are given in References 5 and 33. Bower (Reference 5) was able to predict the surface pressure distribution of an axisymmetric 15 degree boattail with a strong viscous/inviscid interaction method (Figure 59). The method of Wilmoth, described in Reference 33, is a patch method which combines an inviscid flow field, a boundary layer, a mixing layer between the jet and freestream, and a displacement thickness corrected for jet plume entrainment and growth. A comparison of predicted boattail pressures at different nozzle pressure ratios compared to experimental data is shown in Figure 60. This method provides a good prediction of pressure distribution, and is capable of accounting for jet temperature, and jet chemical composition. This is an interactive procedure which uses approximately 30 seconds processing time on a CYBER 175 computer. More work is needed to refine the code for use in describing regions of boundary layer separation.

A strictly supersonic external nozzle boattail flow calculation can be approached by utilizing a small perturbation potential flow solution. Often this can be accomplished by a Method of Characteristics solution.

A more robust technique is a time dependent finite difference solution to the compressible Navier-Stokes equations for turbulent separating flows. Full three-dimensional, time dependent Navier-Stokes solutions including a turbulence model are

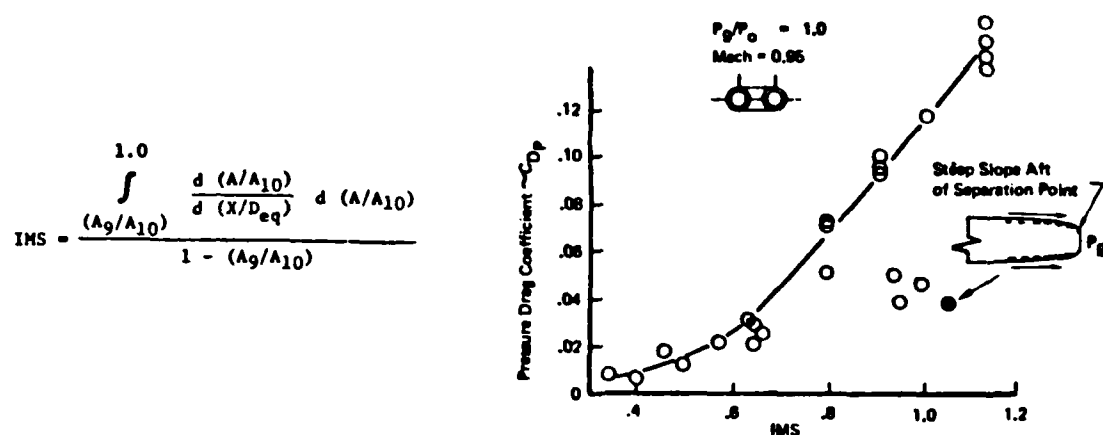


Figure 58. IMS Data Correlation (Reference 7)

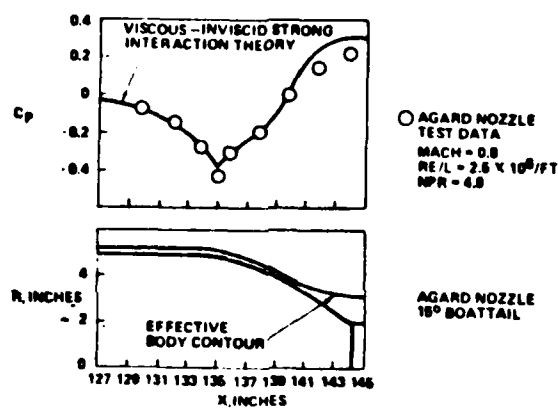


Figure 59. Analytical Prediction of Nacelle Boattail Pressures (Reference 5)

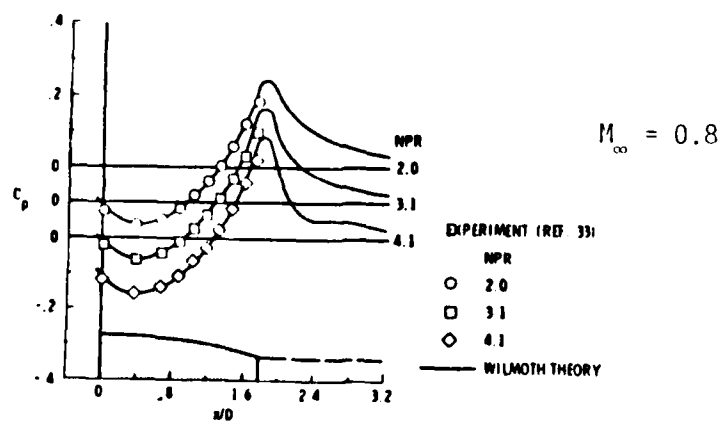


Figure 60. Comparison of Predictions of Patched Method with Experiment (Reference 33)

the goal of many researchers investigating this complicated flow field. These solutions require large computers and elaborate computational grid generation techniques and are being supplemented in the near term with approximate solutions to these equations. Good prediction across the Mach number range of the surface pressures of an axisymmetric afterbody is shown (Figure 61) in a calculation by Swanson (Reference 33). The results required 5 minutes computing time for a supersonic case and approximately 2 hours for a subsonic case on a CYBER 203 computer. A velocity splitting technique for solving the steady state three-dimensional Navier-Stokes equations at transonic speeds for general bodies has been developed by Cosner. This method has shown good agreement between theory and experiment for clean afterbodies with approximately 1/2 hour running times on a CYBER 175 computer (Reference 34).

## 7. TRANSPORT NACELLE ANALYTICAL TECHNIQUES

The predominately subsonic flow field of the transport nacelle has been approached primarily by potential flow codes and by axisymmetric Navier-Stokes solutions. Incompressible, inviscid techniques, corrected for compressibility and iterated to a solution are successful for entirely subsonic flowfields. Results of a low speed inlet calculation are shown in Figure 62. The incompressible solution with compressibility and boundary layer corrections agrees reasonably well with the data. Transonic relaxation potential flow techniques with an iterative boundary layer solution have also been applied to mixed flow problems. Application of these techniques to a transonic cowl is shown in Figure 63. Moderately good agreement is seen between test data and the analysis. Three-dimensional geometries, such as a nacelle pylon, are also solved by linearized compressible potential flow methods. A flow field of a powered nacelle, with the plume represented as a solid body, is predicted with some success (Figure 64).

Potential methods, three-dimensional linearized compressible potential flow solutions, are often utilized for the flow around high bypass ratio engines. The surface of the complex configurations and, to some extent, the inlet and nozzle flows, are represented by flat panels. A semi-empirical compressibility term for the highly curved regions at the inlet leading edge may be employed to account for the high local Mach numbers, Reference 35. A typical application of this approach is presented in Reference 36. The nacelle representation is comprised of 260 panels



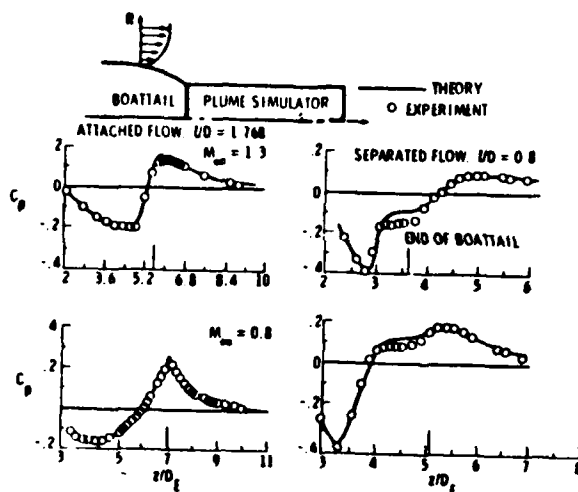


Figure 61. Navier-Stokes Solution by Swanson for Circular Arc Boattail Nozzles with Solid Plume Simulators (Reference 33)

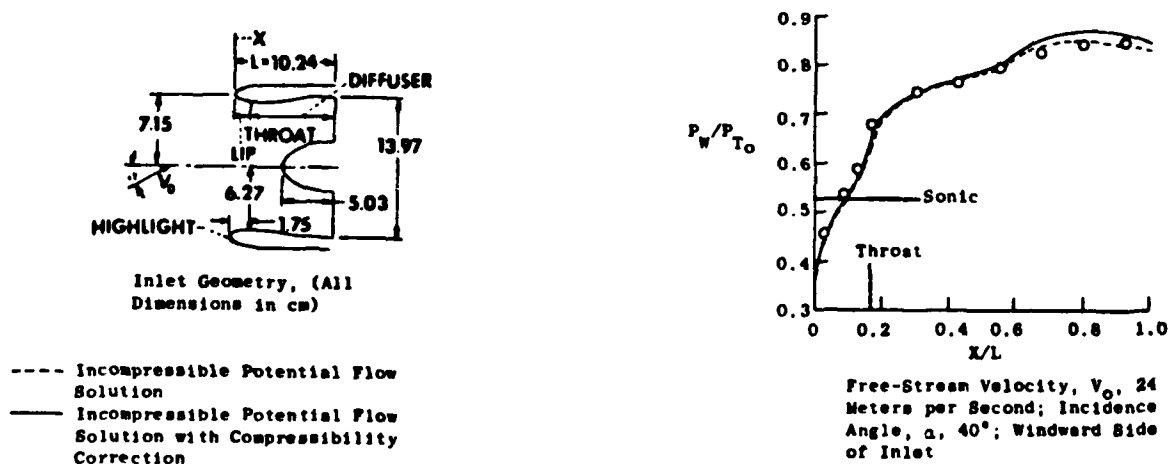


Figure 62. Comparison of Calculated and Measured Internal Surface Pressure Distributions (Reference 5)

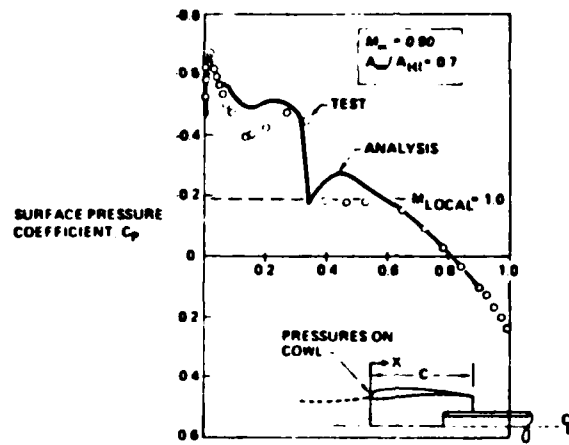


Figure 63. Transonic Cowl Pressure Comparison of Analysis and Test (Reference 5)

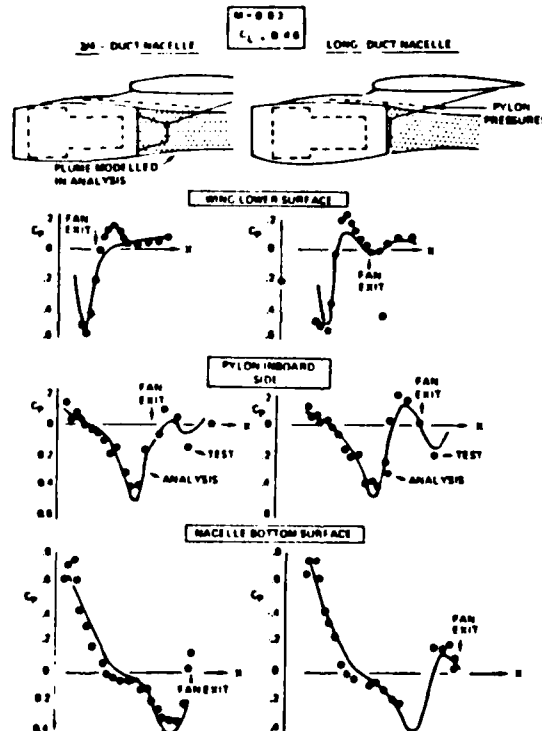


Figure 64. Comparison of Analytical vs. Measured Pressures for Installed Powered Nacelle (Reference 5)

and includes inlet suction, jet spreading, and flow entrainment. The wing/fuselage is represented by 160 panels. The wing pressures (Figure 65) with the jet on and off show good agreement between theory and wind tunnel test. Another application (Figure 66) is from Haberland (Reference 37) where an axisymmetric panel method predicted the inlet cowl pressures for two mass flow ratios. For the most part, the measured and predicted pressures agree. Leakage, a common problem for panel methods, is the difference in calculated and prescribed mass flow rates at the engine face and can be reduced by careful selection and distribution of panels around the cowl.

Euler solutions for transport nacelles are described in References 38 and 39. For a subsonic inlet at approximately 0.8 Mach number and 3 degrees angle-of-attack, a three-dimensional Euler solution agreed well with experimental pressure distributions along the top and bottom centerlines (Figure 67). The computed flowfield Mach contours are shown in Figure 68. On a long duct nacelle calculated with a three-dimensional Euler solver (Reference 39) the authors point out that an undesirable compression and reexpansion of the flow on the nacelle was predicted by the analysis; this encourages use of this method to help sort out propulsion integration problems.

NASA Langley Research Center has developed a Transonic Small Disturbance Theory analysis to predict flows around nacelle, pylon, and fuselage integrations. This method uses a multiple nested computing grid with coarse global grids and fine imbedded grids where needed. This method offers high resolution and flexibility for reasonable resources.

Limited Navier-Stokes solutions have been reported for transport nacelles. A mixed flow solution for a JT9D turbofan engine is summarized in Reference 41. At a Mach number of 0.9 and a nozzle pressure ratio of 2.6, the pressure distribution on the external fan cowl, afterbody, and plug shows good agreement between theory and experiment, Figure 69.

Some conclusions can be drawn from this brief review of analytical techniques for the complex flow field associated with throttle dependent forces. Empirical techniques are useful as predictors in preliminary design if care is exercised in their application and use. Two-dimensional and three-dimensional potential flow methods with boundary layer and compressibility corrections are moderately successful in predicting surface pressure distributions around inlets, nozzles, and

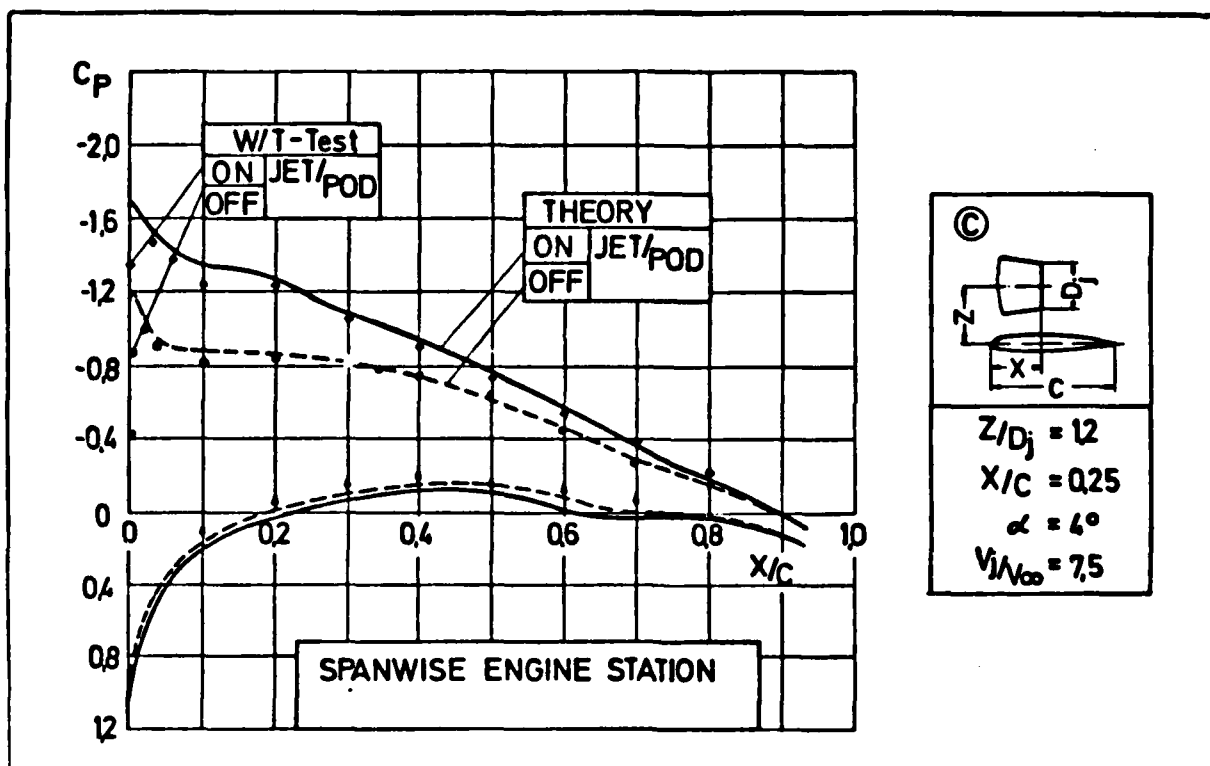


Figure 65. Wing Pressures at Engine Position (Reference 40)

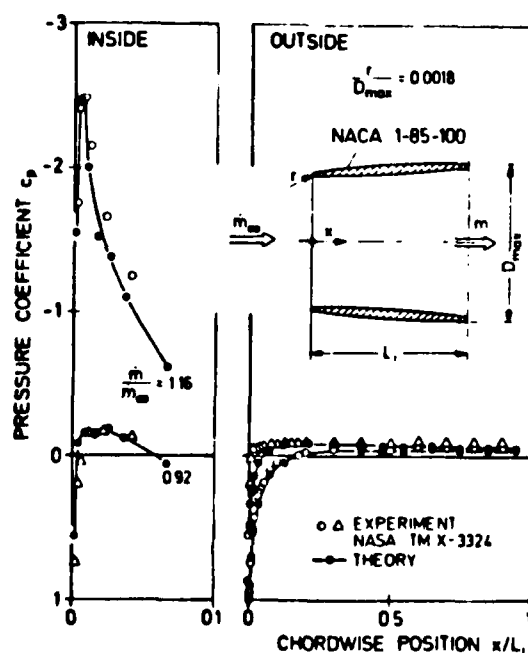


Figure 66. Pressure Distribution at an Axisymmetric Inlet NACA 1-85-100 (Reference 37)

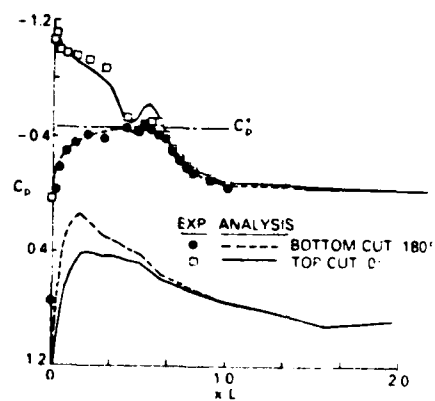


Figure 67. Comparison of Surface Pressure Coefficient  $M_\infty = 0.79$ ,  $MFR = 0.69$ ,  $\alpha = 3.06$  (Reference 38)

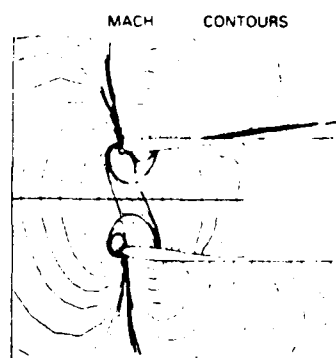


Figure 68. Calculated Mach Contours for Inlet at Angle of Attack (Reference 38)

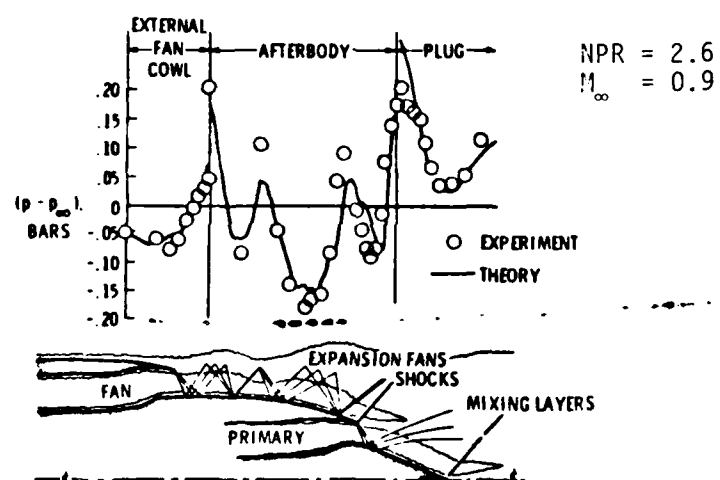


Figure 69. Navier-Stokes Solution of Peery and Forester (Reference 41)

nacelles. Solutions for separated regions and areas of mixed flow are difficult to obtain. Patching methods can provide a good prediction at reasonable cost. The solution of the Navier-Stokes equations is limited by the lack of a good turbulence model, by available data/computational storage, and by cost. All of the methods vary in success relative to the level of accuracy required and the level of resources available. Analytical methods of all levels of complexity can play a role in the prediction of throttle dependent forces. Readers are referred to Boppe (Reference 42) for a more complete summary of the state-of-the-art computational methods used in engine/airframe integration.

## SECTION IV

## WIND TUNNEL/ANALYSIS DETERMINATION OF THROTTLE DEPENDENT FORCES IN FLIGHT

The dynamic nature of an aircraft in flight makes determination of throttle dependent forces difficult, if not impossible. Aircraft are rarely instrumented to measure all of the parameters required, such as mass flow ratio, nozzle total pressure, exit static pressure, and inlet/nozzle surface pressures. Further, the aircraft can vary mass flow ratio or nozzle pressure ratio at a fixed Mach number only over a small range; this precludes determination of spillage or boattail drag at the off-design conditions. The alternative to flight determination of throttle dependent forces is to use wind tunnel data or analytical techniques to predict the throttle dependent forces. These predictions are then verified by correlating the measured or predicted surface pressure distributions with those measured in flight. Plots such as Figures 70 and 71 for the X-15 and XB-70, respectively, show examples of correlations of base pressures measured in flight with wind tunnel and analytical predicted values. This section will describe difficulties and discrepancies in using these correlations and will then present examples of wind tunnel and analytical pressure distributions compared to pressure distributions measured in flight.

## 1. SOURCES OF ERROR - WIND TUNNEL/ANALYSIS TO FLIGHT

Hunt and Gowadia (Reference 1) state that separate determination of inlet and nozzle throttle dependent forces is not possible in flight. Further, when relying on a wind tunnel model to determine these forces, it is not possible to test an accurate scale version of the aircraft due to support interference. In addition, there is no well-established method of reproducing the inlet and nozzle flows simultaneously in the model in order to measure their interference effects. Ayers (Reference 44) notes that prediction of full scale aircraft forces has been historically hampered by the inability to extrapolate nozzle boattail and base effects. This is primarily attributed to model support effects and an inadequate Reynolds number simulation. Due to wind tunnel limitations, model data is rarely acquired at flight Reynolds numbers; therefore, for flow areas with strong viscous effects and separated regions, such as an afterbody/nozzle, the wind tunnel simulation can be questionable. A compilation of possible causes of discrepancies between wind tunnel



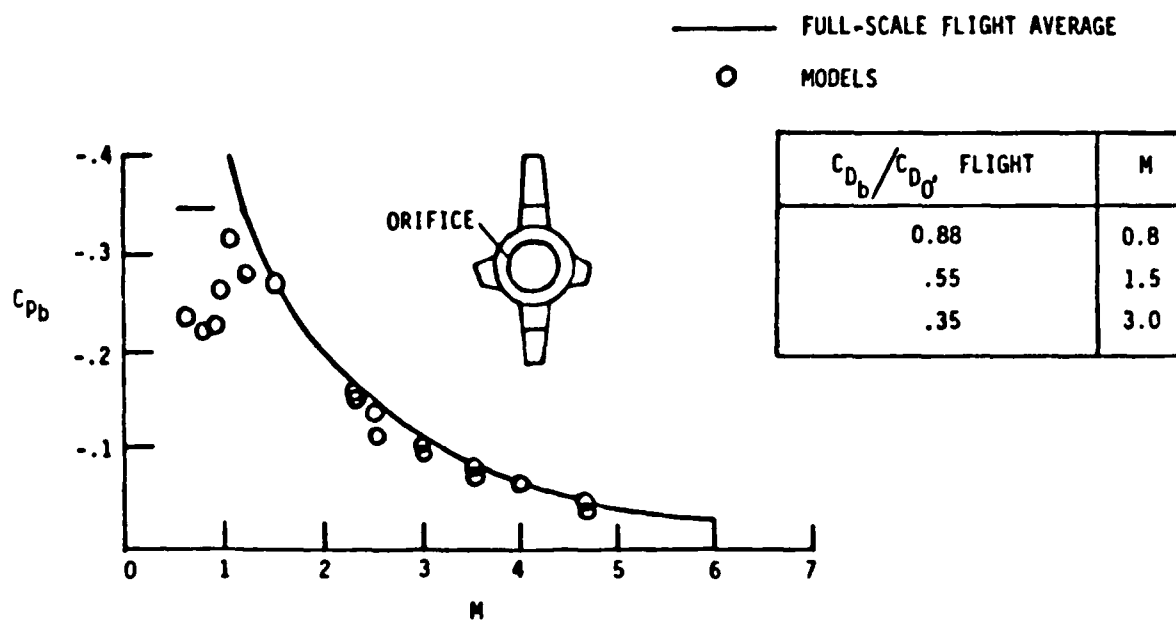


Figure 70. X-15 Fuselage Base Pressure Coefficients (Reference 43)

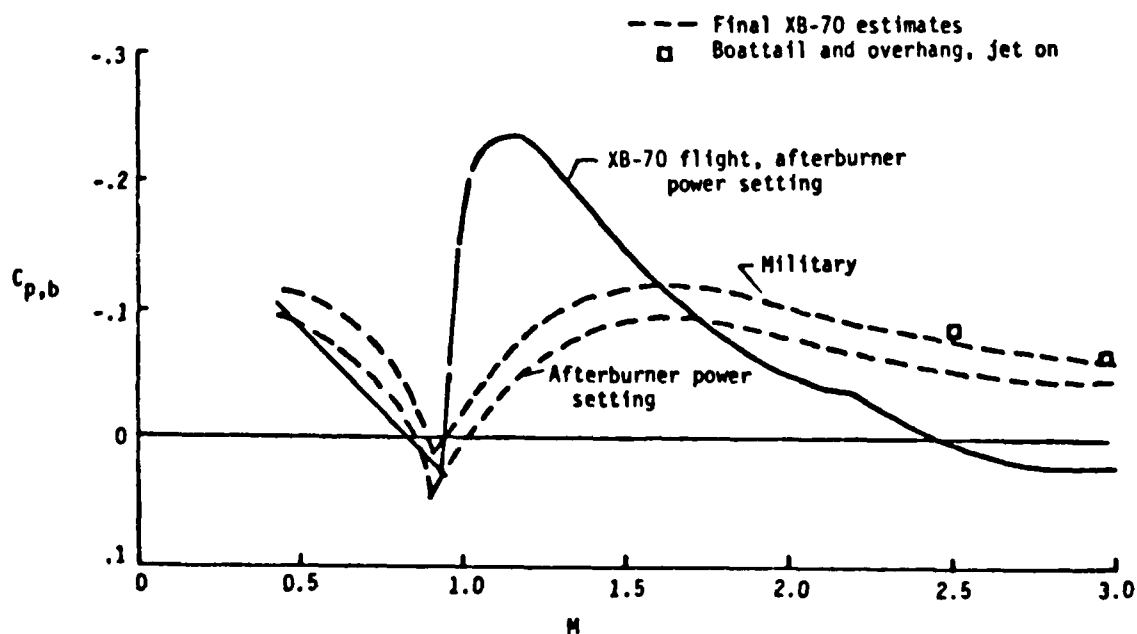


Figure 71. Comparison of Flight-Measured XB-70 Average Base Pressure Coefficient with Predicted Values (Reference 43)

and flight data developed from References 45, 46, and 29 includes: test techniques, wall and support effects, inadequate duplication of inlet/nozzle flow, wind tunnel flow quality, model detail, aeroelastic deformation of the aircraft in flight, scaling and Reynolds number effects, and incorrect assessment of inflight inlet/engine/nozzle operating characteristics.

All of these possible sources of error, plus those graphically presented in Figure 72, do not indicate that the task is impossible, but rather point out the special care and consideration required to simulate these propulsion/airframe interactions. The next section will present four examples of the correlation of wind tunnel data and analysis with flight data where different levels of success have been achieved.

## 2. WIND TUNNEL/ANALYSIS TO FLIGHT CORRELATION - EXAMPLES

Since throttle dependent forces are very difficult to determine in flight, wind tunnel and analytical assessments of these forces must be resolved from surface pressure distributions. Accuracy of these methods is verified by comparing experimentally or analytically predicted pressure distributions with flight data. These comparisons have been performed on several aircraft systems, including the B-1 and F-15, which were the subject of extensive wind tunnel to flight correlations. In these correlations, special attention was paid to the inlet and nozzle. Less detailed comparisons have also been completed for the YF-17 and Tornado aircraft and will be presented in the following section.

### B-1

A correlation between wind tunnel and flight inlet and nozzle pressure data was performed with the objective of eliminating as many of the potential discrepancies between the data sets as possible. Wind tunnel data was taken after the flight test to ensure matching of conditions, and the surface pressure orifice locations were as closely matched as possible. Support interference was determined in a series of wind tunnel tests to remove effects of this parameter. Factors which could not be simulated were wing flexibility and the resulting wing gap between the propulsion nacelle and the lower wing surface, environmental control system (ECS) purge air mass flow and pressure, and absolute Reynolds number. To account for these factors, the model wing was tested to determine the approximate wing gap effect and the ECS

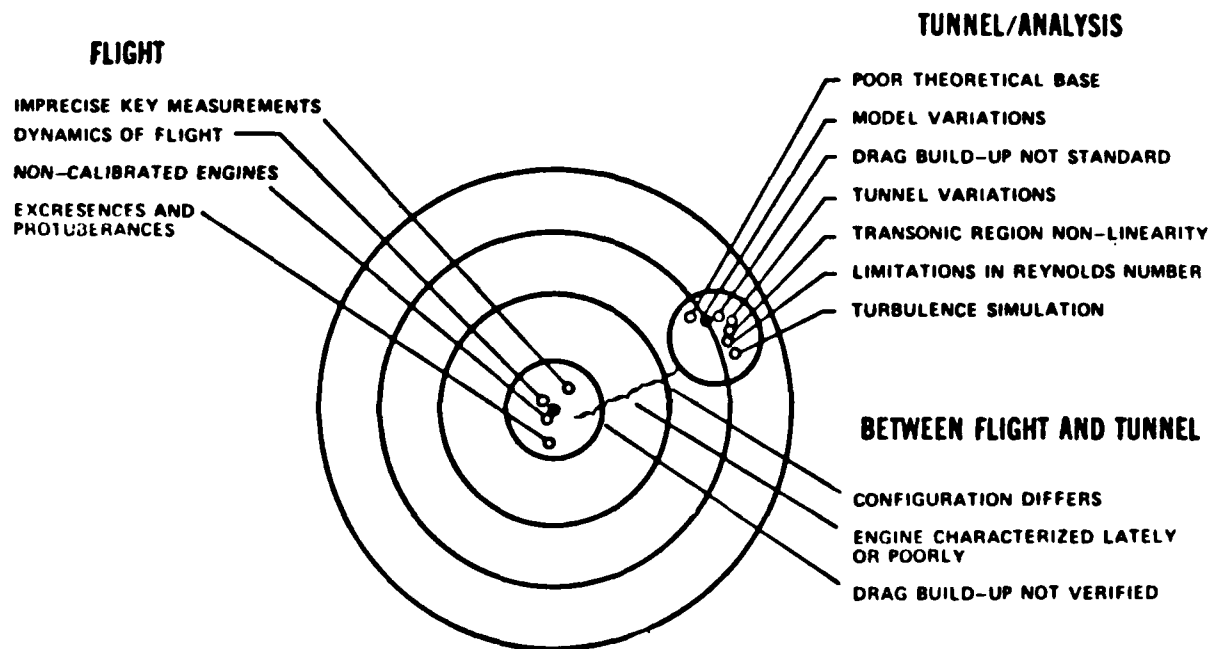


Figure 72. Sources of Error in Throttle Dependent Drag Predictions  
(Reference 46)

air was varied to determine its effect, but an absolute simulation of these parameters was not possible. Absolute Reynolds number was 20 to 40 times greater for the aircraft than the 6 percent propulsion model. In addition to the flight vehicle and the propulsion wind tunnel model, data were also obtained on a 20 percent inlet/forebody model with bypass and bleed and on a 7 percent inlet force model to determine inlet ramp and cowl forces. Pressure taps were matched at 200 locations on the left hand inlet and aft nacelle of the B-1 aircraft and wind tunnel models (Figure 73). In general, the pressures showed good agreement between wind tunnel and flight test data. Agreement was better in the nozzle region than the inlet, and the pressure area integrated drag estimates correlated to within approximately 10 drag counts. It should be noted, however, that differences in local pressures existed but tended to cancel, thus resulting in the final correlation. A comparison of the inlet cowl pressures, shown installed in Figure 74 and as pressure coefficients in Figure 75, shows better agreement for the 6 percent aircraft model than the partial aircraft simulation of the 20 percent model. The 20 percent model's pressure coefficient deviation was attributed to flow field interference from the large cross-sectional area of the mass flow metering system and the downstream model support. Changes of inlet drag with mass flow are shown in Figure 76. The wind tunnel model drag values are consistently higher (3-10 drag counts) but show similar trends with mass flow.

Nozzle surface pressure measurement locations in the afterbody/nozzle region for the flight vehicle and wind tunnel model are shown in Figure 77. Comparison of pressure data yielded results similar to those for the inlet, i.e. the pressure distributions were comparable, with some local pressures higher and some lower. Integrated pressure drag values are within 8 drag counts subsonically and 15 counts supersonically (Figure 78). As before, the data trends are parallel. These differences are attributed to nozzle crossflow, some unaccounted support system interference, inlet fairing effects, incorrect environmental control system air simulation, and inadequate simulation of separated regions on the wind tunnel model.

The issue of independent assessment of inlet and nozzle propulsion flow was also addressed in this study. Varying this inlet's mass flow changes the drag of the reference nozzles by 4 drag counts at the operating condition (Figure 79). Support interference studies provided insight into the magnitude of sting and strut effects. As shown in Figure 80, the model was tested upright and inverted to

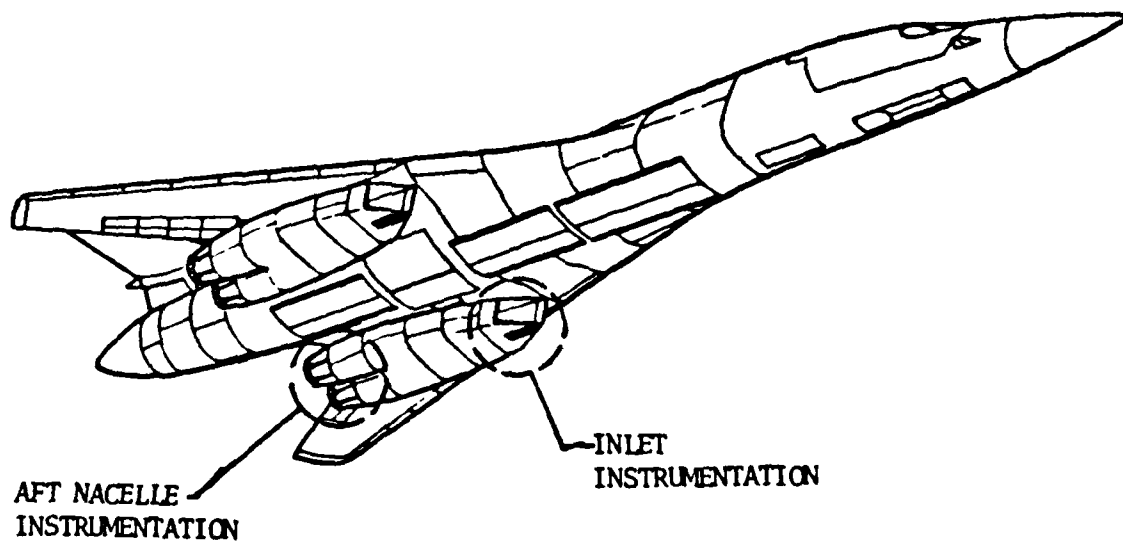


Figure 73. B-1 Nacelle Instrumented Regions (Reference 47)

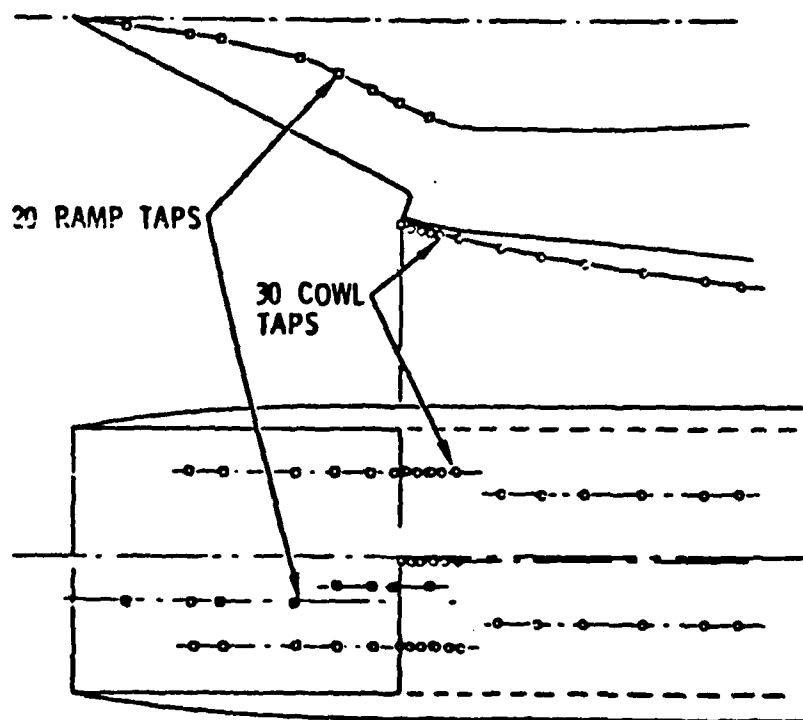


Figure 74. Inlet Surface Pressure Instrumentation Common to the Wind Tunnel Models and Aircraft (Reference 47)

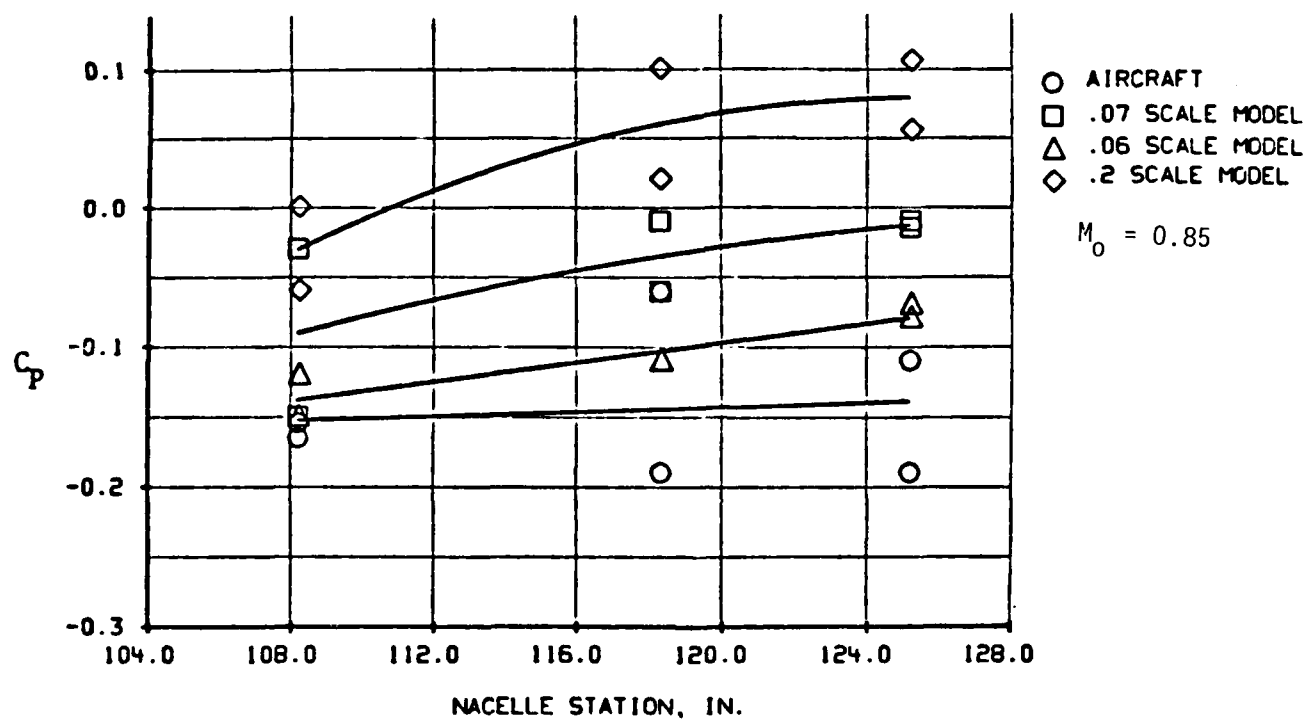


Figure 75. Aircraft and Model Inlet Cowl Pressures (Reference 47)

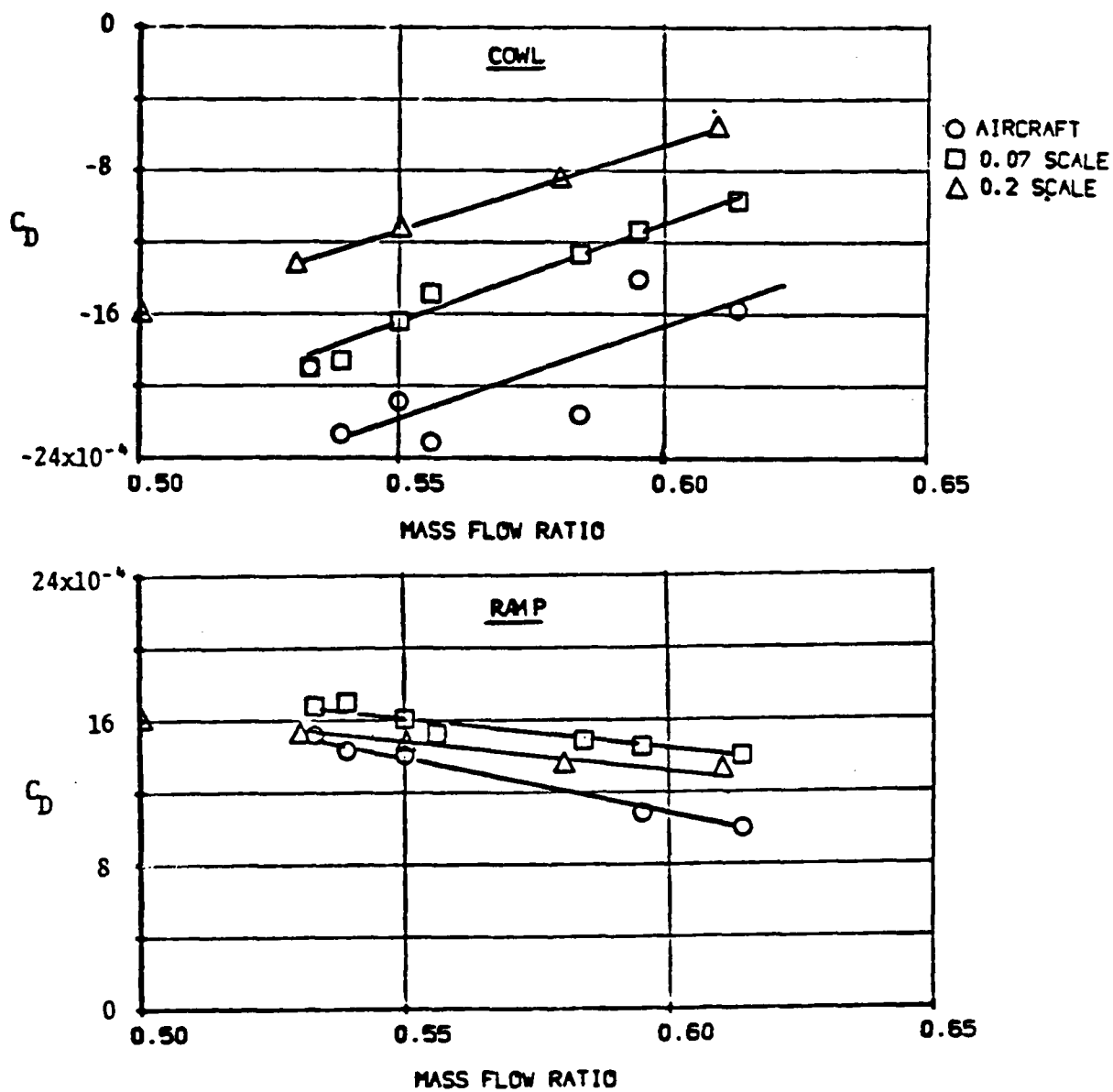


Figure 76. Drag Coefficient Variation with Mass Flow Ratio (Reference 47)

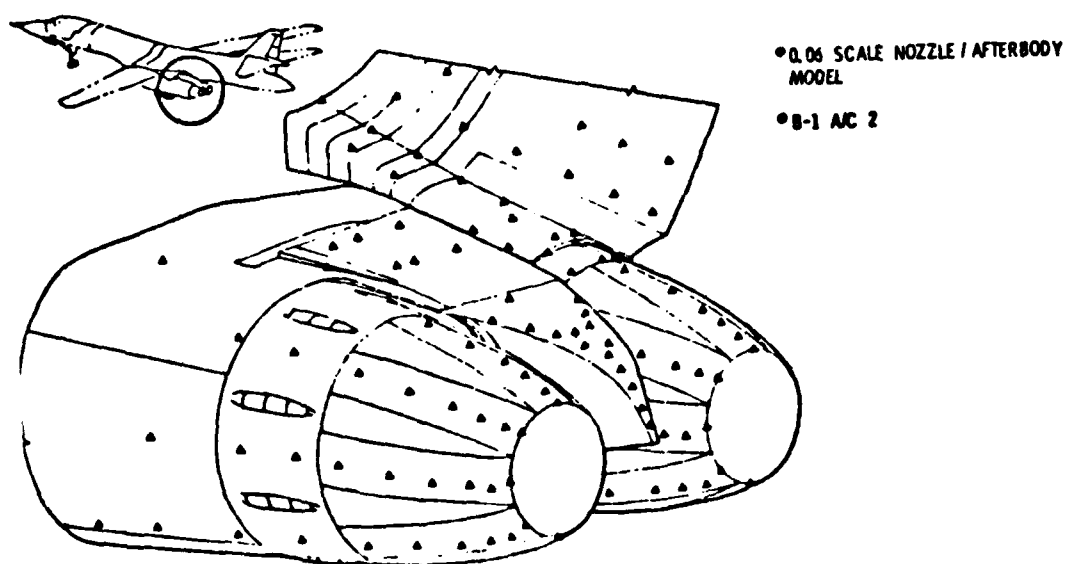


Figure 77. Aft Nacelle Isometric Showing Measurement Locations  
(Reference 48)



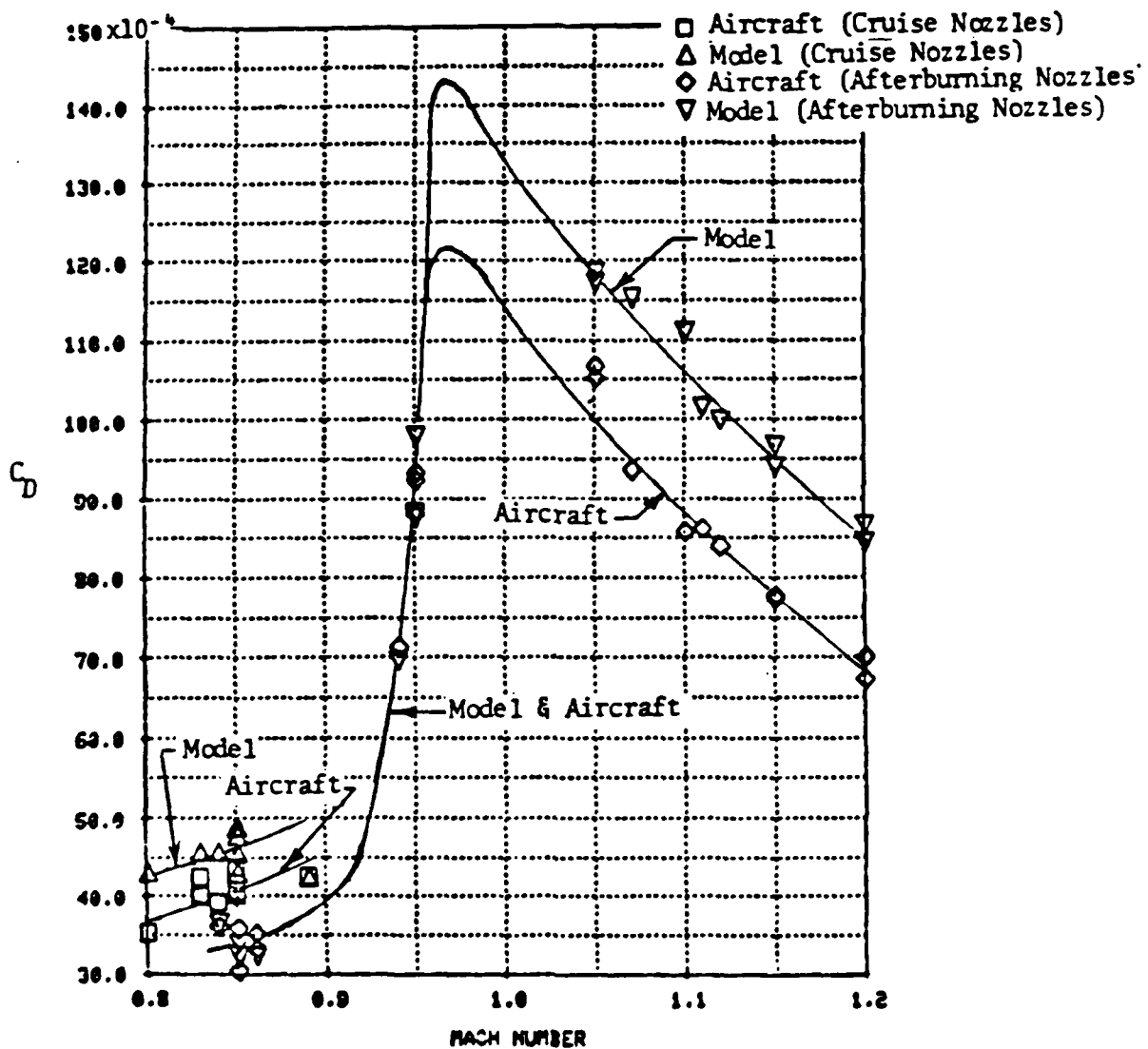


Figure 78. Aft Nacelle Drag - Model and Aircraft (Reference 47)

## INLET MFR EFFECTS

• 0.80 Ma, REF. NOZZLES

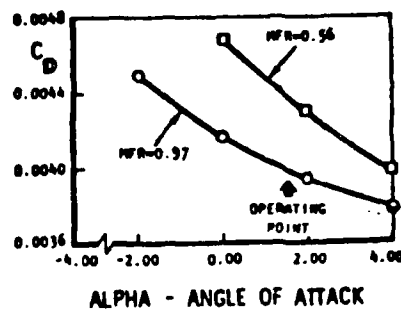


Figure 79. MFR Effect on Aft Nacelle/Nozzle Drag (Reference 48)

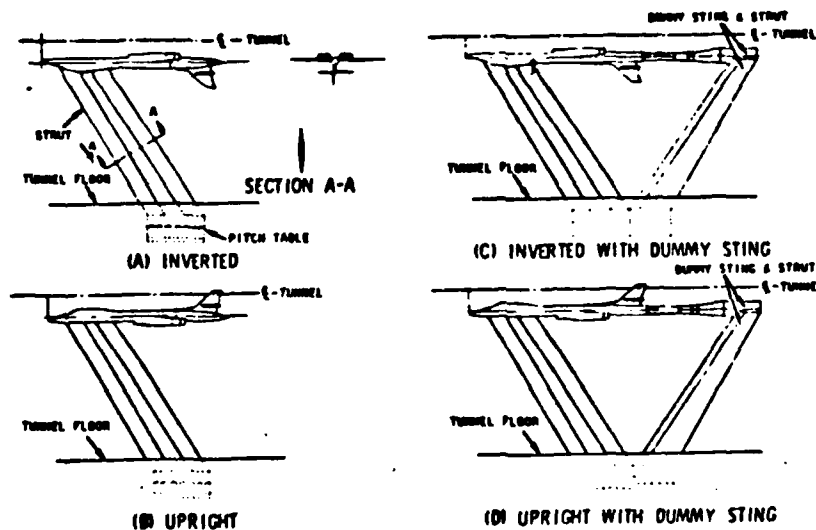


Figure 80. Model Installations (Reference 48)

determine a strut effect. This effect was determined to be 3 drag counts at 0.85 Mach number and 6 drag counts at 1.1 Mach number. The model was also tested to determine a sting interference effect for corrections to the aerodynamic model. Figure 81 illustrates that the effect on the afterbody nozzle drag is 2 to 10 drag counts, depending on Mach number. This correlation effort for the highly interactive flow on the B-1 aircraft nacelle pointed out the difficult technical problems surrounding determination of throttle dependent forces.

#### F-15

The F-15 wind tunnel to flight test data correlation effort is well documented. Representative references include 9, 49, and 50. The 7.5 percent F-15 wind tunnel model and flight vehicle were instrumented with approximately 80 static surface pressures in the inlet and nozzle region. The wind tunnel model was tested at 0.6, 0.9, and 1.2 Mach number over a range of angles-of-attack and mass flows. Not simulated were a variable bypass door, scaled inlet throat probes, or a hot jet exhaust. Pressure coefficient uncertainty targets were  $\pm 0.005$  for the wind tunnel test and  $\pm 0.03$  for the flight test. Flight tolerances desired were: angle-of-attack  $\pm 0.25$ , angle of yaw  $\pm 0.25$ , and Mach number  $\pm 0.01$ . Wind tunnel Reynolds numbers were usually 12 million, compared to a flight Reynolds numbers of 150 to 280 million. Inlet ramp and cowl pressure instrumentation locations are shown in Figure 82. Except downstream of the throat slot bleed/bypass exit, good agreement exists between wind tunnel and flight test data for upper cowl pressures (Figure 83). Similar agreement was evident on the wing fairing (Figure 84). Comparison of the pressure area integrated drag from the wind tunnel and flight vehicle and the wind tunnel force balance measurements (Figure 85) show the drags correlate well at 0.6, 0.9, and 1.2 Mach number across the range of inlet capture ratios. A problem does exist at higher capture ratios for 0.6 Mach number. This discrepancy between the wind tunnel, flight and force balance drag data is attributed to the large flow angularity at the inlet lip for which the pressure area integration cannot account. Additional testing technique development for improving the measurement technique near the inlet lip is required.

Pressure instrumentation locations on the nozzle boattail are illustrated in Figure 86. Nozzle pressures correlate well except for the pressures on the nozzle sides near the interfairing or tail booms. One other point of interest concerning throttle dependent forces is shown in Figure 87. Changing the inlet rotation angle

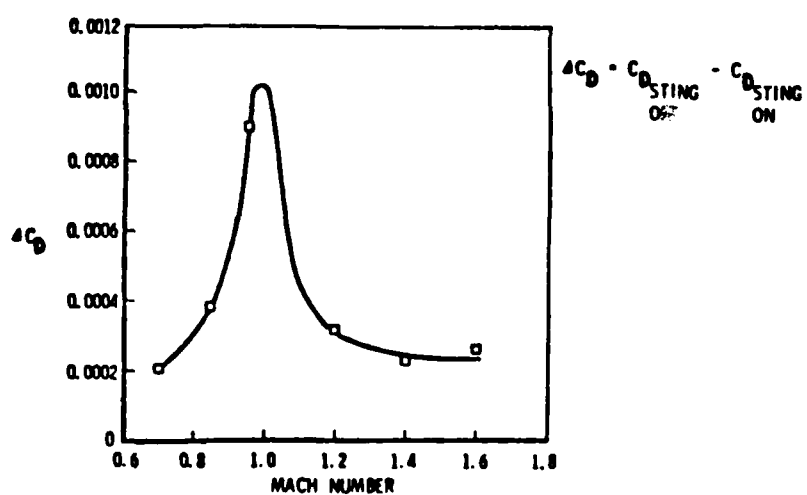


Figure 81. Sting Effects (Nozzle/Afterbody Tests) (Reference 48)

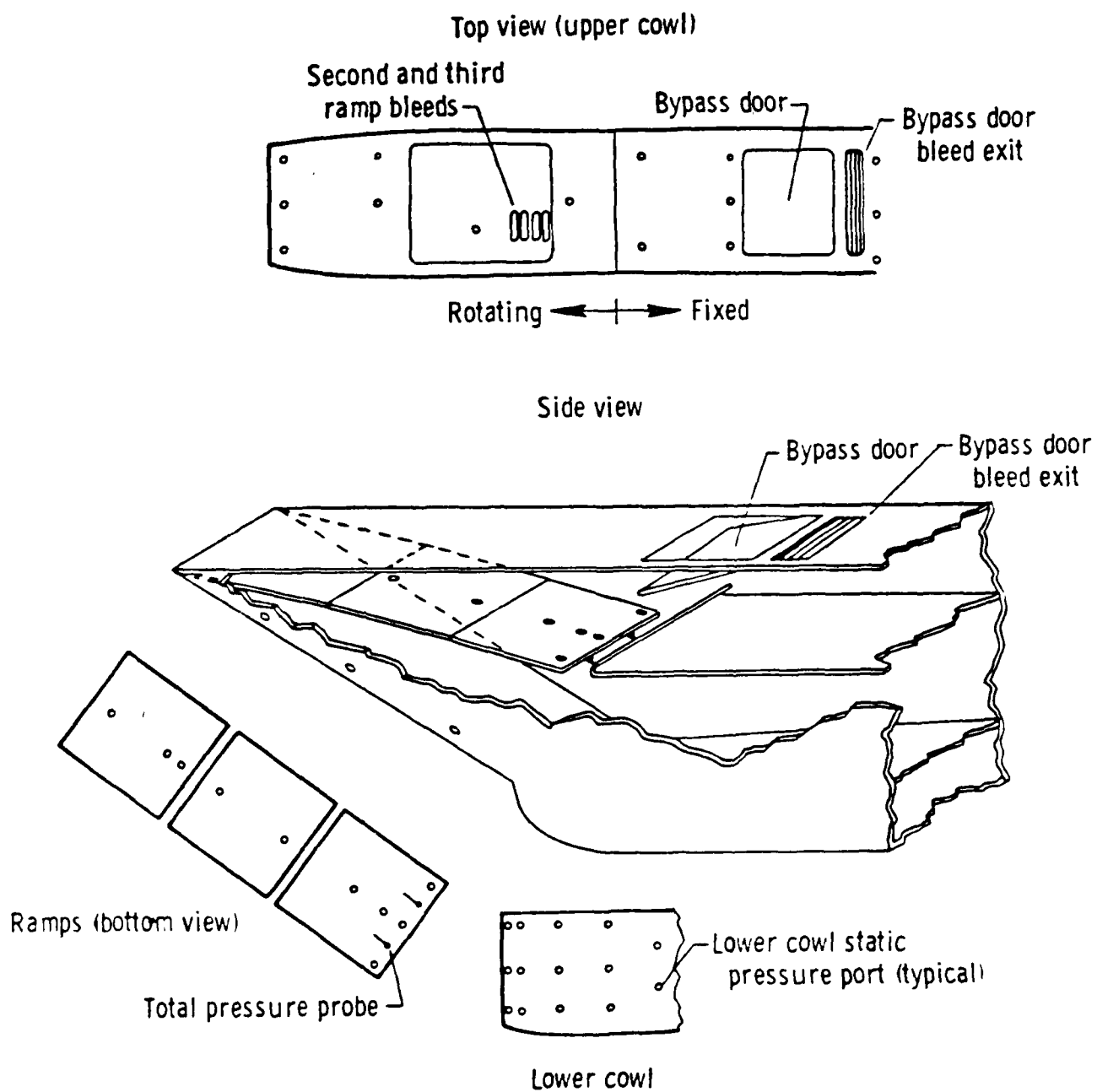


Figure 82. F-15 Inlet Pressure Orifices (Reference 49)

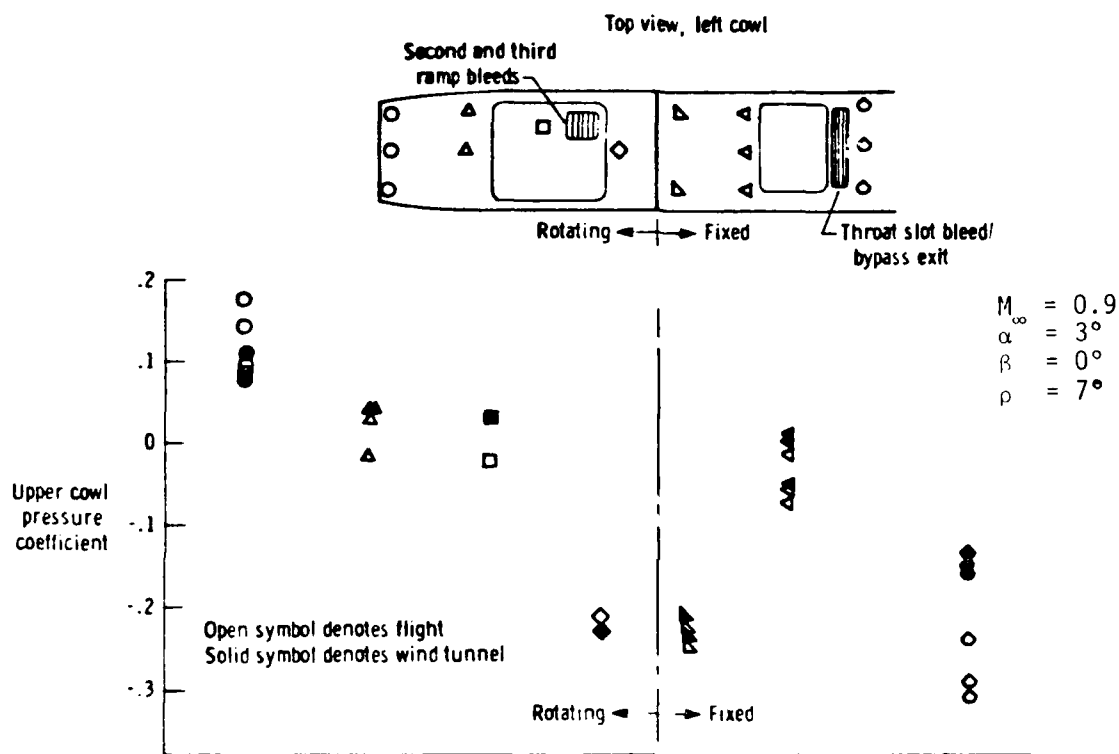


Figure 83. Comparison of Flight and Wind Tunnel Pressure Coefficients for Upper Cowl Surface (Reference 9)

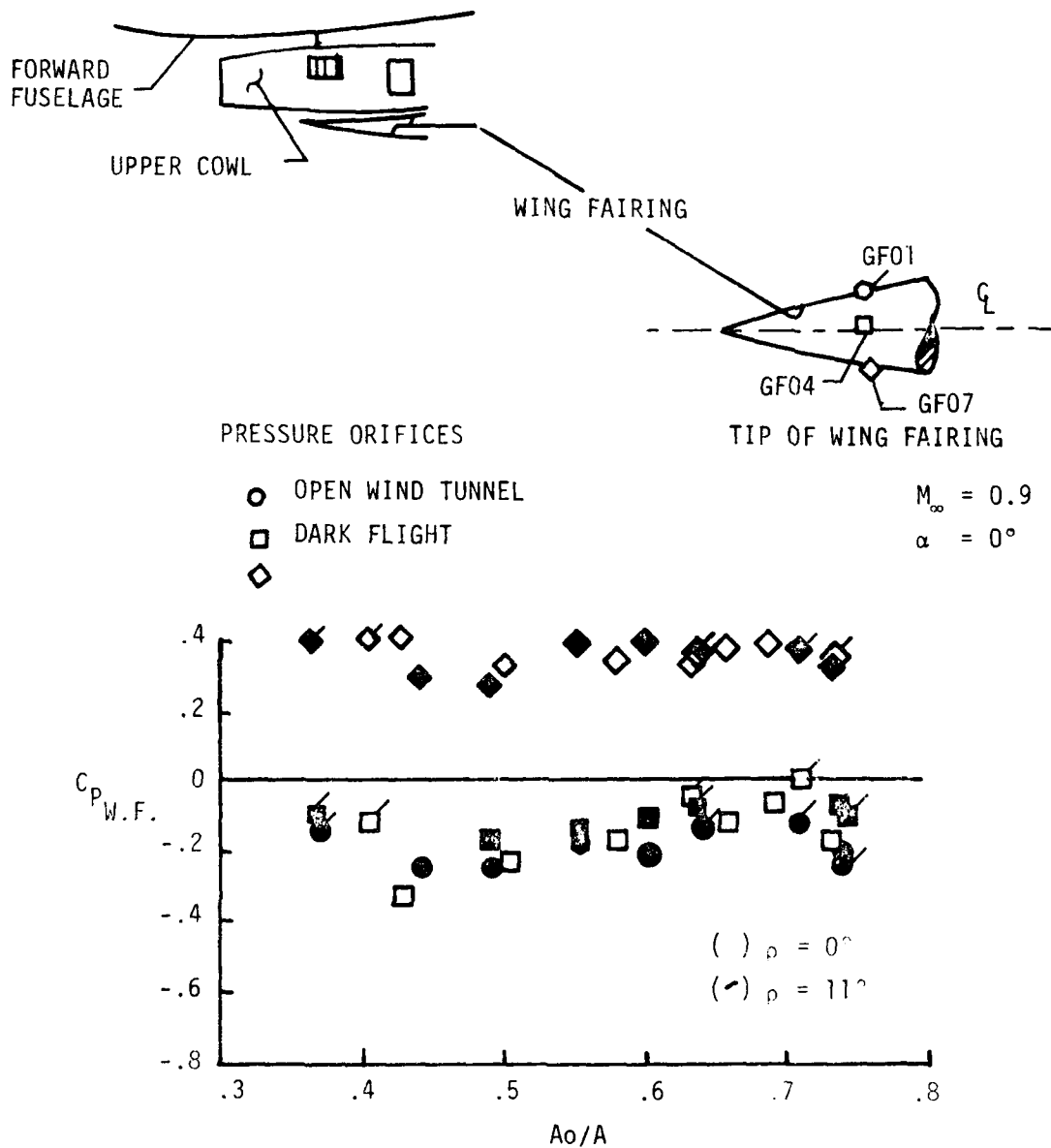


Figure 84. Effect of Capture Area Ratio on Wing Fairing Pressure Coefficients (Reference 49)

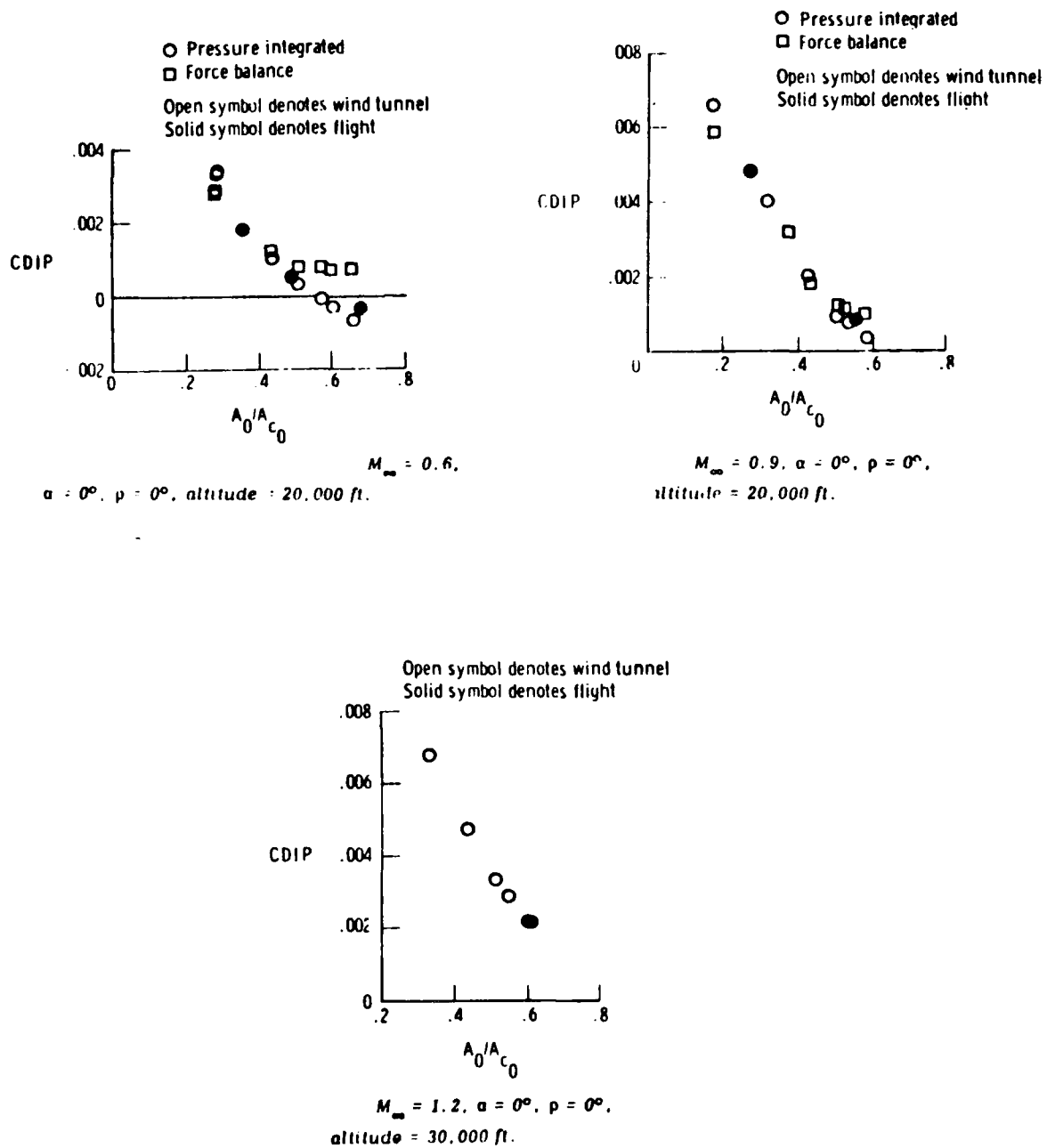


Figure 85. Comparison of Wind Tunnel and Flight Pressure-Integrated Drag (Reference 9)



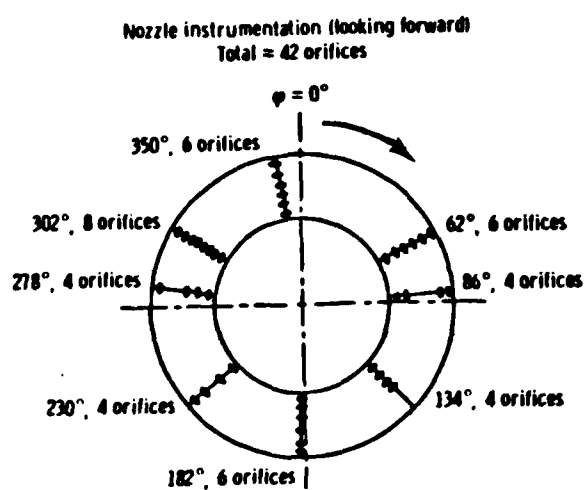


Figure 86. F-15 Nozzle Pressure Orifices (Reference 50)

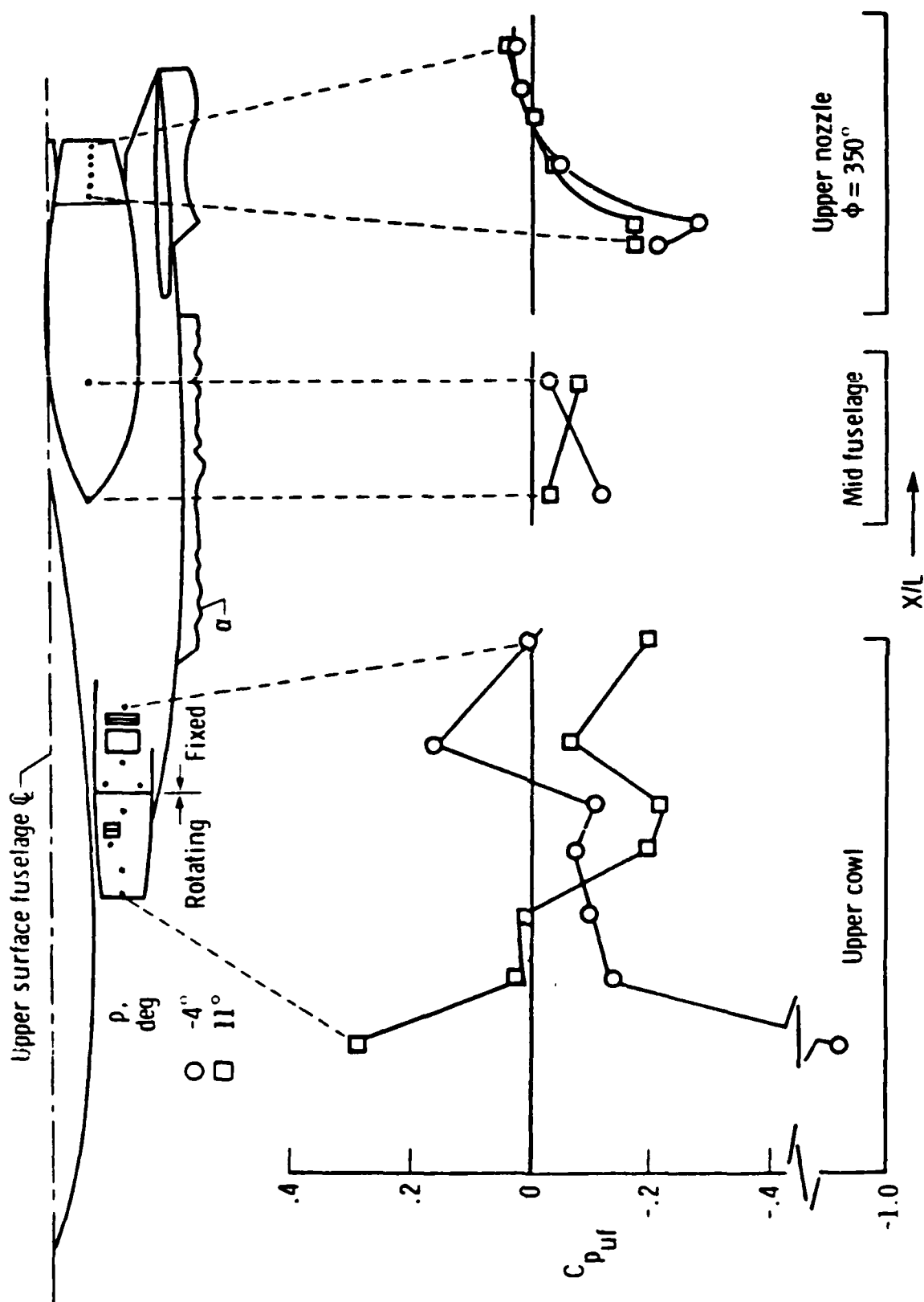


Figure 87. Upper Fuselage Pressure Coefficient (Reference 49)

produces the expected upper cowl pressure changes, but also unexpectedly changes the mid-fuselage and upper nozzle pressures. This illustrates a pressure distribution change over the entire aircraft due to inlet geometry variations. These changes may not be accounted for in conventional testing techniques.

#### YF-17

Flight test surface pressure data correlations were performed with the YF-17 aircraft. Primary emphasis was in the nozzle boattail area (Figure 88). Two wind tunnel models, 10 and 20 percent scale, were tested at Arnold Engineering Development Center from 0.6 to 1.5 Mach number over a range of angles-of-attack and nozzle pressure ratios. Identified model-to-flight sources of error were support interference, cold exhaust simulation, faired inlet, lack of adequate engine bay purge air simulation, inaccurate variable exhaust nozzle and speed brake modeling, and Reynolds number differences. Wind tunnel repeatability was  $\pm 0.0005$  for pressure coefficient,  $\pm 0.1$  degree angle-of-attack, and  $\pm 0.10$  nozzle pressure ratio. Flight test pressure coefficient uncertainties were  $\pm 0.0002$  to  $\pm 0.011$ , depending on altitude and Mach number. To evaluate support interference, the model was held by a sting support with and without a dummy wing tip support (Figure 89). All possible corrections were incorporated. As a result, for both 0.6 and 0.9 Mach number, the wind tunnel and flight pressures correlated well, though some differences were present near the wind tunnel model metric breaks. Pressure comparisons at 0.6 Mach number are presented in Figure 90. Data for 1.2 Mach number, Figure 91, indicates more expansion and recompression was present in the flight data than in the wind tunnel data. This is attributed to the thinner flight boundary layer at higher Reynolds numbers and to the difference in nozzle construction from a solid model to a flight article with flexible nozzle boattail leaves and seals. In general, the support system interference was not significant subsonically but must be considered to achieve good supersonic correlation of wind tunnel and flight test data.

#### TORNADO

The multi-national Tornado aircraft was also the subject of a general correlation of wind tunnel and flight test afterbody pressures. The aircraft and afterbody nozzle (Figure 92) were pressure instrumented in the boattail and base regions to compare with data from the wind tunnel model (Figure 93). Upper and lower surface boattail pressure data are compared to flight test pressures at subsonic speeds in Figure 94. Pressure data on the wind tunnel model show good

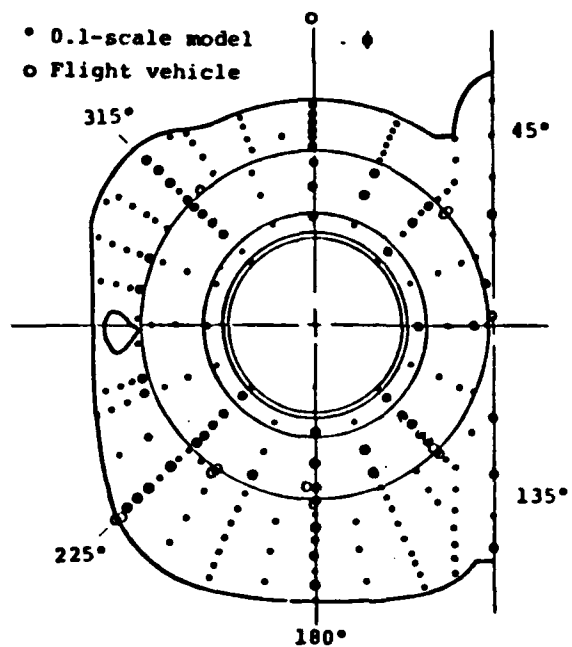


Figure 88. Pressure Orifice Locations-Left Engine Nacelle and Nozzle (Reference 51)

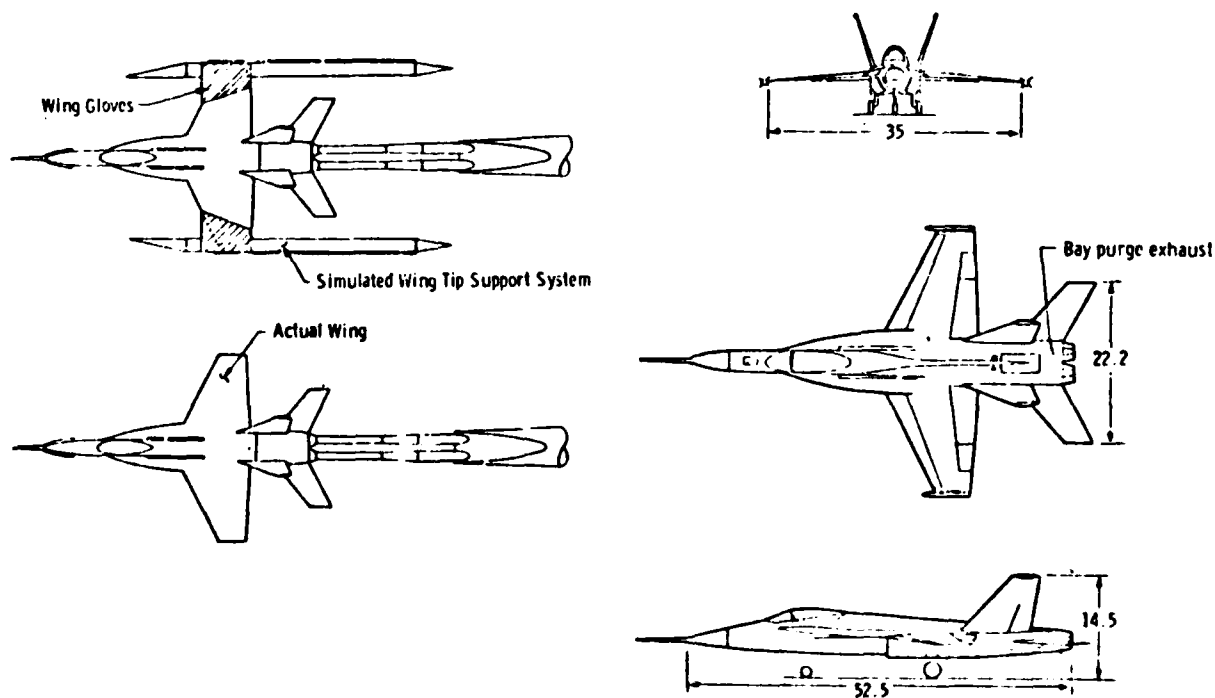


Figure 89. Support System Interference Models and YF-17 Aircraft (Reference 51)

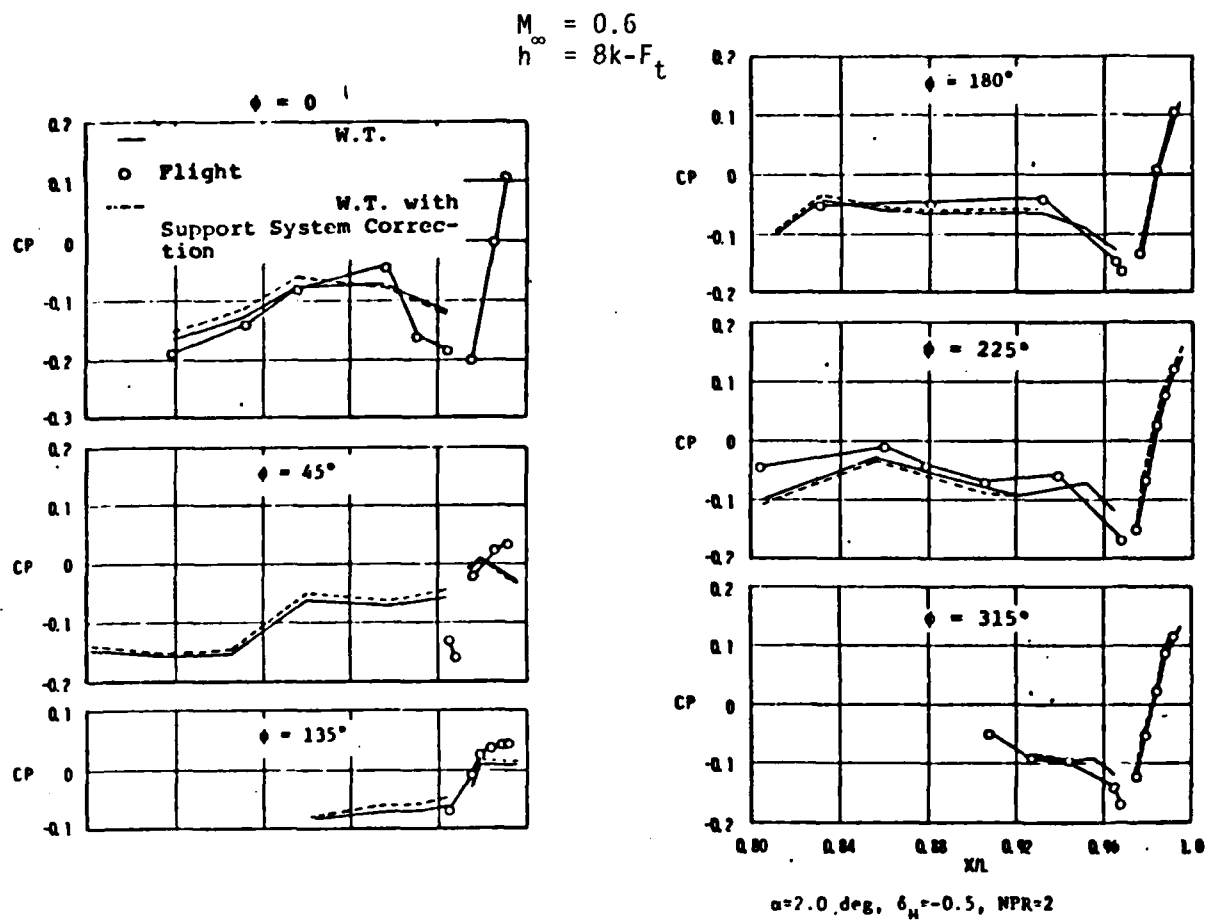
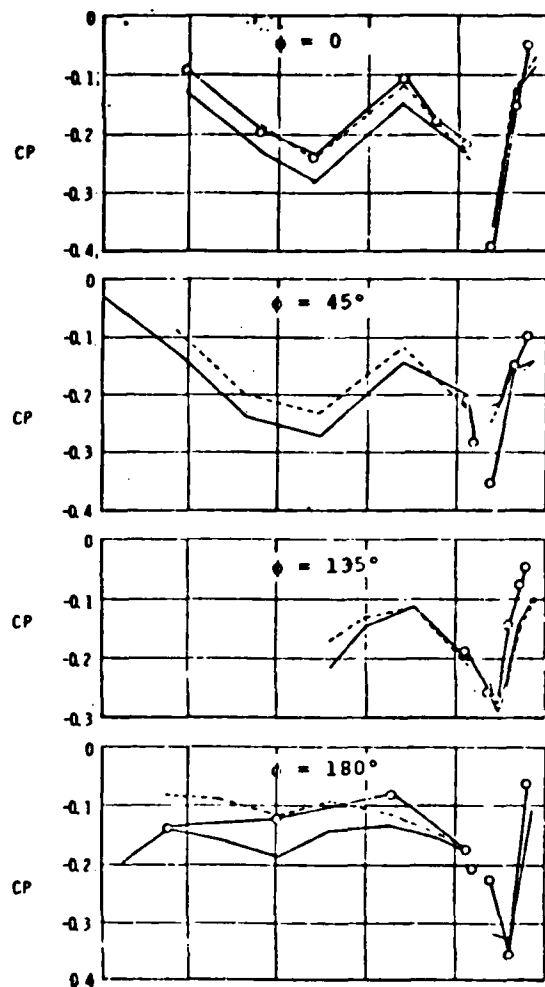


Figure 90. Surface Pressure Distributions-Cruise Nozzle Configuration (Reference 51)



$M=1.2$ ,  $H=27K-ft$ ,  $NPR=6$ ,  $\alpha=2.1$  deg,  $\delta_H=-1.9$  deg

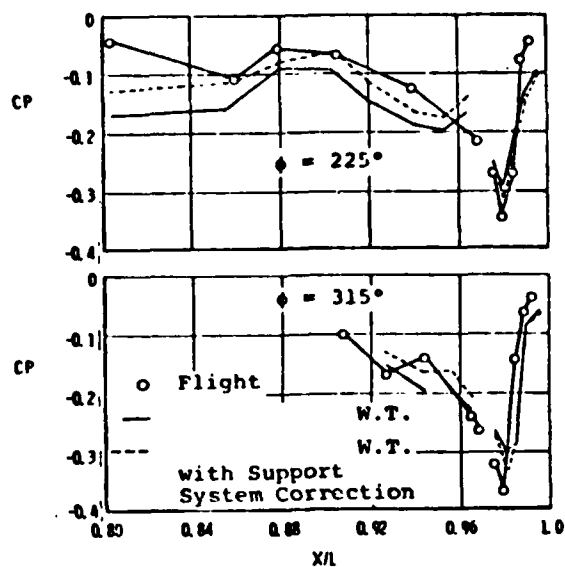
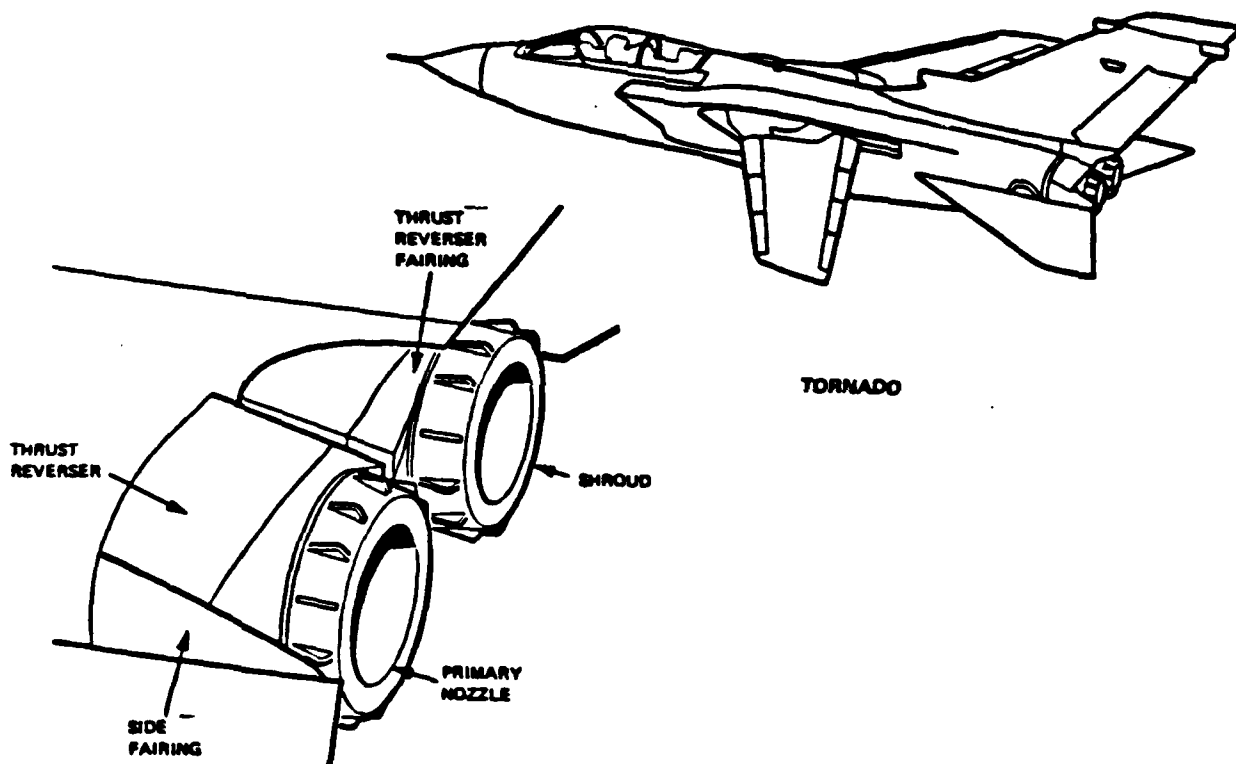


Figure 91. Surface Pressure Distribution Reheat Nozzle Configuration (Reference 51)



PROTOTYPE AFTERBODY

Figure 92. Tornado Prototype Afterbody (Reference 52)

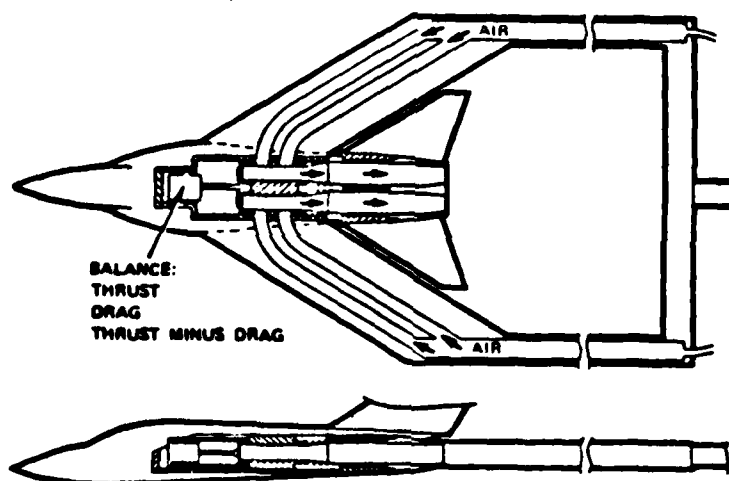


Figure 93. Tornado Afterbody Model (Reference 52)

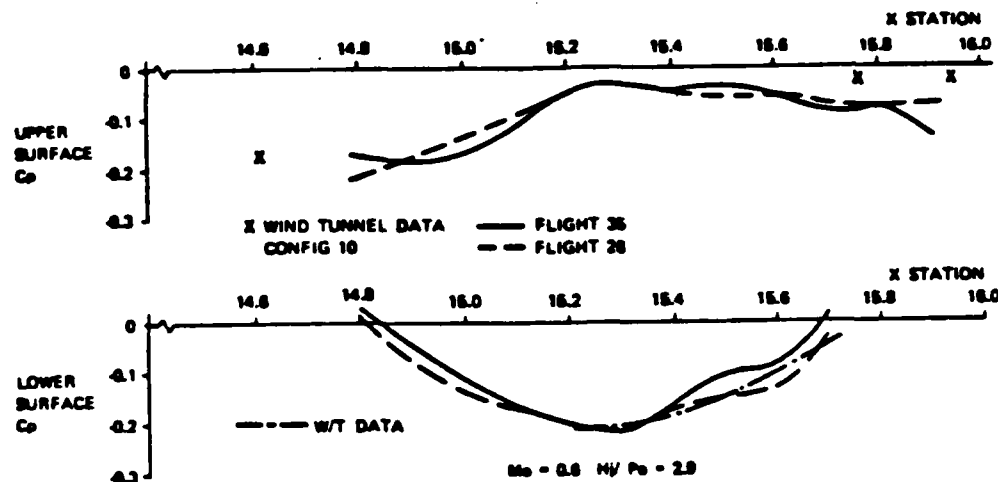


Figure 94. Boattail Surface Static Pressure Distributions (Reference 52)

agreement with flight test data, especially on the lower surface. Base pressures, especially on this nozzle, were good correlating parameters for drag (Reference 52) and were used to monitor drag changes in flight. Wind tunnel and flight test base pressures (Figure 95) are approximately the same level. During flight tests, an unsteady throttle dependent force was identified. A geometric fix to the afterbody flow instability problem, besides reducing the prototype aircraft drag, also identified the usefulness of unsteady pressure measurements as an indication of afterbody flow quality and separation.

Success of wind tunnel/analytical correlations of throttle dependent forces is determined by the care and consideration directed to eliminating or correcting the discrepancies created by the differences in the wind tunnel model and the flight vehicle. Support effects can be corrected with some success. Simultaneous duplication of inlet and nozzle flows is critical if the inlet and nozzle flows are not independent. Extensive pressure instrumentation is required over the inlet and nozzle regions and all other aircraft surfaces influenced by the propulsion stream. The task is not impossible but requires use of engineering skill and resources.



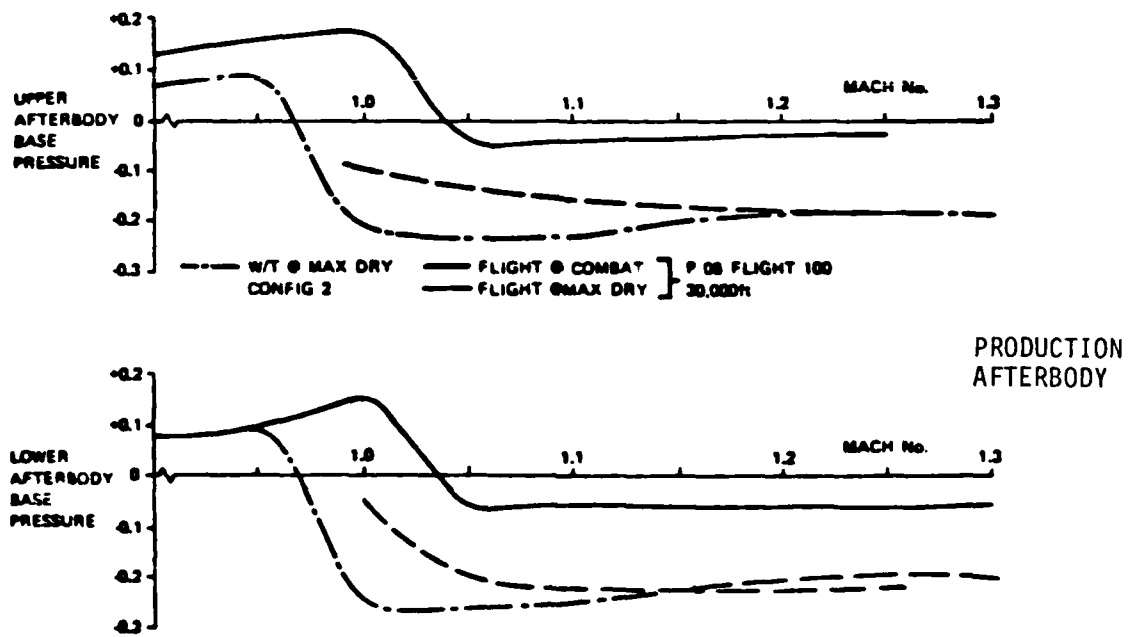


Figure 95. Comparison of In-Flight and Wind Tunnel Base Pressures (Reference 52)

## SECTION V

### FINAL REMARKS

Throttle dependent forces are all forces, internal and external, acting on the engine streamtube and aircraft surfaces that change with engine power setting. These forces can be significant for tactical aircraft which are required to perform a mission over a wide Mach number range and for transport aircraft which have demanding cruise performance requirements. The primary inlet throttle dependent forces are spillage and bypass drag. For the nozzle, these forces are boattail and base drag and jet interference and entrainment. These forces can be determined with varying success by analytical techniques, wind tunnels tests, and in flight tests. Computational methods and test techniques are essential tools and are evolving constantly.

## REFERENCES

1. B. L. Hunt, N. S. Gowadia, Determination of Throttle-Dependent Drag for Fighter Aircraft, AIAA Paper No. 81-1692, August 1981.
2. A. Ferri, "Introductory Lecture - Engine Airplane Interference-Definition of the Problem and Related Basic Fluid Dynamic Phenomena," AGARD LS-53, May 1972.
3. F. Aulehla, K. Lotter, "Nozzle/Airframe Interference and Integration," AGARD LS-53, May 1972.
4. S. A. Thornley, E. C. Carter, "The Measurement of the Transonic Spillage Drag of a Supersonic Intake," AGARD CP-150, September 1974.
5. G. Oates, The Aerothermodynamics of Aircraft Gas Turbine Engines, Aero Propulsion Laboratory WPAFB, Ohio, AFAPL-TR-78-52, July 1978.
6. P. P. Antonatos, "Inlet/Airplane Interference and Integration," AGARD LS-53, May 1972.
7. M. E. Brazier, W. H. Ball, "Accounting of Aerodynamic Forces on Airframe/Propulsion Systems," AGARD CP-150, September 1974.
8. J. G. Doonan, W. H. Davis, Advanced Exhaust Nozzle Concepts Using Spanwise Blowing for Aerodynamic Lift Enhancement, AIAA Paper No. 82-1132, June 1982.
9. L. D. Webb, R. L. Janssen, Preliminary Flight and Wind Tunnel Comparisons of the Inlet/Airframe Interactions of the F-15 Airplane, AIAA Paper No. 79-0102, July 1978.
10. L. G. Nielding, "F-15 Wind Tunnel/Flight Correlation," NASA Wind Tunnel/Flight Correlation, November 1981.
11. F. W. Burcham, et al., Recent Propulsion System Flight Tests at NASA Dryden Flight Research Center, AIAA Paper No. 81-2438, November 1981.
12. J. V. Rejeske, D. J. Stava, A Test Technique for Inlet/Aircraft Drag Evaluation, AIAA 74-1145, October 1974.
13. H. Arnaiz, Techniques for Determining Propulsion System Forces for Accurate High Speed Vehicle Drag Measurements In Flight, AIAA Paper No. 75-964, August 1975.
14. A. E. Fuhs, "Engine Integration and Thrust/Drag Definition," AGARD LS-53, May 1972.
15. Aviation Week and Space Technology, p. 16, November 20, 1972.
16. B. Munniksma, F. Jaarsma, "Jet Interference on a Podded Engine Installation of a Twin Engined Wide Body Aircraft at Cruise Conditions," AGARD CP-150, September 1974.
17. Aerospace Engineering, March 1983.

## REFERENCES (Cont'd)

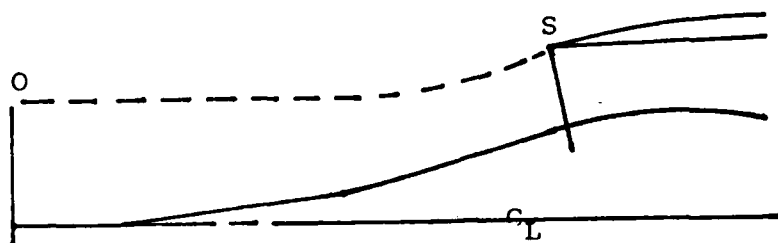
18. R. E. Craig, R. J. Reich, Flight Test Aerodynamic Drag Characteristics Development and Assessment of Inflight Propulsion Analysis Methods for AGM-109 Cruise Missile, AIAA Paper No. 81-2423, November 1981.
19. T. D. Coombes, "A Model Technique for Exhaust System Performance Testing," AGARD CP-150, September 1974.
20. F. Jaarsma, "Experimental Determination of Nozzle Characteristics and Nozzle Airframe Interference," AGARD LS-53, May 1982.
21. G. D. Smith, et al., Analytical and Experimental Investigation of Ejector-Powered Engine Simulators for Wind Tunnel Models, AEDC-TR-76-128, January 1977.
22. R. J. Glidewell, A. E. Fanning, "Twin Jet Exhaust System Techniques," AGARD CP-150, September 1974.
23. A. E. Harris, E. C. Carter, "Wind Tunnel Test and Analysis Techniques Using Powered Simulators for Civil Nacelle Installation Drag Assessment," AGARD CP-301, May 1981.
24. B. Ewald, "Engine Jet Simulation Problems in Wind Tunnel Tests," AGARD CP-150, September 1974.
25. T. L. Kennedy, An Evaluation of Wind Tunnel Test Techniques for Aircraft Nozzle Afterbody Testing at Transonic Mach Number, AEDC TR-80-8, November 1980.
26. F. Aulehla, G. Besiok, "Reynolds Number Effects on Fore and Aftbody Pressure Drag," AGARD CP-150, September 1974.
27. F. Aulehla, G. Besiok, "Fore and Aftbody Flow Field Interaction with Consideration of Reynolds Number Effects," Messerschmitt Bolkow Blohm UFE 1279, October 1976.
28. A. Pope, Wind Tunnel Testing, John Wiley & Sons, Inc., 1950.
29. P. P. Antonatos, et al., "Assessment of the Influence of Inlet and Afterbody/Nozzle Performance on Total Aircraft Drag," AGARD CP-124, April 1973.
30. D. D. Knight, Improved Numerical Simulation of High Speed Inlets Using the Navier-Stokes Equations, AIAA Paper No. 80-0383, January 1980.
31. J. A. Ross, I. McGregor, A. J. Priest, "Some RAF Research on Shielded and Unshielded Fuselage Mounted Air Intakes at Subsonic and Supersonic Speeds," AGARD CP-301, May 1981.
32. F. Marconi, et al., Development of a Computer Code for Calculating the Steady Super/Hypersonic Inviscid Flow Around Real Configurations, NASA CR-2675, 1975.
33. I. Putnam, J. Mace, A Survey of Aft Body Flow Prediction Methods AIAA Paper No. 81-1694, August 1981.
34. J. Mace, R. Cosner, Analysis of Viscous Transonic Flow Over Aircraft Forebodies and Afterbodies, AIAA Paper No. 83-1366, June 1983.

## REFERENCES (Concluded)

35. N. Voogt, et al., "Aerodynamic Aspects of a High Bypass Ratio Engine Installation on a Fuselage Afterbody," AGARD CP-301, May 1981.
36. S. R. Ahmed, "Prediction of the Optimum Location of a Nacelle Shaped Body on the Wing of a Wing-Body Configuration by Inviscid Flow Analysis," AGARD CP-150, September 1974.
37. C. Haberland, et al., "Calculation of the Flow Field Around Engine-Wing Configuration," ICAS-80-4.1, October 1980.
38. T. J. Barber and D. C. Ives, et al., Computational Design and Validation Test of Advanced Concept Subsonic Inlets, AIAA-84-1329, June 1984.
39. W. B. Compton, J. L. Whitesides, Three-Dimensional Euler Solutions for Long-Duct Nacelles, AIAA-83-0089, January 1983.
40. G. Krenz, "Interference Between Wing and Intake/Jet," AGARD CP-150, September 1974.
41. K. M. Peery and C. K. Forester, Numerical Simulation of Multi-Stream Nozzle Flows, AIAA 79-1549, July 1979.
42. C. W. Boppe, Elements of Computational Engine-Airframe Integration, AIAA-84-0117, January 1984.
43. T. G. Ayers, "Report of the Wind Tunnel/Flight Correlation Panel," NASA Dryden Flight Research Center.
44. T. G. Ayers, "Review of the 1980 Wind Tunnel/Flight Correlation Panel," NASA Wind Tunnel/Flight Correlation, November 1981.
45. AGARD/Flight Mechanics Panel, Ground/Flight Test Techniques and Correlation, Symposium program and abstracts, October 1982.
46. R. H. Smith, "Problems in Correlation Caused by Propulsion Systems," NASA Wind Tunnel/Flight Correlation, November 1981.
47. F. J. Schoelen, B-1 Inlet and Nozzle Flight Performance Determination Program, AIAA Paper No. 81-1852, August 1981.
48. G. K. Richey, et al., Wind Tunnel/Flight Test Correlation on the B-1 Nacelle Afterbody/Nozzle, AIAA Paper No. 76-673, July 1976.
49. J. Nugent, L. D. Webb, "Selected Results of the F-15 Propulsion Interaction Program," NASA Ames Tetwoq Meeting, May 1982.
50. L. D. Webb, J. Nugent, Selected Results of the F-15 Propulsion Interactions Program, AIAA Paper No. 82-1041, June 1982.
51. E. J. Lucas, et al., Comparison of Nozzle and Afterbody Surface Pressures from Wind Tunnel and Flight Test of the YF-17 Aircraft, AIAA Paper No. 78-992, June 1978.
52. D. C. Leyland, Lessons from Tornado Afterbody Development, British Aerospace.

## BASIC DEFINITIONS

1. Additive Drag ( $D_{ADD}$ ) - Static pressure force exerted, in the wind direction, on the inlet streamtube, between freestream conditions and the inlet stagnation point, with the inlet operating at zero external bleed flow. Alternatively it may be looked upon as the total momentum change of the inlet air from freestream to the inlet stagnation point, with the inlet operating at zero external bleed flow.



2. Additive Drag Correlation Factor ( $K_{ADD}$ ) - The change in spillage drag from the mass flow ratio at which the additive drag is zero to an operating mass flow ratio, divided by the theoretical additive drag:

$$K_{ADD} = (D_{ADD} - \Delta D_{Lip}) / D_{ADD} \text{ (theoretical)}$$

If it is assumed that the correction factor is not a function of mass flow ratio (a common assumption) the additive drag correction factor is the change in spillage drag divided by the change in theoretical additive drag between any two mass flow conditions.

$$K_{ADD} = \Delta D_{Spill} / \Delta D_{Add} \text{ (theoretical) [if } K_{ADD} \neq f(\text{MFR})]$$

3. Aerodynamic Reference Configuration (Reference Configuration) - Configuration tested on external aerodynamics model. Usually a fixed configuration with a flow through duct propulsion system.
4. Aerodynamic Reference Model - Wind tunnel model used to determine the forces and moments of the reference aircraft configuration.

BASIC DEFINITIONS (Cont'd)

5. Afterbody - Total fuselage and/or nacelle from the fuselage maximum cross section to the nozzle exit station, including base area.
6. Afterbody Drag - Boattail plus base drag.
7. Base Area - Cross sectional area projected normal to the fuselage reference line of any geometrically definable area aft of the maximum cross section station that is known to be totally in a separated flow region.
8. Base Drag - Drag attributable to a base area.
9. Bleed Drag - ( $D_{bl}$ ) - Wind direction component of total momentum loss from freestream to exit station of the bleed air, plus the incremental change in external drag, at constant inlet airflow, from no bleed to the operating bleed. Note that in the case of external bleed drag (bleed air taken off ahead of the inlet lip station), although the definition is identical, there is an important difference. In this case the bleed flow alters the inlet stagnation streamtube shape, even at a constant inlet airflow. Therefore the incremental change in external drag includes a change in the "spillage drag" in addition to the change in external drag due to the perturbations at the bleed exit station.
10. Boattail - Amount of fuselage and/or nacelle closure between two stations. Measured by planar cuts normal to the fuselage reference line through various aircraft sections (less any base closure between the stations).
11. Boattail Drag - Total drag (pressure plus friction) on the nozzle boattail minus base drag (does not include tail surfaces).
12. Bypass Drag ( $D_{by}$ ) - Wind direction component of total momentum loss from freestream to exit station of the bypass air plus the incremental change in external drag, at constant inlet airflow, from no bypass to the operating bypass.
13. Capture Area, Design ( $A_{Des}$  or  $A_{Ref}$ ) - For variable capture area inlets this is the capture area setting at which the inlet contours are designed.

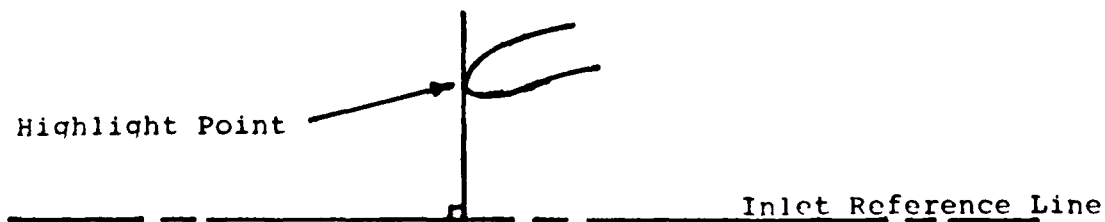
## BASIC DEFINITIONS (Cont'd)

14. Capture Area, Inlet ( $A_c$ ) - Area enclosed by the locus of most forward points (measured normal to the inlet reference line) on the inlet cowl, sideplates and first ramp or boundary layer diverter, projected in the freestream direction.
15. Cowl Length ( $l_{max}$ ) - Length from cowl lip station to the fuselage or nacelle maximum cross section station measured along the fuselage reference line.
16. Datum Configuration - Configuration used as a basis of comparison with other configurations of the same type.
17. Drag Polar - A plot of drag versus lift. For bookkeeping purposes it is presented for the operating reference configuration.
18. Drag Polar Exhaust Increments - Lift, drag and pitching moment differences between the aerodynamic reference and operating reference exhaust system configurations which are allocated to the aircraft drag polar.
19. Drag Polar Inlet Increments - Lift, drag and pitching moment differences between aerodynamic reference and operating reference inlet configurations which are allocated to the aircraft drag polar.
20. Engine Air - All air entering the engine compressor face including all air removed from or injected into the engine airstream aft of the compressor face. This will include for example high compressor bleed air, fan bleed air, nozzle bleed air (e.g. jet flaps) and secondary air injected into the nozzle flow. The lone exception to this definition will be tertiary nozzle air which will be defined as an external flow stream.
21. Exhaust System Force Model - Wind tunnel model used to determine the relative forces and moments of the aerodynamic reference, operating reference, and operating exhaust system configurations.
22. Exit Station (e) - The most downstream station, measured along the fuselage reference line, at which the internal airflow is completely confined by solid surfaces.



BASIC DEFINITIONS (Cont'd)

23. External Drag ( $D_{ext}$ ) - Pressure plus friction force in the wind direction on the external surface of the aircraft, minus the static force on all external surfaces effected by the propulsion airstreams.
24. External Surfaces - All aerodynamic surfaces not included in the internal surfaces.
25. Friction Force, Calculated - Skin friction force obtained from skin friction coefficient correlations and model local flow conditions.
26. Fuselage Boattail - Closure of the fuselage and/or nacelle from maximum cross section to customer connect, less any base closure between the stations (does not include tail surface).
27. Fuselage Boattail Angle ( $B_{11}$ ) - Chord line from customer connect to maximum nacelle/fuselage cross sectional area station.
28. Fuselage Boattail Drag (Afterbody Boattail Drag) - Total drag (pressure plus friction) on the afterbody (does not include base drag).
29. Gross Thrust - ( $F_g$ ) (Uninstalled Gross Thrust) - The static force vector generated by the engine operating with Mil Spec total pressure recovery at the compressor face and no customer bleed or horsepower extractions. Here the static force will include the total momentum of all propulsion air streams at their respective exit station and all static friction and pressure forces on any external surfaces effected by the propulsion streams.
30. Highlight Point - A point at which a line normal to the inlet reference line is tangent to the inlet leading edge contour.

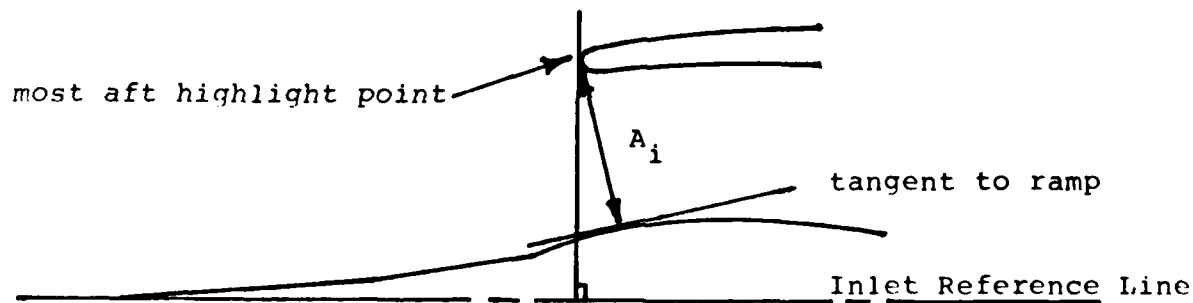


## BASIC DEFINITIONS (Cont'd)

31. Inlet Airflow - All air which enters the inlet at the cowl lip station. Includes bleed taken out aft of the lip station but does not include bleed removed forward of this station.

32. Inlet Force Model - Wind tunnel model used to determine the relative forces and moments of the aerodynamic reference, operating reference, and operating inlet configurations.

33. Inlet Lip Area ( $A_i$ ) - Physical duct cross sectional area measured from the most aft highlight point (usually the cowl centerline highlight point) to the ramp/centerbody at an angle normal to the ramp centerbody. Pitot (open nose) inlets are considered as an axisymmetric inlet with a zero (0) degree centerbody for the purpose of this definition.



34. Installed Gross Thrust ( $F_{g_{inst}}$ ) - The static force generated by the engine operating with the installed total pressure recovery at the compressor face and with installed customer bleed air and horsepower extractions. Static force is defined the same as in Gross Thrust.

35. Installed Net Thrust ( $F_{n_{inst}}$ ) - Installed Gross Thrust minus the ram drag ( $m_{eng} V_o$ ) of all engine air. (Installed Net Thrust does not include throttle dependent drag increments.)

36. Integrated Pressure Force - Force obtained by assigning surface areas to selected model static pressure taps and mathematically combining the pressure X area terms in axial and normal directions.

## BASIC DEFINITIONS (Cont'd)

37. Internal Drag ( $D_{INT}$ ) - Pressure plus friction force, positive in the wind direction, on the internal surfaces of the aircraft. ( $D_{INT} = -F_{INT}$ ).
38. Internal Surface - All internal surfaces from the locus of inlet stagnation points (stagnation points on the cowl lip, sideplates and forward ramp or boundary layer gutter leading edge) to the respective propulsion air exit stations at which exit momentum is defined.
39. Internal Thrust ( $F_{INT}$ ) - The pressure plus friction force developed on all internal surfaces.
40. Lift - ( $L$ ) - External pressure plus friction force exerted on the aircraft in a direction normal to the wind direction in the plane of symmetry.
41. Lip Suction Increment - Change in the external drag (usually a reduction) due to a change in inlet airflow from baseline to operating conditions with the inlet operating at zero external bleed flow.
42. Net Thrust ( $F_n$ ) - (Uninstalled Net Thrust) - Uninstalled Gross Thrust minus the ram drag ( $\dot{m}_{eng} V_o$ ) of all engine air.
43. Nozzle Boattail - Closure on the nozzle from customer connect to nozzle exit stations.
44. Nozzle Boattail Angle ( $\beta$ ) - Chord line from nozzle exit to customer connect.
45. Nozzle Drag - (Nozzle of the nozzle boattail).
46. Operating Configuration - Configuration representing an actual aircraft operating condition for which performance is being predicted.
47. Operating Reference Configuration (Baseline or Datum Configuration) - Configuration for which the drag polar is derived and from which all propulsion installation force increments are taken. Usually a function of flight Mach Number only.

## BASIC DEFINITIONS (Cont'd)

48. Operating Reference Configuration Forces - The external forces and the additive forces at operating reference conditions resolved into lift, drag, and side force components.
49. Operating Reference Configuration Moments - The moments associated with external forces, the ram drag, the additive forces, and the gross thrust at operating reference conditions resolved into pitching, yawing, and rolling moments.
50. Propulsion Air Stream - All exit streams used in the calculation of gross thrust. Since the exact definition of this will vary from configuration to configuration (e.g. engine air used in jet flaps, or spanwise blowing) this must be well defined for each specific configuration.
51. Propulsive Force ( $F_p$ ) - (Installed Propulsive Force) Installed Net Thrust minus all throttle dependent force increments.
52. Ram Drag ( $D_{ram}$ ) - Product of the flight velocity ( $V_o$ ) and the engine air mass flow rate ( $\dot{m}_{eng}$ ).
53. Reference Capture Area ( $A_{ref}$ ) - The design capture area projected in the direction of the inlet reference line. Used in inlet drag coefficient.
54. Reference Configuration - Aerodynamic reference configuration.
55. Scrubbing Drag - Incremental force (pressure plus friction) in the wind direction on all afterbody external surfaces between the zero nozzle flow condition and the operating condition.
56. Side Force - Pressure plus friction force exerted on the aircraft in a direction normal to the wind direction and normal to the plane of symmetry.
57. Spillage Drag - ( $D_{spill}$ ) - Incremental change in additive drag plus lip suction due to a change in inlet airflow from operating reference to operating conditions with the inlet operating at zero external bleed flow.

## BASIC DEFINITIONS (Concluded)

58. Subsonic Duct Angle - ( $\theta_{sd}$ ) - Equivalent cone expansion half angle of the subsonic diffuser from the throat section to the compressor face station neglecting the engine bullet nose.
59. Throat Area, Inlet ( $A_t$ ) - Minimum physical duct cross section area measured at angle of minimum cross section (cannot occur in opening of bleed/bypass slots).
60. Throttle Dependent Exhaust Increments - Force and moment differences between operating reference and operating exhaust system configuration which are allocated to the propulsive force.
61. Throttle Dependent External Drag Increments ( $\Delta D_{TD}$ ) - Throttle dependent exhaust drag increment plus the throttle dependent inlet drag increment.
62. Throttle Dependent Inlet Increments - Force and moment differences between the operating inlet configurations which are allocated to the propulsive force.
63. Throttle Dependent Moments - The power setting dependent moment increments between operating reference conditions.
64. Total Momentum - Sum of the momentum flux (velocity times mass flow rate  $\dot{m}V$ ) and pressure forces (area times pressure increment above ambient  $A(P-P_o)$ ).
65. Trimmed Drag Polar - The drag polar of a series of configurations (due to varying control surfaces) for which all moments are zero at each individual point.